FIRAT UNIVERSITY
GRADUATE SCHOOL OF NATURAL AND APPLIED SCIENCES
T Ü R K İ Y E

SYNTHESIS, CHARACTERIZATION AND QUANTUM CHEMICAL CALCULATIONS OF SUBSTITUTED 1,2,4-TRIAZOLE DERIVATIVES.

Rebaz Anwar OMER

Doctoral Thesis

DEPARTMENT OF CHEMISTRY

Program of
Division of Organic Chemistry

MAY 2022

FIRAT UNIVERSITY
GRADUATE SCHOOL OF NATURAL AND APPLIED SCIENCES
TÜRKİYE

Department of Chemistry

Doctoral Thesis

SYNTHESIS, CHARACTERIZATION AND QUANTUM CHEMICAL CALCULATIONS OF SUBSTITUTED 1,2,4-TRIAZOLE DERIVATIVES.

Author
Rebaz Anwar OMER

Supervisor
Prof. Dr. Metin KOPARIR

MAY 2022

ELAZIG

FIRAT UNIVERSITY
GRADUATE SCHOOL OF NATURAL AND APPLIED SCIENCES
T Ü R K İ Y E

Department of Chemistry

Doctoral Thesis

Title:	Synthesis, Characterization and Quantum Chemical Calculations of Substituted 1,2,4-Triazole Derivatives.
Author:	Rebaz Anwar OMER
Submission Date:	14 April 2022
Defense Date:	23 May 2022

THESIS APPROVAL

This thesis, which was prepared according to the thesis writing rules of the Graduate School of Natural and Applied Sciences, Fırat University, was evaluated by the committee members who have signed the following signatures and was unanimously approved after the defense exam made open to the academic audience.

Signature

Supervisor:	Prof. Dr. Metin KOPARIR Firat University, Faculty of Science	Approved
Chair:	Prof. Dr. Mustafa KARATEPE Firat University, Faculty of Science	Approved
Member:	Prof. Dr. Niyazi BULUT Firat University, Faculty of Science	Approved
Member:	Prof. Dr. Ahmet ÇETIN Bingol University, Faculty of Science and Literature	Approved
Member:	Assist. Prof. Dr. Kamuran SARAÇ Bitlis Eren University, Faculty of Science	Approved

This thesis was approved by the Administrative Board of the Graduate School on

.... / .... / 20 ....

Signature

Prof. Dr. Kürşat Esat ALYAMAÇ
Director of the Graduate School

DECLARATION

I hereby declare that I wrote this Doctoral Thesis titled "Synthesis, Characterization and Quantum Chemical Calculations of Substituted 1,2,4-Triazole Derivatives." in consistent with the thesis writing guide of the Graduate School of Natural and Applied Sciences, Firat University. I also declare that all information in it is correct, that I acted according to scientific ethics in producing and presenting the findings, cited all the references I used, express all institutions or organizations or persons who supported the thesis financially. I have never used the data and information I provide here in order to get a degree in any way.

23 May 2022

Rebaz Anwar OMER

PREFACE

Rebaz Anwar OMER
ELAZIG, 2022

TABLE OF CONTENTS

Page

ABSTRACT

Synthesis, Characterization and Quantum Chemical Calculations of Substituted 1,2,4-Triazole Derivatives.

Rebaz Anwar OMER

Doctoral Thesis

FIRAT UNIVERSITY
Graduate School of Natural and Applied Sciences

Department of Chemistry

May 2022, Page: iv + 130

This thesis are planned in two main stages experimental and theoretical studies.

Stage 1: Synthesis and characterization of structures to be studied in the thesis

In this step, N-phenyl-2- (thiophene-2-carbonyl) hydrazine-1-carbothioamide and N-ethyl-2-(thiophene-2-carbonyl) hydrazine-1-carbothioamide were obtained by the reaction of thiophene-2-carbohydrazide with phenyl isothiocyanate and ethyl isothiocyanate respectively in the presence of ethyl alcohol. The obtained N-phenyl-2-(thiophene-2-carbonyl) hydrazine-1-carbothioamide and N-ethyl-2-(thiophene-2-carbonyl) hydrazine-1-carbothioamide was added base (KOH) to give the ring closure reaction. result of the ring closure reaction is obtained the 4-phenyl-5- (2-thiophene) -2,4-dihydro-3H-1,2,4-triazole-3-thione and 4-ethyl-5-(2-thiophene)-2,4-dihydro-3H-1,2,4-triazole-3-thione. The 4-phenyl-5- (2-thiophene) -2,4-dihydro-3H-1,2,4-triazole-3-thione compound obtained in the second step was converted to compound 1- (3-methyl-3-mesityl) -cyclobutyl-2 - {[5- (thiophen-2-yl) -4-phenyl-4H- 1,2,4-triazol-3- yl] sulfanyl}-ethanone by reaction with 2-chloro-1- (3-methyl-3-mesityl-cyclobutyl) -ethanone in dry acetone containing potassium carbonate.

Also 4-ethyl-5-(2-thiophene)-2,4-dihydro-3H-1,2,4-triazole-3-thione which was prepared in a second step is reacted with four different coumarin compounds to obtain compounds containing coumarin, 3,4,5-trisubstituted 3,4,5-trisubstituted 1,2,4-triazole sulfonyl compounds. Organic compounds prepared by us have been experimentally characterized by spectroscopic methods such as FT-IR, ^{1}H-NMR, and ^{13}C-NMR after beıng purified by appropriate purification methods.

Stage 2: Theoretical characterization of the substances to be synthesized in the thesis:

In addition to the characterization studies of the experimentally obtained compounds, theoretical calculations were made at the cc-PVDZ basis set level by using the Gaussian 09W and GaussView 5.1 packages of molecules and the Density Functional Theory (DFT) method. As a result of the studies, it was seen that experimental and calculated values were in good agreement.

The molecular electrostatic potential (MEP), charge distribution on the atoms, and thermodynamic parameters for all compounds were evaluated. Different parameters were calculated for all compounds using B3LYP/cc-Pvdz, those parameters are including energy of the highest occupied molecular orbital (E_{HOMO}), energy of the lowest unoccupied molecular orbital (E_{LUMO}), energy bandgap ($\Delta E = E_{LUMO} - E_{HOMO}$), dipole moment ($\mu$), hardness ($\eta$), softness ($\sigma$), electronegativity ($\chi$), electrophilicity index (ω), nucleophilicity (ε) index and The fraction of transferred electrons (ΔN) which is related to transfer electron between the inhibitor and metal surface.

Keywords: 1,2,4-triazole, Thiophene, Sulfanyl, Cyclobutane, Coumarin, B3LYP/cc-Pvdz, Inhibitor.

ÖZET

Sübstitüe 1,2,4-Triazol Türevlerinin Sentez, Karakterizasyon ve Kuantum Kimyasal Hesaplamaları

Rebaz Anwar OMER

Doktora Tezi

FIRAT ÜNİVERSİTESİ
Fen Bilimleri Enstitüsü
Kimya Anabilim Dalı

Mayıs 2022, Sayfa: iv + 130

Bu tez deneysel ve teorik çalışmalar olmak üzere iki ana aşamada planlanmıştır.

Aşama 1: Tezde çalışılan yapıların sentezi ve karakterizasyonu

Bu aşamada, N-fenil-2-(tiyofen-2-karbonil)hidrazin-1-karbotioamid ve N-etil-2-(tiyofen-2-karbonil)hidrazin-1-karbotioamid, etil alkol varlığında sırasıyla etil izotiyosiyanat ve fenil izotiyosiyanat ile tiyofen-2-karbohidrazidin reaksiyonundan elde edilir. Elde edilen N-fenil-2-(tiyofen-2-karbonil) hidrazin-1-karbotioamid ve N-etil-2-(tiyofen-2-karbonil) hidrazin-1-karbotioamid, halka kapanmasını vermek üzere baz (KOH) ilave edildi. Halka kapanma reaksiyonunun sonucu, 4-fenil-5-(2-tiofen)-2,4-dihidro-3H-1,2,4-triazol-3-tiyon ve 4-etil-5-(2-tiyofen)-2,4-dihidro-3H-1,2,4-triazol-3-tiyon elde edildi.

İkinci aşamada elde edilen 4-fenil-5-(2-tiyofen) -2,4-dihidro-3H-1,2,4-triazol-3-tiyon bileşiği, bileşik 1-(3-metil-3)'e dönüştürüldü. -mesitil) -siklobütil-2 - {[5-(tiofen-2-il)-4-fenil-4H-1,2,4-triazol-3-il]sülfanil}-etanon, 2-kloro-1 ile reaksiyona sokularak - (3-metil-3-mesitil-siklobutil) -etanon, potasyum karbonat içeren kuru aseton içinde. 2-kloro-1-(3-metil-3-mesitil-siklobütil)-etanon sentezi, literatür talimatına göre sentezlendi. Ayrıca ikinci aşamada hazırlanan 4-etil-5-(2-tiyofen)-2,4-dihidro-3H-1,2,4-triazol-3-tiyon dört farklı kumarin bileşiği ile reaksiyona sokularak elde edilen bileşikler aşağıdakileri içerir: kumarin, 3,4,5-tri-ikameli 3,4,5-tri-ikameli 1,2,4-triazol sülfonil bileşikleri. Tarafımızdan hazırlanan organik bileşikler, uygun saflaştırma yöntemleriyle saflaştırıldıktan sonra deneysel olarak FT-IR, ^{1}H-NMR ve ^{13}C-NMR gibi spektroskopik yöntemler ile karakterize edilmiştir.

Aşama 2: Tezde sentezlenen maddelerin teorik karakterizasyonu:

Ayrıca deneysel olarak elde edilen bileşiklerin karakterizasyon çalışmalarının yanı sıra, moleküler Gaussian 09W ve GaussWiew 5.1 paket programları ve Yoğunluk Fonksiyonel Teorisi (DFT) metodu kullanılarak cc-PVDZ temel seti seviyesinde teorik olarak da hesaplamalar yapıldı. Yapılan çalışmalar sonucunda deneysel ve hesaplanan değerlerin uyum içerisinde oldukları görülmüştür.

Tüm bileşikler için moleküler elektrostatik potansiyel (MEP), atomlar üzerindeki yük dağılımı ve termodinamik parametreler değerlendirildi. B3LYP/cc-Pvdz kullanılan tüm bileşikler farklı parametreler hesaplandı. Bu parametreler arasında en yüksek dolu moleküler orbitalin enerjisi (E_{HOMO}), en düşük boş moleküler orbitalin enerjisi (E_{LUMO}), enerji bant aralığı (ΔE= E_{LUMO} - E_{HOMO}), dipol momenti (μ), sertlik (η), yumuşaklık (σ), elektronegatiflik (χ), elektrofiliklik indeksi (ω), nükleofilisite (ε) indeksi ve inhibitör ve metal yüzey arasında elektron transfer etmek ile ilgili olan Aktarılan elektronların oranı (ΔN) bulunur.

Anahtar Kelimeler: 1,2,4-triazol, Tiyofen, Sülfanil, Siklobütan, Kumarin, B3LYP/cc-Pvdz, İnhibitör.

LIST OF FIGURES

x

LIST OF TABLES

LIST OF APPENDICES

SYMBOLS AND ABBREVIATIONS

Symbols

Δ	: heating
•	: Radical

Abbreviations

Ac	: Acetic acid
eq	: equivalent
h	: hours
^{0}C	: Degree of Celsius
DMF	: Dimethyl sulfoxide
M	: Mole
-H	: loss of hydrogen
+H	: added of Hydrogen
cm	: Centimeter
IR	: infrared spectroscopy
FT-IR	: Fourier transform infrared
ppm	: parts of gas per million parts of air
NMR	: Nuclear magnetic resonance
MHz	: mega hertz
g	: gram
mm	: millimole
Temp	: Temperature
DFT	: Density Functional Theory
TMS	: Tetramethylsilane
a.u.	: atomic unit
K	: kelvin
Kcal	: kilocalorie per mole
C	: Compound

1. INTRODUCTION

Triazole compounds have become a highly attractive field of research because of their available application such as drug substances, agricultural drugs, artificial acceptors, multimolecular ligands, etc. [1-3]. The triazole ring is, which is aromatic with three nitrogen atoms, a five-member heterocyclic compound, and is an electronically rich system [4]. These compounds have a wide range of biological effects because triazole derivatives can easily bind to various enzymes and receptors in the biological system via weak interaction such as coordination bond, ion-dipole, cation-π, π- π, van der Waals forces, the hydrophobic effect [5-8]. Triazole compounds have the ability to create multimolecular structures, which is a unique characteristic [9, 10]. In this way, special importance is placed on triazole compounds especially in the development of new molecules drug [2, 11, 12]. Furthermore, the triazole ring can be employed as an appealing linker to unite several pharmacophores to create bifunctional medicinal compounds. Thus, it provides a convenient and efficient way to develop biologically active and functional various molecules. In the construction of novel therapeutic molecules, the triazole ring is also an essential isostere of substances such as imidazole, oxazole, pyrazole, and thiazole.

Some triazole-based compounds have been widely produced and explored for their biological activity in the study and development of novel medications. In particular, triazole compounds as antifungal drugs are an important role in clinical treatment and it is the first choice for the treatment of fungal infections. Many triazole derivatives are being used as clinical drugs due to their potent pharmacological activity, low toxicity, low side effects, high bioconjugation, good pharmacokinetic properties, drug targeting, drug delivery diversity, broad-spectrum and better healing, or become candidates for the treatment of various diseases.

The biological activity of the sulphonyl derivatives of 1,2,4-triazoles is diverse. As example to these can display diuretics, neuroleptics [13], antituberculosis [14, 15], antimicrobials [16-18] antiphlogistics [19], antimycotics[20], anti-HIV [21]. In addition, substitute sulphonyl-1,2,4-triazoles can be used in agriculture and industry [13, 22] as complexing agents having the ability to coordinate metal ions with various donor centers [13, 23, 24] and as precursors in organic synthesis [25].

Wang and colleagues reported a novel sulphonyl triazole see Figure 1.1, as a non-nucleoside HIV-1 reverse transcriptase inhibitor in their study [26].
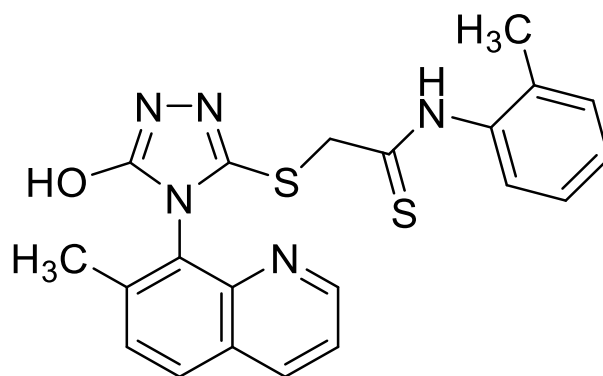
Figure 1.1. sulphonyl triazole

Kaplancyk and colleagues have synthesized 3-alkylsulphonyl-1,2,4-triazole derivatives [27] and investigated antituberculosis activity. Tests performed in the presence of in vitro have shown that these compounds act as anti-tuberculosis agents at a significant level see Figure 1.2.
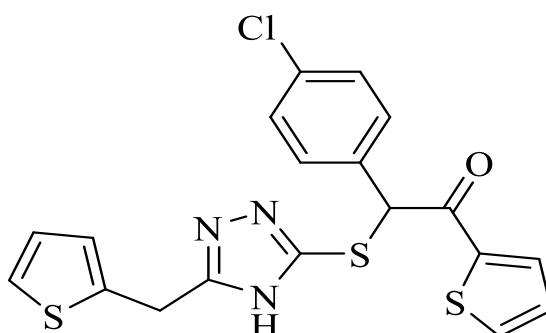
Figure 1.2. 3-alkylsulphonyl-1,2,4-triazole derivatives

Nahworld and colleagues have synthesized sulphonyl-1,2,4-triazole derivatives see Figure 1.3 [28], which have potent antiviral activity against efavirenz and nevirapine resistant viruses.
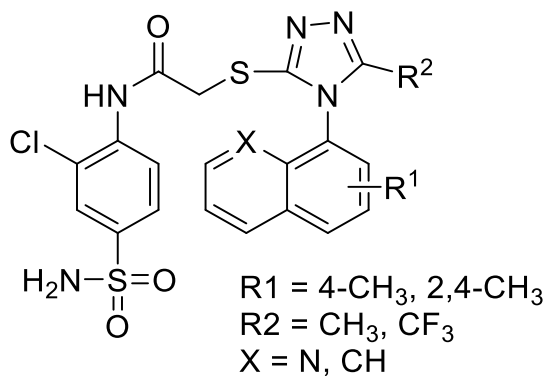
Figure 1.3. sulphonyl-1,2,4-triazole derivatives

It is known that 3-substitue cyclobutane carboxylic acid derivatives exhibit anti-inflammatory, antidepressant [29] activity. In addition, the cyclobutane ring in the structure of some polymers is impart different properties to these polymers. Such polymers have liquid crystal properties and they form a class of biopolymers suitable for photodegradation [30, 31].

Zhu and colleagues have synthesized 3-(phenylcyclobutyl) -1,2,4-triazole derivatives [32] in their study they measured values of inhibition against 11β-hydroxysteroid dehydrogenase enzyme in the presence of both in vitro and in vivo. As a result of the measurements, 1,2,4-triazole compounds containing the fluoro substituted cyclobutyl group see Figure 1.4, reported very good inhibition.
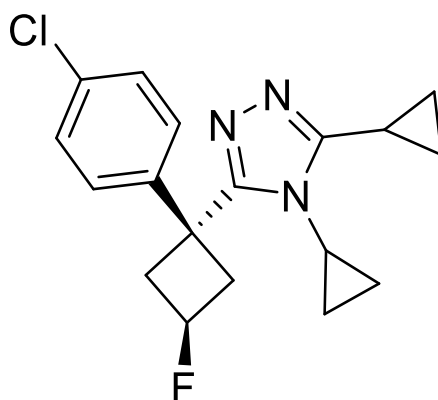
Figure 1.4. 1,2,4-triazole compounds containing the fluoro substituted cyclobutyl group

Ahmedzade and colleagues in a study in 2003 have synthesized thiazole derivatives containing 1,1,3-trisubstituted cyclobutane ring see Figure 1.5 [33], they have investigated antimicrobial activities against fungi and yeast. As a result of the antibacterial and antifungal

studies carried out, they reported that these substances showed high activity especially against *Escherichia coli*, *Rhodotorula rubrum* and *Kluyveromyces fragilis* species.
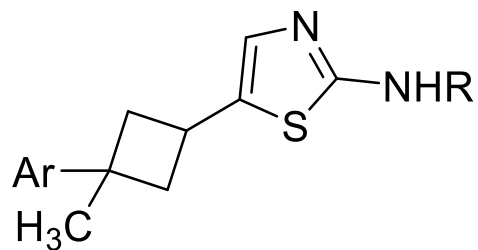
Figure 1.5. synthesized thiazole derivatives containing 1,1,3-trisubstituted cyclobutane ring

2. 1,2,4-TRIAZOLES

Three nitrogen atoms are arranged in a five-membered ring in this arrangement known as "triazacyclopentadiene" or simply triazole look Figure 2.1. There are two different isomer groups according to the relative position of the three nitrogen atoms. Each of these isomers has two different tautomers than the nitrogen atom to which hydrogen is attached.

1H-1,2,3- Triazole   2H-1,2,3- Triazole   1H-1,2,4- Triazole   4H-1,2,4- Triazole
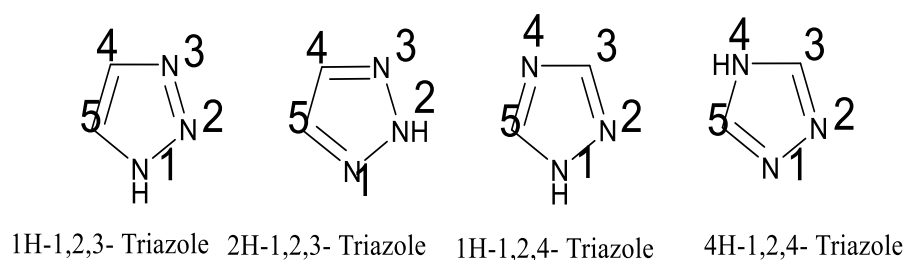
Figure 2.1. Simple triazole derivatives

In these aromatic rings, the state of electronic of the nitrogen atoms carrying hydrogen is the same as the electronic state of the nitrogen atom in the pyrrole. The electronic state of other nitrogen atoms is like the state of nitrogen atoms that do not carry hydrogen in diazoles [34, 35].

2.1. Synthesis 1,2,4-trizole derivatives

The first studies on the triazole ring started in 1885 by Bladin and Pelizzari when hydrazine reacted with formamide to synthesize the main ring [36] The formation reaction is shown in Figure 2.2 and the mechanism shown in Figure 2.3.
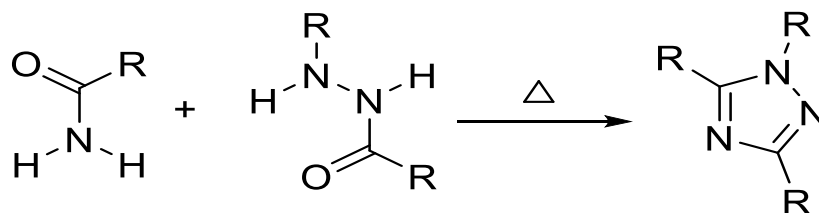
Figure 2.2. 1,2,4-Triazole ring formation reaction.
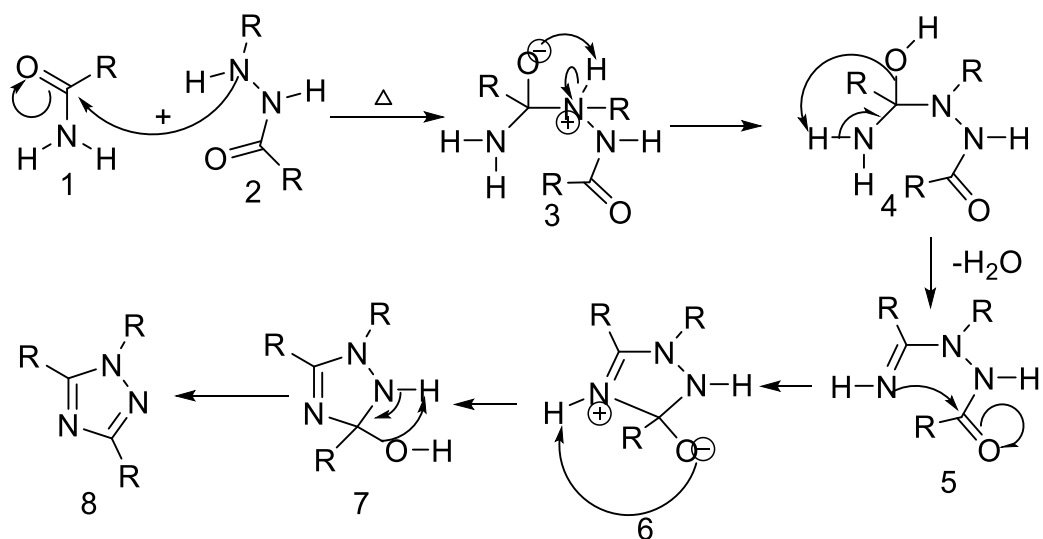
Figure 2.3. Mechanism of pellizzari reaction.

In this reaction, different methods have been tried for the synthesis of 1,2,4-triazole, as the yield is low and variable. In 1914, chemist Karl Brunner successfully synthesized substituted 1,2,4-triazole derivatives by reacting to various imides and hydrazines. This reaction is known as the Einhorn-Brunner reaction [37-41] The formation reaction is shown in Figure 2.4 and the mechanism is shown in Figure 2.5.
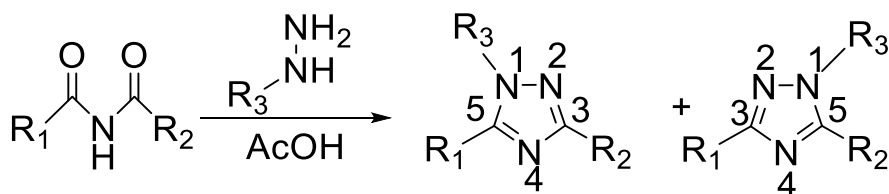
Figure 2.4. Formation of 1,2,4-triazole by Einhorn-Brunner reaction.
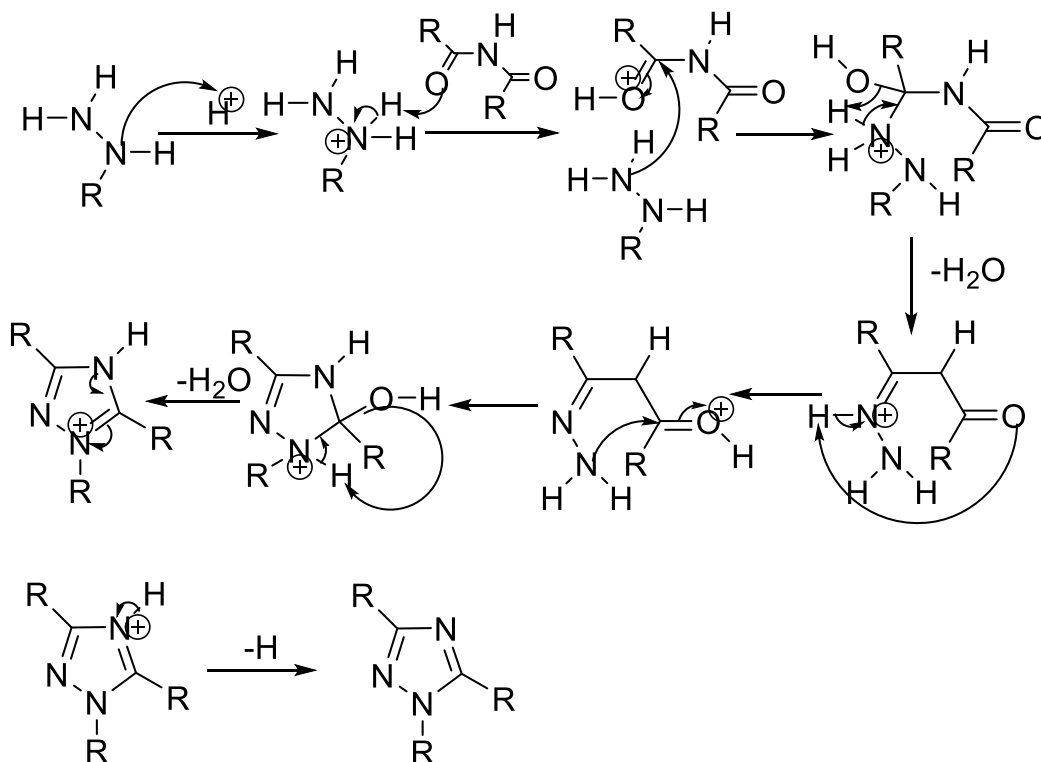
Figure 2.5. Einhorn-Brunner reaction mechanism

2.2. Other methods

In 1974, Conde et al. the mixture of cyano compound and aluminum chloride in dry o-dichlorobenzene were mixed then added with phenyl benzohydrazidoyl chloride heated for 20 minutes at 120-130 °C. This mixture is then basic with chilled dilute sodium hydroxide then extracted with ethyl acetate. Dilute organic part 1,2,4-triazole compound was obtained by washing with hydrochloric acid and water [42]. The related reaction is in Figure 2.6.
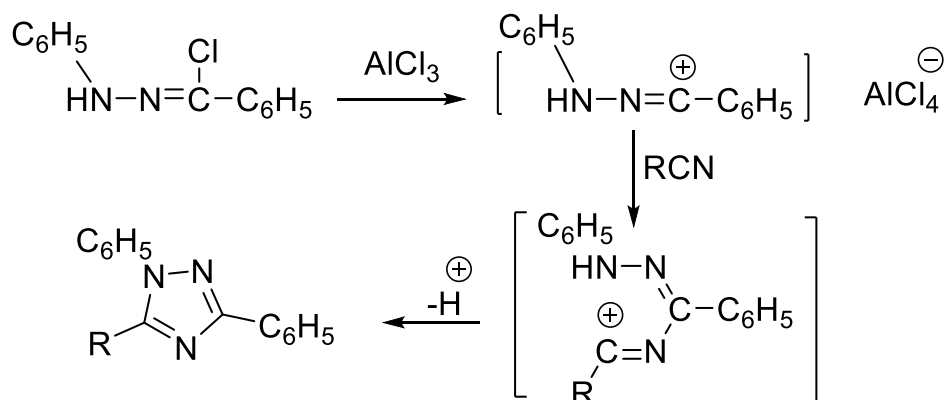
Figure 2.6. Hand reaction of 1,3-diphenyl-5-alkyl-1H-1,2,4-triazole.

The reaction of hydrazone and aliphatic amines under aerobic oxidative conditions. It gives 1,3,5-trisubstituted 1,2,4-triazole compounds. The reaction is given in Figure 2.7. and the mechanism in Figure 2.8.
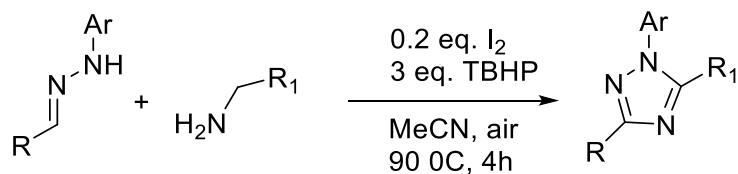
R: Ar, alkyl
R1: Ar, alkyl, Br

Figure 2.7. Formation recreation of 1,3,5-trisubstituted 1,2,4-triazole compounds as a result of the reaction of hydrazone and aliphatic amines.

The reaction occurs by the interaction of hydrazone and amine at 90°C under the catalyst of iodide and tert-butyl hydroperoxide (TBHP). The yield varies between 34% and 92% depending on the type of hydrazone and amine used.
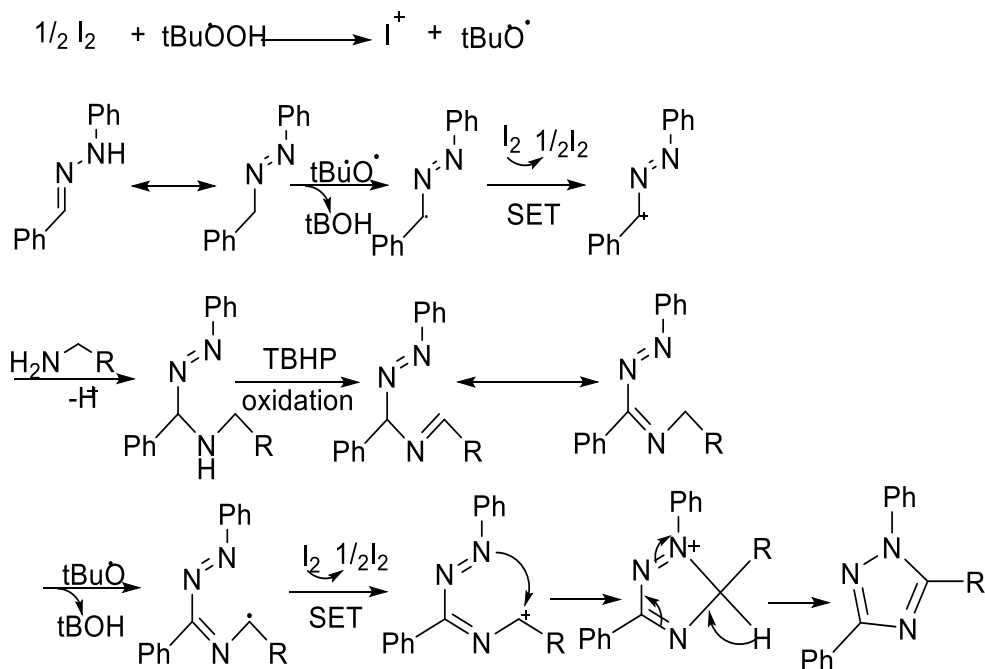
Figure 2.8. The formation mechanism of 1,3,5-trisubstituted 1,2,4-triazole compounds as a result of the reaction of hydrazone and aliphatic amines (SET = single-electron-transfer).

8

Castenedo et al. In a study published in 2010, succeeded in obtaining 1,3,5-trisubstituted-1,2,4-triazole derivatives as a result of the reaction of carboxylic acid, pyramid amidine, and monosubstituted hydrazines [43]. The reaction is as in Figure 2.9.
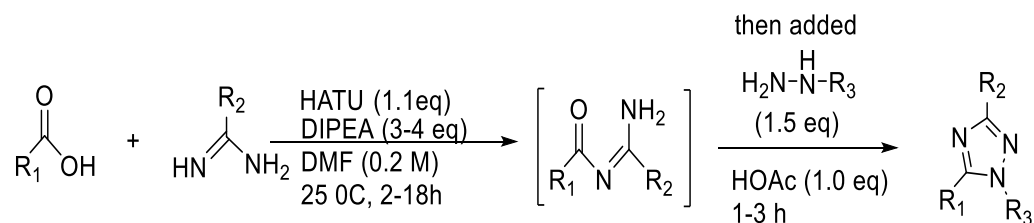
Figure 2.9. The reaction of 1,3,5-trisubstituted-1,2,4-triazole derivatives from carboxylic acid, primary amidine, and monosubstituted hydrazines.

2.3. Synthesis 1,2,4-Triazole-5-thions

2.3.1. From thiosemicarbazide and its derivatives

In 1896, 1,2,4-Triazol-5-thion (Figure 2.10) was first obtained by Freund by heating 1-formyl-3-thiosemicarbazide to 190 ^{0}C then dried [44].
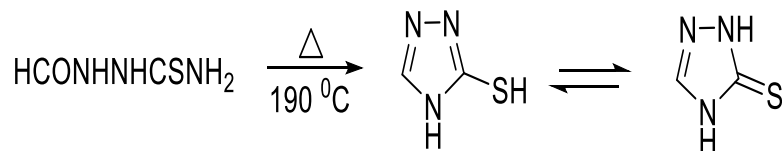
Figure 2.10. 1,2,4-Triazol-5-thion

One of the most widely used methods for the synthesis of 1,2,4-Triazole-5-thions by cyclization of 1-acyl-4-substituted-3-thiocemicarbazides with acylhydrazines substituted isocyanates see Figure 2.11 [45-47].
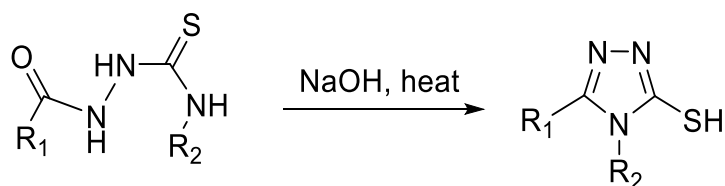
Figure 2.11. 1,2,4-Triazole-5-thions derivatives

9

4-Substituted-3-thiosemicarbazide derivatives acylation with carboxylic acid chlorides to obtained 4,5-disubstituted-1,2,4-triazole-3-thiones look Figure 2.12 [48-50].
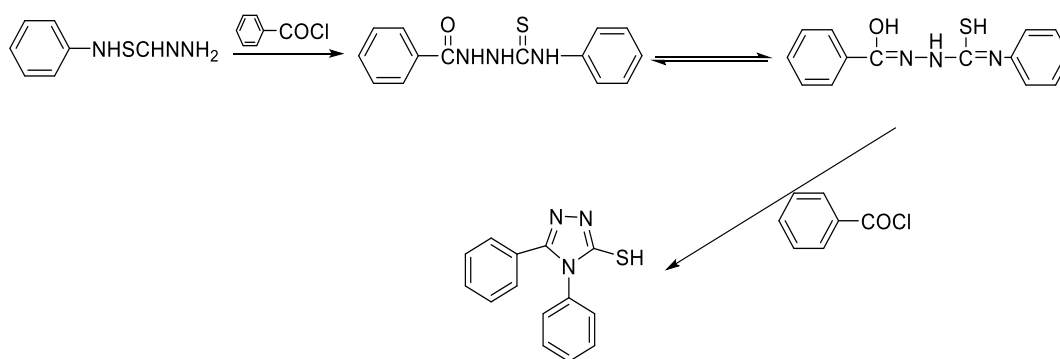
Figure 2.12. 4,5-disubstituted-1,2,4-triazole-3-thiones

2.3.2. Dithiocarbazic Acid Salts

Acylhydrazines with carbon-sulfur in alcohol at room temperature at the basic environment, as a result of the reaction, is dithiocarbazate salt which is a reaction with hydrazine the 4-amino-5-alkyl-1,2,4-triazole-3-thion was formed [51] look the Figure 2.13.
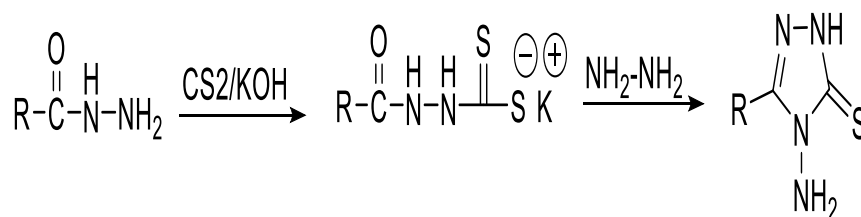
Figure 2.13. Synthesis of 4-amino-5-alkyl-1,2,4-triazole-3thion from dithiocarbazic acid salts.

In the study of Reid and Heindel, 3-aryldithiocarbazate was reacted with hydrazine hydrate to formed 4-amino-5-phenyl-2,4-dihydro-3H-1,2,4-triazole-3-thion. It is reacted with methyl bromoacetate, acid chloride, methylene iodide, and chloroacetonitrile, to synthesized 4-amino-5-phenyl-1,2,4-triazole derivatives in 60-70% yields Figure 2.14 [52-54].
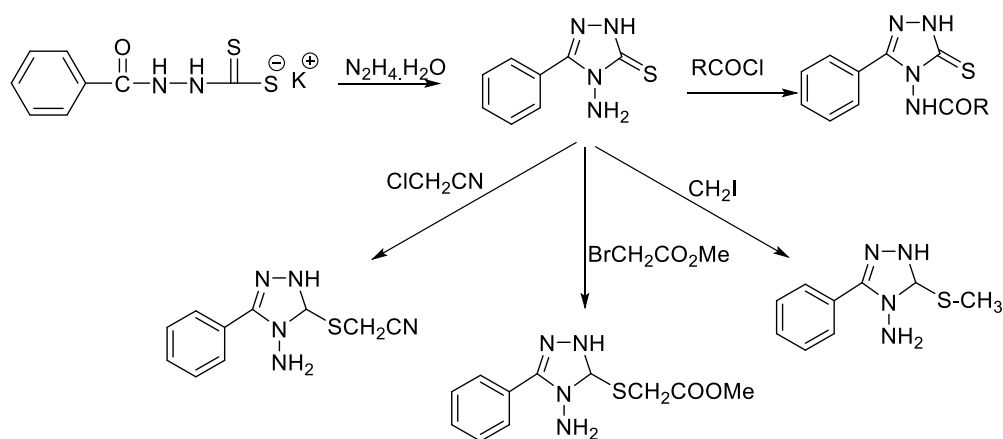
Figure 2.14. Synthesis of 4-amino-5-phenyl-1,2,4-triazole derivatives from 3-aryldithiocarbazic acid salts.

According to the Reid and Heindel procedure, carboxylic acid hydrazides in ethanolic KOH, then react with CS_2 and give high-efficiency potassium 3-aroildithiocarbazate salts. This salt, which is formed, forms a 5-aryl-2-mercapto-1,3,4-oxadiazole compound by ring closure with pyridine or anhydrous KOH. 4-amino-5-alkyl-3-mercapto-4H-1,2,4-triazole were formed when reacted with excess NH_2NH_2 in Figure 2.15 [55].

However, after the 3-aroildithiocarbazate salt is activated with methyl iodide, if the dithiocarbazate formed is reacted with hydrazine, the result of the ring-closing reaction gives 4-amino-5-alkyl-3-mercapto-4H-1,2,4-triazole.
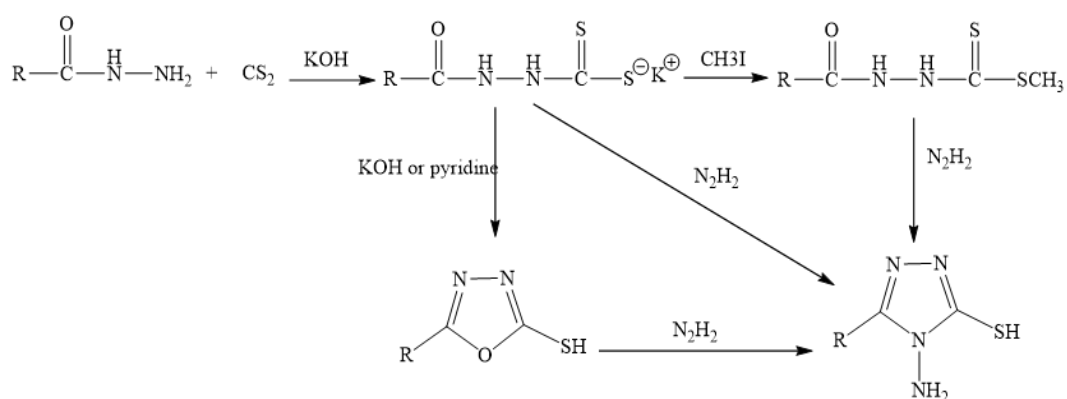
Figure 2.15. Reid and Heindel procedure, for synthesized 4-amino-5-alkyl-3-mercapto-4H-1,2,4-triazole

2.4. Properties of Triazoles

2.4.1. Acidity and basicity

Although 1,2,4-Triazole compounds show weak acid properties (pKa = 10.04 for protonation), they are more basic than 1,2,3-triazoles (pKa = 2.45 for proton removal). The basic feature of 1,2,4-triazole is that the imidazolium-type cation is stabilized mesmerically in Figure 2.16.
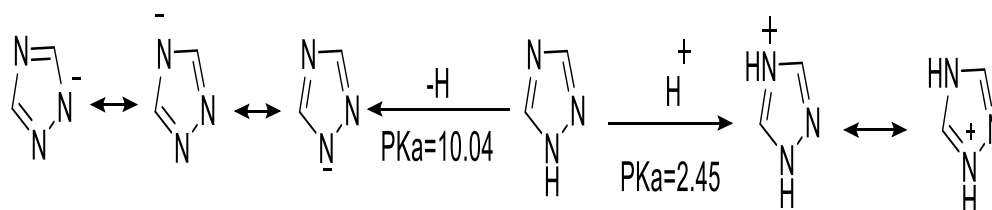
Figure 2.16. 1,2,4-Triazoles proton intake and proton administration

2.4.2. Reactivity

1,2,4-triazoles are similar to 1,2,3-triazoles in their aromatic properties and stability. Oxidizers are oxide the side chain, cannot break the ring. Triazoles, KMnO4, CrO3, etc. They are usually resistant to oxidants but are sensitive to reducers. Hydrogen in the nitrogen atom is replaced with metals.

Hydrogen at position 1 in triazoles is alkylated with alkali halides or diazomethane in an alkaline medium see Figure 2.17.
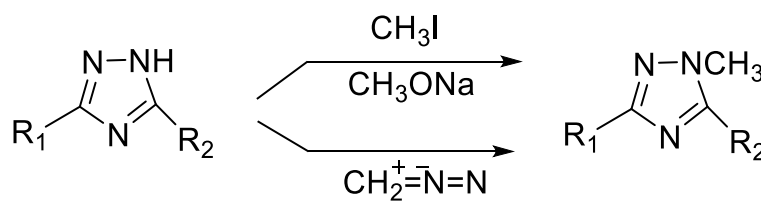
Figure 2.17. 1,2,4-Triazole derivative

On the other hand, 3,4-disubstituted-1,2,4-triazoles are number five with alkyl halides. while alkylating from their positions, they are acylated with acyl chloride, see Figure 2.18.
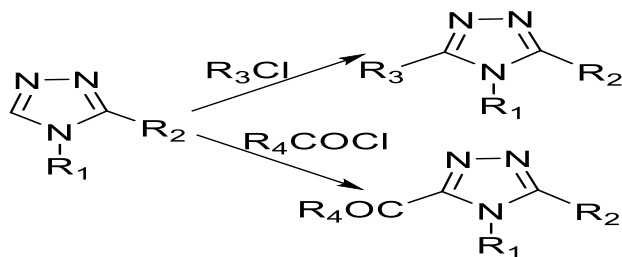
Figure 2.18. 3,4,5-Trisubstituted-1,2,4-triazoles

Preparation of 3- and 5-Substituted Derivatives from the positions of the ring is also possible. Triazoles can be easily halogenated, N-Cl of halogenated products, N-Br, and N-I-1,2,4-triazole derivatives are interesting. Because the connection between nitrogen and halogen can be easily broken and give a displacement reaction.

In 1,2,4-triazoles, nitration, sulfonation, and Friedel-Crafts alkylation and acylation do not give electrophilic substitution reactions that require acidic conditions. But they form 3-hydroxymethyl-1,2,4-triazoles with formaldehyde at 130 ° C.

3. THIOPHENE

Thiophene Figure 3.1 is a heterocyclic compound consist of a five-member ring with one heteroatomic Sulphur and the formula is C_4H_4S. Thiophene and derivative are found in petroleum and col. The structure of thiophene may be present in many natural products and is used in many pharmacologically activities. The thiophene derivatives were very well known for their therapeutic applications in medicinal chemistry. Simple thiophene is Liquid and stable compounds like benzene in boiling point and small [56, 57]. Thiophene was found as a benzene contaminant [58]
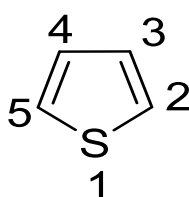
Figure 3.1. Thiophene

3.1. Synthesis of Thiophene

The major thiophene synthesis including Paal Knorr synthesis, aminothiophene (Gewald), Fiesselmann synthesis, and Hinsberg thiophene synthesis.

3.1.1. Paal Knorr Synthesis

From the reaction of 1, 4-Dicarbony1 with the source of sulfur to give thiophene [59, 60], Figure 3.2.
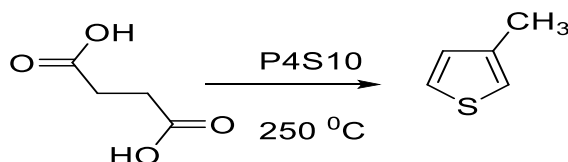
Figure 3.2. Paal Synthesis of Thiophene

The reaction of diketone with P2O5 under the condition of Paal synthesis was produced a higher yield of thiophene see Figure 3.3.
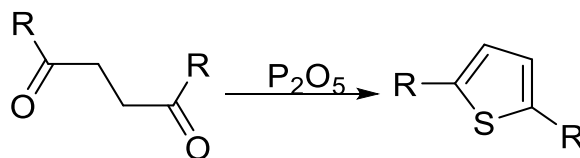
Figure 3.3. The reaction of diketone with P2O5 under the condition of Paal synthesis

According to the above reaction the proposed mechanism Figure 3.4 to formation the initial thione (X= S or O) which is tracked by cyclization and tautomerizations [61].
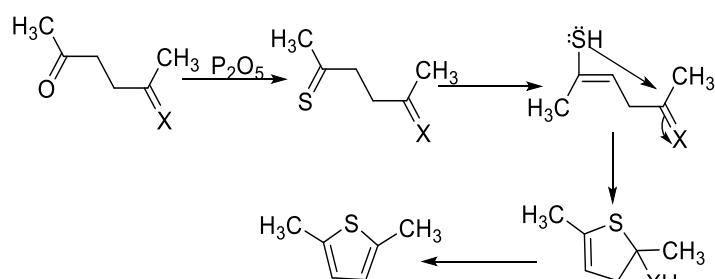
Figure 3.4. Mechanism reaction for Paal synthesis

3.1.2. Aminothiophene (Gewald)

In 1966 Gewald has reported this method [62]. This method was consisting the condensation reaction between Ketones has methyl group with β-ketonitrile under base condition and sulfur element, the cyclization was formed, see Figure 3.5.
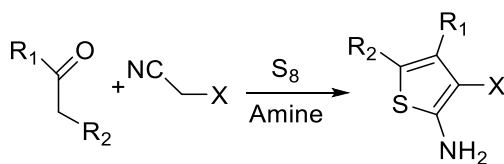
Figure 3.5. Condensation reaction between Ketones with β-ketonitrile and sulfur element, the cyclization was formed

3.1.3. Fiesselmann Synthesis

Fiesselamann synthesis of thiophene by condensation of thioglycolic and α, β-acetylenic esters to formed 3-hydroxyl-2-thiophene carboxylic acid [63]. According to the following reaction (Figure 3.6).
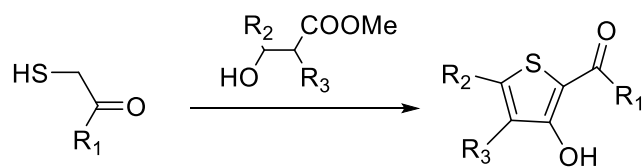
Figure 3.6. Fiesselamann synthesis

3.1.4. Hinsberg thiophene synthesis.

The Hinsberg synthesis (Figure 3.7) is the condensation between 1,2-dicarbonyl compounds with diethyl thiodiacetatet to produce thiophene [64]. The product is ester acids by stop mechanism, but the reactions always happened through hydrolysis to isolate di-acids.
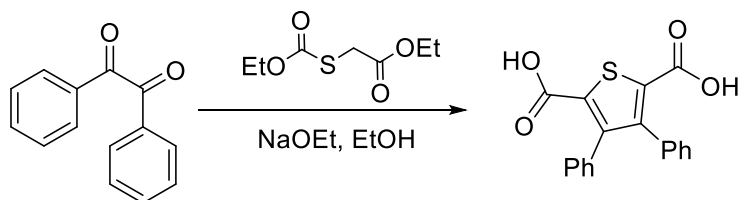
Figure 3.7. Hinsberg synthesis

3.1.5. Synthesis thiophene from industrial

On an industrial scale, thiophene can be synthesized by the high-temperature reaction between n-butane and sulfur see Figure 3.8.
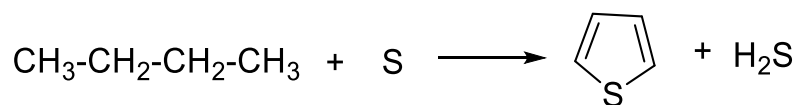
Figure 3.8. Synthesized thiophene from the reaction between n-butane and sulfur with high-temperature

The commercial method used for the synthesis of thiophene in industrial is a mixture of acetylene with hydrogen sulfide through a tube contain alumina at a higher temperature of 400 ^{0}C, see Figure 3.9.
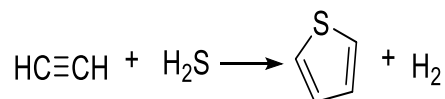
Figure 3.9. Synthesis of thiophene in industrial

Thiophene can also be synthesis by the reaction of phosphorous trisulphide and sodium succinate with heating see Figure 3.10 [65].
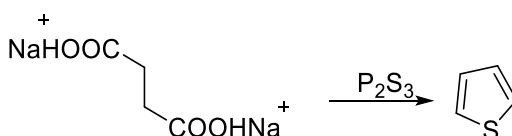
Figure 3.10. Synthesis thiophene by the reaction of phosphorous trisulphide and sodium succinate with heating

3.2. Properties of thiophene

3.2.1. Physical properties

Thiophene is a colorless liquid at room temperature, with a Slightly good smell reminiscent of benzenes, which thiophene shares certain similarities with it. The basis way for separation thiophene and benzenes is sulphonation reaction, due to the reactivity of thiophene with sulphonation. Due to their close boiling points (4 ^{0}C) between thiophene and benzene, which are difficult to distinguish by distillation at ambient pressure. Thiophene is classified as aromatic, while theoretical results indicate less aromatic compared with benzene. Thiophene is a toxic and flammable compound. Thiophene is water-insoluble but soluble in organic solvents like ether and alcohols. Thiophene melting points -38 ^{0}C, and the boiling point is 84 ^{0}C.

Thiophene's critical temperature was calculated by the sealed-tube method and equal to 579.4 K. A resonance energy equal to 20 Kcal/mol for thiophene was determined from the heat combustion and the thermochemical bond energies (Figure 3.11). The electron pairs on sulfur in the pi-electron system are greatly delocalized [66, 67]. Thiophene has a degree of stabilization higher than the equivalent furan, because sulfur has a larger bending radius and Consequently, sulfur could better tolerate a positive charge as a result of inductive sulfur pull.
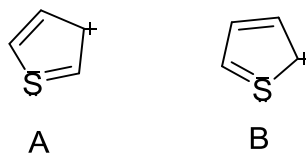
Figure 3.11. Thiophene resonance

3.2.2. Chemical properties of thiophene

Thiophene is a stable and readily available compound, the chemistry of the derivatives of thiophene matter has constant investigation. The sulfide of thiophene does not normally undertake the oxidations. Thiophene is subjected to electrophilic substitution: sulphonation reaction, nitration, the addition of halogen, Friedel-Crafts acylation reactions, etc. Thiophene even undergoes the Remer Tiemann reactions to the formation of diazonium salt [68, 69].

The reaction of thiophene, Nucleophilic reaction of thiophene (Figure 3.12) faster than the counterpart of benzenoid, this due to delocalization charge on the sulfur atom [60].
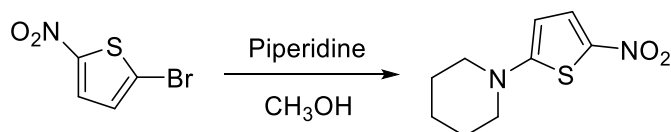
Figure 3.12. Nucleophilic reaction of thiophene

Thiophene Friedel Craft acylation reaction gave higher yield with controlling condition, see Figure 3.13 [70].
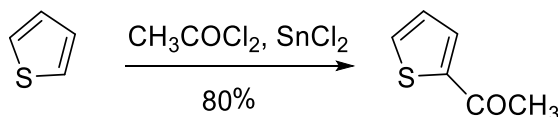
Figure 3.13. Thiophene Friedel Craft acylation reaction

Thiophene sulphonation see Figure 3.14, with sulphuric acids, the results is thiophene-2-sulfonic acid[71].

18

Pyridinium hydrogen sulfate   thiophene-2-sulfonic acid
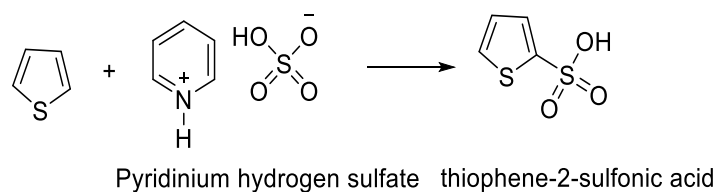
Figure 3.14. Thiophene sulphonation

Thiophene nitration see Figure 3.15, should occur in the absence of nitrous acid because it can result in an explosive reaction. To avoid this, nitronium tetrafluoroborate or acetyl nitrate were used [72, 73].
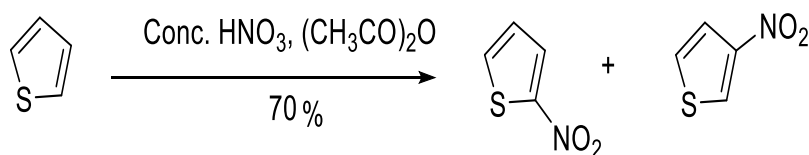
Figure 3.15. Thiophene nitration

Halogenation of thiophene see Figure 3.16, was very fast at room temperature even lower at zero degrees in a dark place, however the halogenation of thiophene 10^8 times faster than benzene [74].
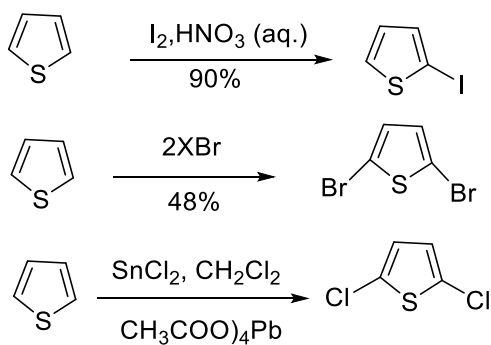
Figure 3.16. Halogenation of thiophene

4. CYCLOBUTANE AND DERIVATIVES

Cyclobutane is an alicyclic compound with the formula $(C_2H_4)_2$ closed since it is a polar molecule only has Van der Walls interactions. Although it is a colorless and flammable gas at room temperature, it is insoluble in water. The boiling point is 12 and the Melting point is -80 ℃. Cyclobutane itself has no commercial or biological significance, but its more complex derivatives are very important in biology and biotechnology. The four carbon atoms in the cyclobutane are not on the same plane, the ring is typically in a folded or creased conformation. Each of the carbon atoms makes an angle of 25 with the plane formed by the other three carbon atoms. Thus, the driving force caused by each carbon atom is minimized. This conformation is also known as the "butterfly" Figure 4.1.
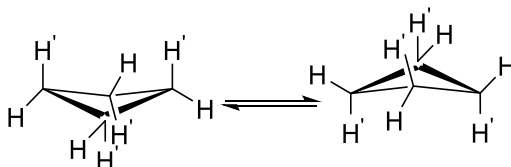
Figure 4.1. Butterfly conformations of the cyclobutane molecule.

4.1. Stereoisomerism in cyclobutane

In cyclobutane, the carbons are prevented from rotating around their axis due to the ring. As a result, a geometric isomer has formed. For the geometric isomer to form in the cyclobutane, there must be at least two groups. In this case, mostly-isomers of cyclobutane are formed Figure 4.2, when three groups are attached to the cyclobutane asymmetric carbon atom is formed and its optical isomer is seen.
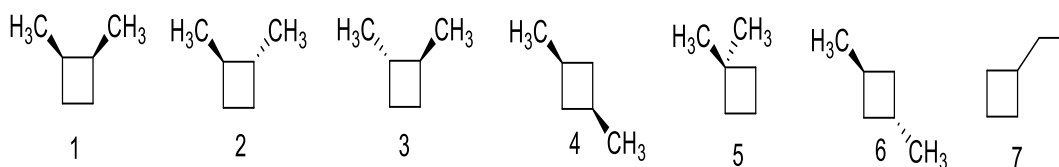
Figure 4.2. possible constitutional isomer for di-substituted

4.2. Reactions of Cyclobutane

The most suitable way to obtain cyclobutane is the Wurtzy method with 1,4-dihalobutane. This method is possible to obtain cyclobutane derivatives as in Figure 4.3. The yield in Wurtzy method is lower, using dilute hexane or pentane solutions can be increased the yield [75].

$$X\diagdown\diagup\diagdown\diagup X \quad + \quad 2Na \longrightarrow \square \quad + \quad 2NaX$$

X= Halojen
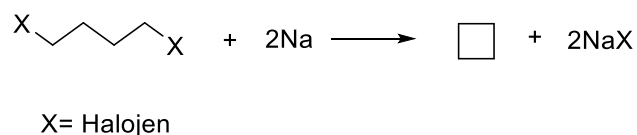
Figure 4.3. Cyclobutane production from 1,4 dihalobutans by Wurtz method.

Cyclobutane is formed by catalytic hydrogenation of cyclobutene. The first of the reaction hydrogen gas is sent to the nickel in the phase and H-H sigma bond opening under the effect of metal metal-H bond is formed. In the next stage, cyclobutane is sent to metal, and pi bonds are formed by interacting with the metal and cyclobutane. Figure 4.4. The formed cyclobutane moves away from the metal surface. The reaction takes place at 180 °C.

$$\square \quad \xrightarrow{H_2/Ni} \quad \square$$
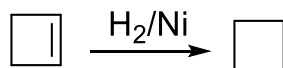
Figure 4.4. Preparation Cyclobutane from cyclobutane by catalytic hydrogenation.

Cycloaddition reactions are a kind of Diels-Alder reaction, with a light effect. cyclobutane may occur [76]. The reaction occurred in Figure 4.5.

$$\begin{matrix} CH_2 \\ \| \\ CH_2 \end{matrix} \quad + \quad \begin{matrix} CH_2 \\ \| \\ CH_2 \end{matrix} \xrightarrow{h\nu} \square$$
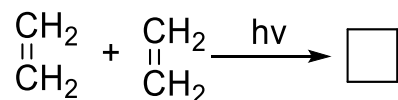
Figure 4.5. Formation of cyclobutane [2 + 2] by photochemical reaction.

Cyclobutane gives a radical halogenation reaction like straight-chain alkanes. It is opened to the public as a result of the impact of hydrogen on cyclobutane in palladium catalysis. Cyclobutane is resistant to HI and KMnO4 in the cold, and it's not a fragmentation reaction.

21

4.3. Spectroscopic Properties of Cyclobutane

In 1,3-substituted cyclobutane derivatives -the dihedral angle in the case of the cis-trans state is smaller. While the dihedral angle is 30º in the Cis, this angle is 140º in the case of -trans. If the dihedral angle is small in the -cis position, the atoms will generate a strong repulsion force between the electron clouds, and these will cause the protons to appear in the higher area or lower ppm values in the 1H-NMR spectrum. Cyclobutane ^{1}H-NMR peaks are in the range of 2-3 ppm, depending on the change of groups and structure. In the FT-IR spectrum, the peaks of these protons appear at 2980-2900 cm^{-1}as C-H strain vibrations. At 1325 cm^{-1}, the C-H bending peak appears [77].

4.4. The Importance of Cyclobutane Derivatives in the Literature

The first example that can be given to cyclobutane derivatives is cyclobutane carboxylic acid. In 1887, William Perkin succeeded in obtaining cyclobutane carboxylic acid as shown below as a result of a series of reactions. Figure 4.6.
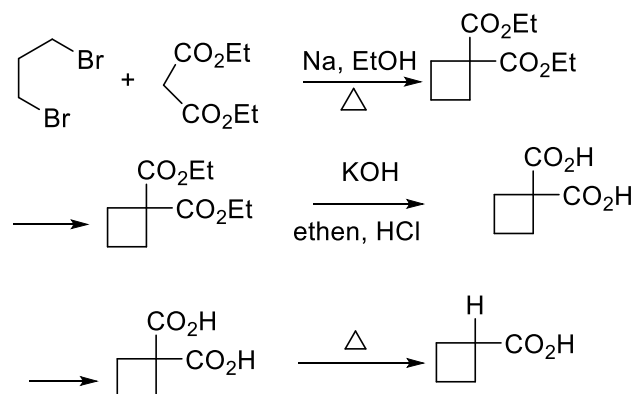
Figure 4.6. Synthesis of cyclobutane carboxylic acid from malon ester and 1,5-dibromopropane.

This reaction is a two-step reaction. It is an intramolecular reaction in the second stage. Malonic acid ester turns into malonic acid when hydrolyzed. In general, dicarboxylic acids are not stable at high temperatures. They lose 1 mol of CO_2 at 150-200 ºC and turn into monocarboxylic acid[78].

Akhmedov (1991) et al. Unsaturated derivatives of epichlorohydrin with aromatic hydrocarbons along with Lewis acids for the synthesized chlorine hydrinos containing 1,1,3-tri-substituted cyclobutane ring with high efficiency, see Figure 4.7 [79].
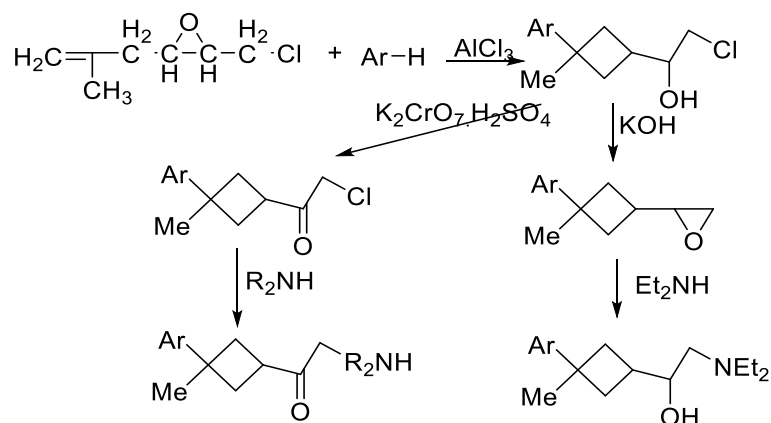
Figure 4.7. 1,1,3-tri-substituted cyclobutane ring

Akhmedov (1991) et al. Benzene allyl-substituted 2- (2-propenyl) -3chloromethyloxirane and the formation of the following products from reactions next to AlCl3 were determined. (Ar (Benzene, toluene) see Figure 4.8.
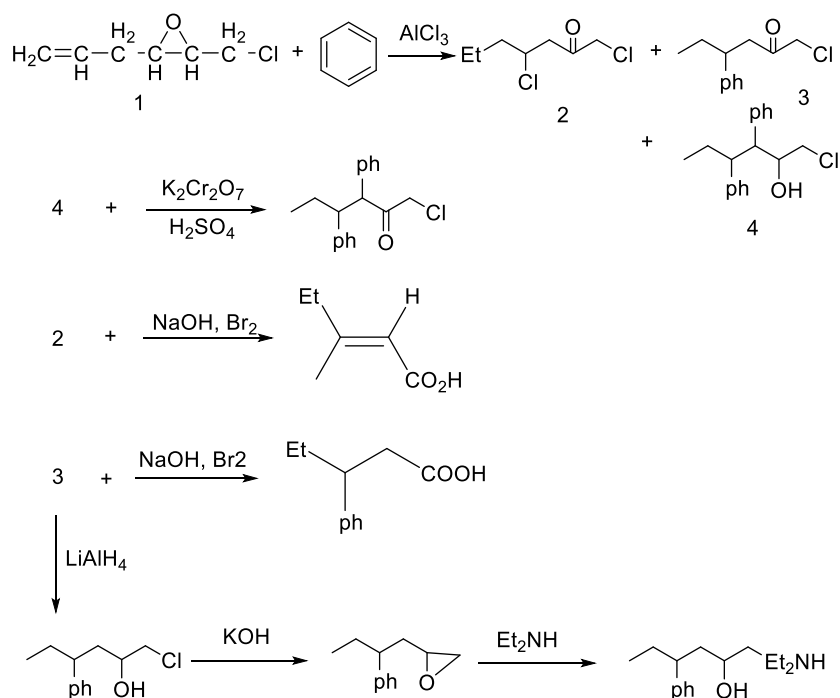
Figure 4.8. Synthesis of oxirane compounds

There are two important features in the synthesis of cyclobutane derivatives in the literature. The first is the use of malon esters as the starting material in general, and the second is the synthesis of cyclobutane carboxylic acid derivatives as the cyclobutane derivative.

5. COUMARIN

Coumarin and derivatives of coumarin are natural products that are found from different parts including fruit, leaves, seeds and roots [80-82]. Coumarins are benzopyrone compounds that naturally occur [83]. Coumarin has antibacterial, antioxidant, anti-inflammatory, and anti-cancer because it had makes a bond such as a hydrogen, hydrophobic, coordination, and van der Waals bonds with proteins and enzymes [84, 85]. Coumarins also play an essential part in the food, and industries (soap and perfume) [86, 87]. Furthermore, coumarin is used in electronic requests such as Optical improvement, dye and fluorophores. Coumarin was synthesized by different methods like Pechmann reaction [88] and Perkin reaction [89] and Knoevenagel reaction [90]. Pechmann reaction is synthesis coumarins from phenol and ß-ketoester in a 4-substituted group.

5.1. Synthesis coumarin derivatives

6-ethoxy-4-methylcoumarin (Figure 5.1) was synthesized from 4-ethoxyphenol and ethyl acetoacetate in present sulfuric acid [80].
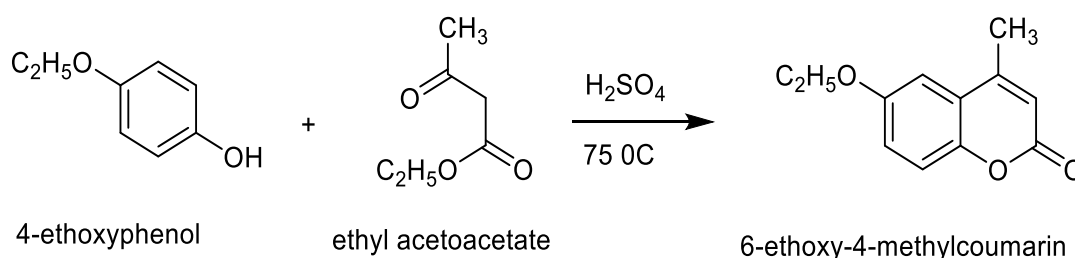
Figure 5.1. Synthesized 6-ethoxy-4-methylcoumarin

Synthesis 4-(Chloromethyl)-7-methylcoumarin (Figure 5.2) from 3-methylphenol and ethyl 4-chloro-3-oxobutanoate in present sulfuric acid as a catalyst [91].
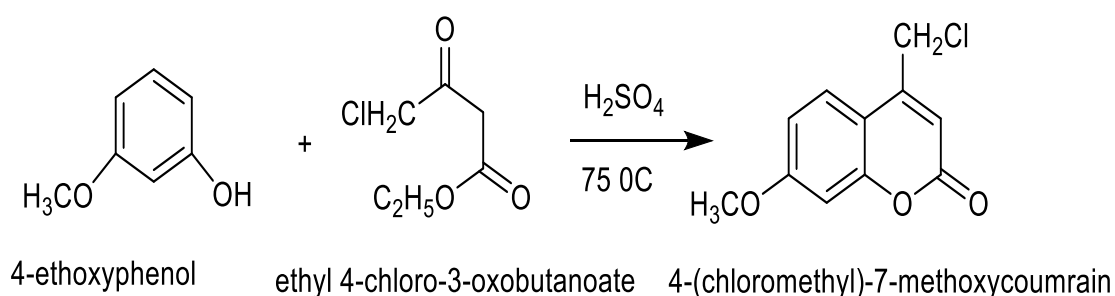
Figure 5.2. Synthesized 4-(Chloromethyl)-7-methylcoumarin

Synthesized 8-t-buthyl-4-methyl-2H-chromen-2-one (Figure 5.3) from 2-(tert-butyl) phenol with ethyl acetoacetate [83].
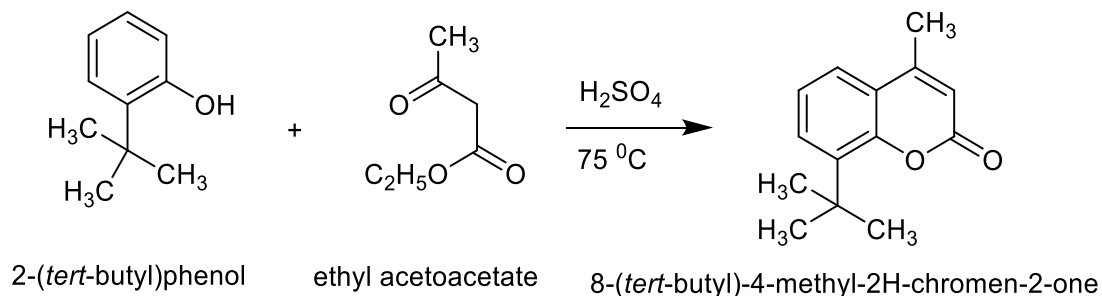
Figure 5.3. Synthesized 8-t-buthyl-4-methyl-2H-chromen-2-one

Synthesized 2-oxo-2H-chromen-4-yl 4-nitrobenzoate (Figure 5.4) from 4-hydroxy-2H-chromen-2-one with 4-nitrobenzoyl chloride [92].
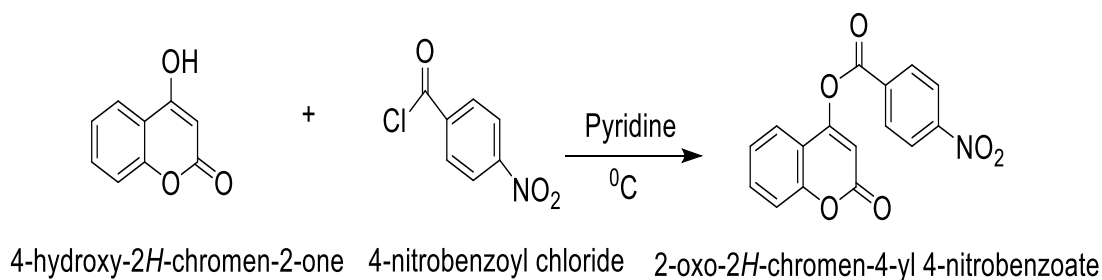
Figure 5.4. Synthesized 2-oxo-2H-chromen-4-yl 4-nitrobenzoate

Shuguang et al was synthesized novel coumarin derivatives see Figure 5.5:
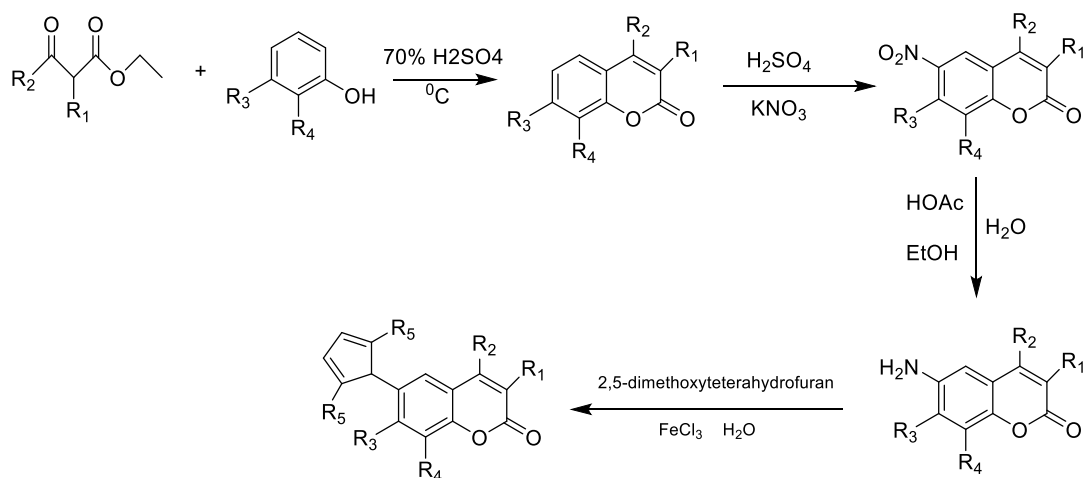
Figure 5.5. Novel coumarin derivatives

Synthesis phenyl coumarin from 2-hydroxybenzaldehyde and 2-phenylacetyl chloride in present tetra butyl ammonium hydrogen sulfate and potassium carbonite see Figure 5.6 [93].
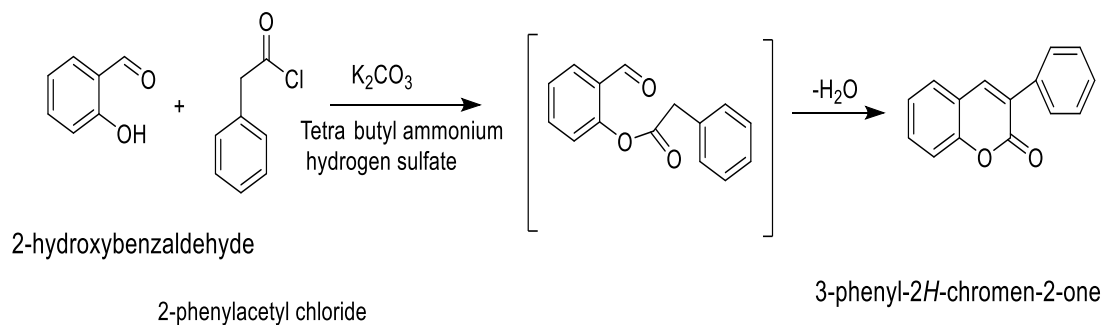
Figure 5.6. Synthesis phenyl coumarin

6. MATERIAL AND METHODS

6.1. Equipment and Tools Were Used

- As glass material; a round bottom flask of various sizes, dropping funnels, separating funnels, funnels, beakers, glass road, burettes, capillary tubes, and test tubes.
- Electronic Balance for weighing: Chyo J.L.180.
- Perkin Elmer Spectrum One FTIR spectrophotometer for IR spectra.
- Bruker 400 MHz NMR spectrometer for receiving ^{1}H-NMR spectra.
- Bruker 400 MHz NMR spectrometer for receiving ^{13}C-NMR spectra.
- Memmert M50 model oven for the drying process.
- Melting point determination device (Gallenkamp).
- Magnetic and mechanical mixers.
- Thermometers of 100 and 360 °C.
- Automatic pipettes.
- Desiccator.

6.2. Chemical Substances Were Used

6.2.1. Reagents

Thiophene-2-carbohydrazide, 4-(chloromethyl)-7-methyl-2H-chromen-2-one, 4-(chloromethyl)-6,8-dimethyl-2H-chromen-2-one, 4-(chloromethyl)-6,7-dimethyl-2H-chromen-2-one, potassium carbonate, 4-(chloromethyl)-7,8-dimethyl-2H-chromen-2-one, potassium hydroxide, ethyl isothiocyanate, phenyl isothiocyanate, Sodium dichromate, calcium chloride over anhydrous, 2-chloro-1-(3-methyl-3-(2,4,6-trimethyl cyclohexyl)cyclobutyl) ethan-1-ol.

6.2.2. Solvents

Ethyl alcohol, diethyl ether, acetone, methanol, hydrochloric acid, Sulfuric acid, and DMSO-d6 for NMR spectra.

6.3. Experimental Part

6.3.1. 4-phenyl-5-(thiophen-2-yl)-2,4-dihydro-3H-1,2,4-triazole-3-thione (1)

To prepared the reaction needed reflux, a round bottle flask (two nicks), magnetic bar, and thermometer. The reaction flask was filled with 10 mmol thiophene-2-carbohydrazide and 50 ml absolute ethyl alcohol. 10 mmol phenyl isothiocyanate was added once the reflux process began. Solid thiosemicarbazide began to form in the reaction flask after about 4 hours. Dissolution began after 15 mmol KOH was added to the material. The reaction was stopped after 6 hours, and the precipitate was generated in ice water with HCl at a pH of 3-4. The solid precipitate was filtered, rinsed with ice water, then crystallized in a combination of alcohol and water. FT-IR, ^{1}H-NMR, and ^{13}C-NMR techniques were used to illuminate the structure of the product. Figure 6.1 depicts the general reaction of the product.

Yield 70%. Melting point: 163-164 °C; FT-IR (KBr, cm^{-1}): 3039-3105 (vAr-H), 1611, 1478, 1415(vC-N, vC=N, vC-N-C in triazole) respectively, 1573 (vC = N), 1259 (vC = S), 681 (vC-S-C); ^{1}H NMR (400 MHz, DMSO-d6, ppm): 6.64-7.72 (8H, Ar-H), 13.98 (s, 1H, SH); ^{13}C NMR (100 MHz, DMSO-d6, ppm): 117.34, 126.82, 128.70, 129.35, 130.22, 132.03, 146.64, 168.18. Molecular Weight (C$_{12}$H$_9$N$_3$S$_2$) 259g/mol.
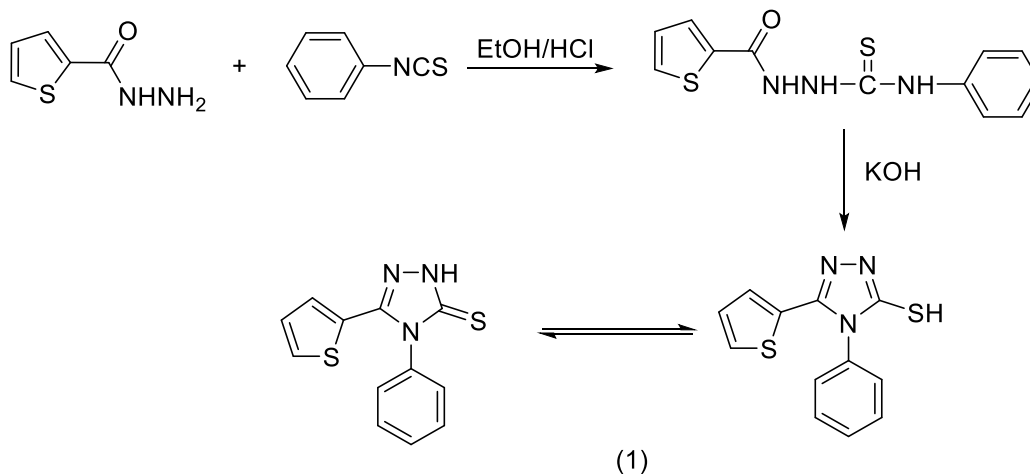
Figure 6.1. Reaction for synthesis 4-phenyl-5-(thiophen-2-yl)-4H-1,2,4-triazole-3-thiol (1)

6.3.2. 4-ethyl-5- (thiophen-2-yl) -2,4-dihydro-3H-1,2,4-triazole-3-thione (2)

To prepared the reaction needed reflux, a round bottle flask (two nicks), magnetic bar, and thermometer. The reaction flask was filled with 10 mmol thiophene-2-carbohydrazide and 50 ml absolute ethyl alcohol. 10 mmol ethyl isothiocyanate was added once the reflux process began. Solid thiosemicarbazide began to form in the reaction flask after about 4 hours. Dissolution began

after 15 mmol KOH was added to the material. The reaction was stopped after 6 hours, and the precipitate was generated in ice water with HCl at a pH of 3-4. The solid precipitate was filtered, rinsed with ice water, then crystallized in a combination of alcohol and water. FT-IR, ^{1}H-NMR, and ^{13}C-NMR techniques were used to illuminate the structure of the product. Figure 6.2 depicts the general reaction of the product.

Yield 84%. Melting point: 187-188 °C; FT-IR (KBr, cm^{-1}, υ): 3072-3107(υ Thiophen group) 2870-2960 (υC-H), 1570 (υC=N), 1260 (υC=S), 715 (υC-S-C); ^{1}H NMR (400 MHz, DMSO-d$_6$, δ, ppm): 1.23 t (3H, N-CH$_2$-CH$_3$), 4.22 q (2H, -N-CH$_2$-CH$_3$), 7.27 dd (1H, Thio-H), 7.68 d (1H, Thio-H) 7.86 d (1H, Thio-H), 13.98 s (1H, SH); ^{13}C-NMR (100 MHz, DMSO-d$_6$, δ, ppm): 13.7, 39.7, 126.8, 128.9, 129.3, 130.3, 146.3, 168.5. Molecular Weight (C$_8$H$_9$N$_3$S$_2$): 211g/mol.

(2)
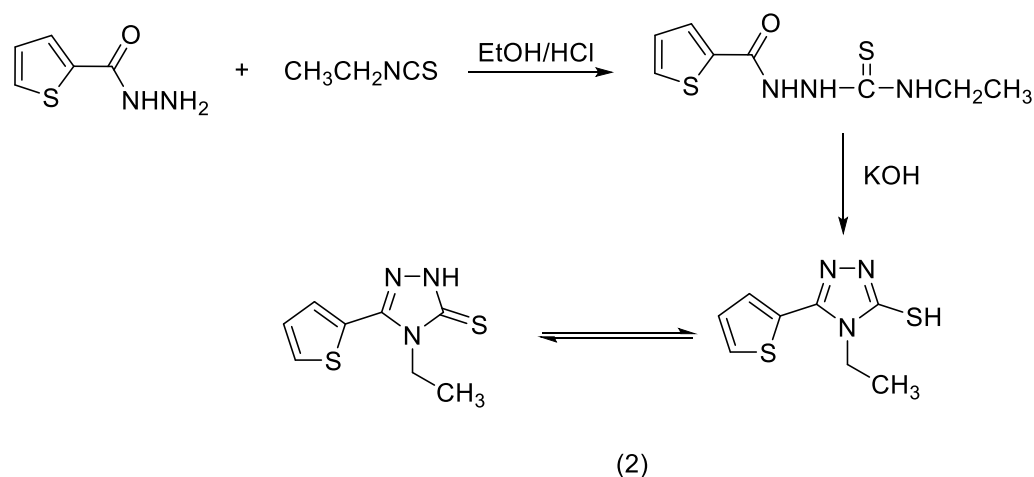
Figure 6.2. Reaction for synthesis 4-ethyl-5-(thiophen-2-yl)-4H-1,2,4-triazole-3-thiol (2)

6.3.3. 2-chloro-1- (3-methyl-3-mesityl-cyclobutyl) –ethanone (5)

The synthesis of 2-(chloromethyl)-3-(2-methylallyl)oxirane (3) that we used in our study was prepared as follows by the method of the literature [79].

By dissolving 300 ml of acrolein in 300 ml of CC14, a 4-neck 2-liter reaction flask was attached to the mechanical stirrer. On the other hand, the reaction temperature is kept constant in a liquid nitrogen environment at 20-22 ^{0}C. Also, 300 g of KMnO4 was added periodically to the 3-spouted reaction flask and chlorine gas was obtained with HCl dropwise. Chlorine gas was dried in the H$_2$SO$_4$ trap and chlorine gas was introduced into the reaction medium for 7-8 hours. Chlorine gas was continued to be given until the alcohol turned green. It is stirred overnight at room temperature. CCl$_4$ was removed in the rotary evaporator and distilled at 20 mm Hg and 55-60 °C. The distillery trap was recognized with 40-50% base solution, see Figure 6.3.

Figure 6.3. Reaction mechanism for synthesized 2,3-dichloropropanal

The glass trap was cooled to -60 °C in a liquid nitrogen environment, and by adding 50 ml of hexane, 231g of isobutane gas was collected from the tube by liquefying the isobutene gas into the glass trap. Prepare 489 g of dichloraldehyde, 22 ml of SnCl4. A 4-orifice reaction flask fitted with a previously driven CaC1$_2$ tube, a dropping funnel, and a thermometer was attached to the mechanical stirrer. Prepared aldehyde and isobutylene were put into the reaction flask. SnC1$_4$ was added drop by drop with a dropping funnel at -50 to -60 ^{0}C. Another 50-60 ml of hexane was added and it was stirred for another 4 hours at -15 to -20 ^{0}C under the mechanical stirrer for 2 hours. Then it was cooled to -50 and hydrolyzed by adding water dropwise. The filtrate was taken into the separation funnel and extracted with water and ether. With MgSO$_4$ it was dried and the ether-hexane solvent was evaporated on the rotary evaporator overnight, and 740 g of hydrochloride was obtained, see Figure 6.4.

Figure 6.4. Reaction mechanism for synthesized 1,2-dichloro-5-methylhex-5-en-3-ol

A dropping funnel, thermometer and reflux flask were attached to the 4-mouthed reaction flask and 270 g of KOH and 300 ml of water solution were put into the reaction flask and under mechanical stirrer, 300 g of chlorhydrin at 20-25 ^{0}C was added dropwise and mixed for 7-8 hours at 30-40 ^{0}C. When the color of the reaction mixture was red, the reaction was extracted and neutralized by washing with water and ether. It was dried with MgSO$_4$ and the solvent was removed

on the rotary evaporator. 183 g of epoxide was removed by vacuum distillation at 20 mm Hg and 83-90 ^{0}C. Yield 76%, look Figure 6.5.
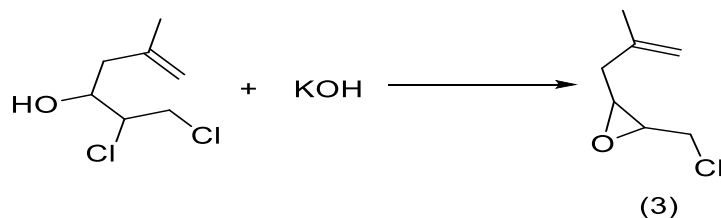
Figure 6.5. Synthesis of 2-(chloromethyl)-3-(2-methylallyl)oxirane

A dropping funnel, thermometer and calcium chloride tube were attached to the 4-mouthed reaction flask and placed in a mechanical mixer. 1500 ml of mesitylene, 167 g of anhydrous AlCl$_3$ were added and 183 g of epoxide was given dropwise at (11-12) ^{0}C. It was stirred for 2 hours and the mixture was decomposed with 15% HCl. It was neutralized with 5% NaOH. Ether-Water extraction was done. It was dried with MgSO$_4$ and the solvent was removed on the rotary evaporator. Distillation in vacuum obtained 247 g of product at 2 mm Hg, 185-187 ^{0}C. Efficiency 71%, see Figure 6.6.
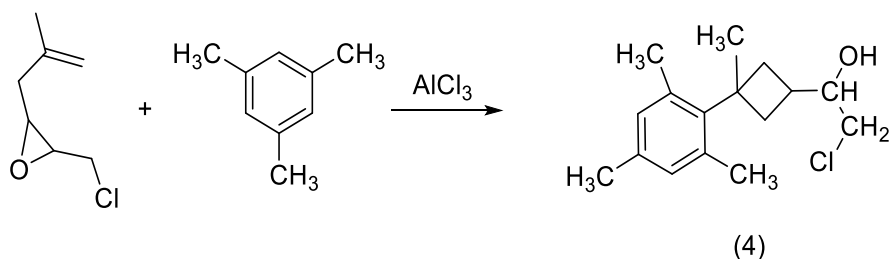
Figure 6.6. Synthesis of 2-chloro-1-(3-mesityl-3-methylcyclobutyl)ethan-1-ol

Four-neck conical flask 1000ml fitted with a thermometer, funnel, stirrer and condenser, added Sodium dichromate (0.29 mol), 2-chloro-1-(3-methyl-3-(2,4,6 trimethyl cyclohexyl)cyclobutyl) ethan-1-ol (0.52 mol) which is prepared according to the literature [79] then added water (50 ml). from the neck of the funnel added H$_2$SO$_4$ (75 ml) (68% v/v) during 7-8h at room temperature. At the same temperature, the reaction was agitated for 18 hours. The solid product was formed and filtered, to remove all diethyl ether used CaCl$_2$ over anhydrous, then recrystallized with ethyl alcohol. FT-IR, ^{1}H-NMR, and ^{13}C-NMR techniques were used to illuminate the final product. Figure 6.7 depicts the general reaction of the product.

Yielded, 55%; melting point: 97-98 ^{0}C; FT-IR (KBr, cm^{-1}, υ): 3156 (υAr-H), 1745 (υC=O), 1650 and 1612 (υC=C in ring),; ^{1}H-NMR (400 MHz, DMSO-d$_6$, δ, ppm): 1.50 (s,3H, -CH$_3$-(cyclobutane), 2.41 (s, 9H, -CH$_3$ (mesitylene), 2.36-2.52 (m, 4H, -CH$_2$)- (cyclobutane), 3.48 (p, 1H, -CH- (cyclobutane), 4.55 (s, 2H, CH$_2$-Cl), 6.75(s, 2H, Ar-H); ^{13}C-NMR (100 MHz, DMSO-d$_6$, δ, ppm): (5 peaks for CH$_3$ and CH$_2$ s), (20.45, 20.75, 25.24, 37.68, 130.29); (7 pieces of CH and aprotic carbons), 39.77, 40.21, 48.42, 130.29, 134.06, 143.94, 203.90. Molecular Weight (C$_{16}$H$_{21}$OCl): 246.5g/mol.
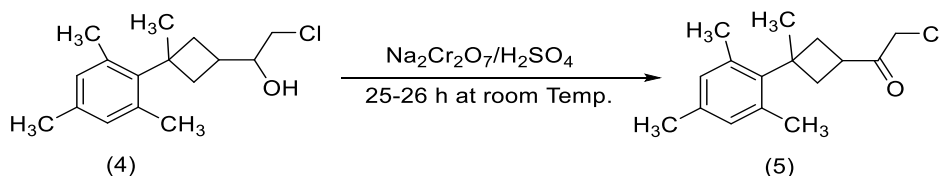
Figure 6.7. Reaction for synthesis 2-chloro-1-(3-methyl-3-mesityl-cyclobutyl)-ethanone (5)

6.3.4. 1-(3-methyl-3-mesityl) -cyclobutyl-2 –[[5-(thiophen-2-yl)-4-phenyl-4H-1,2,4-triazol-3- yl] sulfanyl]-ethanone (6)

At room conditions, 2 mmol (0.276 g) K$_2$CO$_3$ dissolved in 30 ml dry acetone. To this solution, 2 mmol (0.530 g) of 2-chloro-1- (3-methyl-3-mesityl cyclobutyl) ethanone added to the solution at room conditions. Then, 2 mmol (0.423 g) 4-phenyl-5-(thiophen-2-yl)-2,4-dihydro-3H-1,2,4-triazole-3-thione dissolved in 10 ml of dry acetone was added dropwise to this solution, 6 hours stirred at room conditions with a magnetic stirrer. After removing the excess solvent from the environment with the evaporator under low pressure, the solid formed was washed with ice water and filtered and dried. The obtained substance was purified by crystallization in ethyl alcohol. FT-IR, ^{1}H-NMR, and ^{13}C-NMR techniques were used to illuminate the structure of the product. Figure 6.8 depicts the general reaction of the product.

Yield is 55%; melting point: 102-104 ^{0}C; FT-IR (KBr, cm^{-1}, υ): 2955-3059 (υAr-H), 2866-2910 (υC-H), 1697 (υC=O), 1498 (υC=N), 1131 (υN-N), 1045 (υC-S), 774 (C-S-C); ^{1}H NMR (400 MHz, DMSO-d6, δ, ppm): 1.50 (s, 3H, -CH$_3$ (cyclobutane), 2.14 (s, 9H, -CH3 (mesitylene), 2.47-2.50 (m, 4H, -CH$_2$- (cyclobutane), 3.56 (p, 1H, -CH- (cyclobutane), 4.23 (s, 2H, S-CH$_2$-), 6.69-6.70 (m, 3H, Ar-H) , 6.99 (m, 1H, Ar-H), 7.50-7.51 (m, 2H, Ar-H), 7.64-7.68 (m, 4H, Ar-H) 13C NMR (100 MHz, DMSO-d6, δ, ppm): 20.5, 21.4, 25.2, 39.0, 40.9, 127.5, 128.2, 128.5, 129.3, 130.5, 130.7, 131.3, 133.7, 134.9, 143.7, 150.4, 151.8, 205.3. Molecular Weight (C$_{28}$H$_{29}$N$_3$OS$_2$): 487.6g/mol.
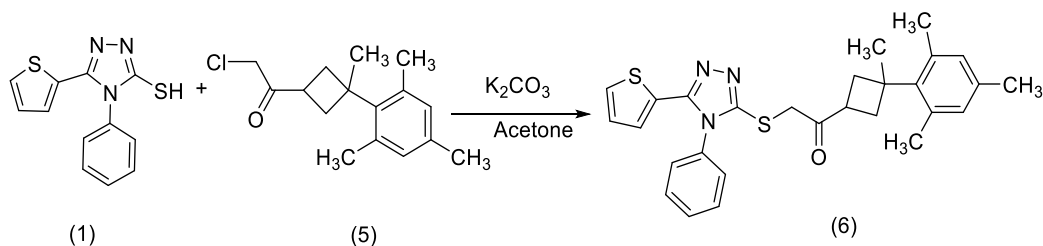
Figure 6.8. Reaction of synthesis 1- (3-methyl-3-mesityl) -cyclobutyl-2–[[5- (thiophen-2-yl)-4-phenyl-4*H*-1,2,4-triazol-3-yl] sulfanyl]-ethanone (6)

6.3.5. 4-((((4-ethyl-5-(thiophen-2-yl)-4H-1,2,4-triazol-3-yl)thio)methyl)-7-methyl-2H-chromen-2-one (7)

In 30 ml of dry acetone, the potassium carbonate (K_2CO_3) (0.02 mol) was dissolved, added 4-(chloromethyl)-7-methyl-2H-chromen-2-one (0.02 mol). At room temperature, 4-Ethyl-5-(thiophene-2-yl)-4H-1,2,4-triazole-3-thiol (0.02 mol) dropwise was added to this solution for 6 hours. The solid product was filtrated and dried with recrystallized by ethyl alcohol. FT-IR, [^1]H-NMR, and [^13]C-NMR techniques were used to illuminate the structure of the product. Figure 6.9 depicts the reaction of the product.

Yield is 65%; Melting point: 145-147 ^{0}C; FT-IR (KBr, cm^{-1}, υ): 2937–3081 (υAr-H), 1717 (υC=O), 1439 (υ C=N), 938 and 1266 (υO-C), 560-740 (υS-C); [^1]H-NMR (400 MHz, DMSO-d$_6$, δ, ppm): 1.17 (t, 3H, N-CH$_2$-CH$_3$), 3.39 (s, 3H, Ar-CH$_3$,) 4.09 (q, 2H, N-CH$_2$-CH$_3$), 4.62 (s, 2H, S-CH$_2$), 6.32 (s,1H, H-C-C=O), 7.27 (m, 3H, Ar-H + thiophene-H), 7.57 (s, 1H, Ar-H), 7.85 (m, 2H, Ar-H + thiophene-H) ; [^13]C-NMR (100 MHz, DMSO-d$_6$, δ, ppm): 15.3, 21.2, 33.8, 40.2, 114.4, 115.6, 117.2, 125.4, 125.9, 128.0, 128.7, 129.6, 143.5, 149.4, 150.3, 151.4, 153.9, 160.1. Molecular Weight (C$_{19}$H$_{17}$N$_3$O$_2$S$_2$): 383g/mol.
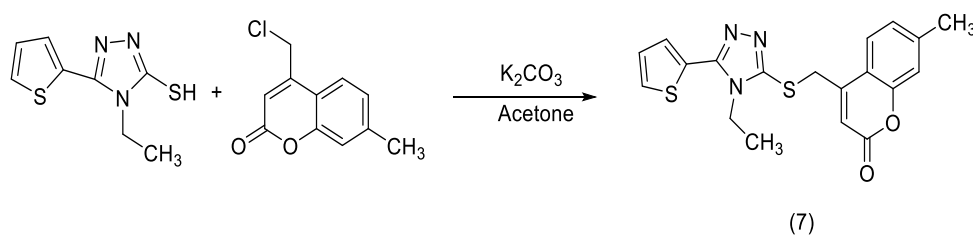
Figure 6.9. Reaction of synthesis 4-((((4-ethyl-5-(thiophen-2-yl)-4H-1,2,4-triazol-3-yl)thio)methyl)-7-methyl-2H-chromen-2-one (7)

6.3.6. 4-((((4-ethyl-5-(thiophen-2-yl)-4H-1,2,4-triazol-3-yl)thio)methyl)-6,8-dimethyl-2H-chromen-2-one (8)

In 30 ml of dry acetone, the potassium carbonate (K2CO3) (0.02 mol) was dissolved, added 4-(chloromethyl)-6,8-dimethyl-2H-chromen-2-one (0.02 mol). At room temperature, 4-Ethyl-5-

(thiophene-2-yl)-4H-1,2,4-triazole-3-thiol (0.02 mol) was added dropwise to this solution for 6 hours [94]. The solid product was filtrated and dried with recrystallized by ethyl alcohol. FT-IR, ^{1}H-NMR, and ^{13}C-NMR techniques were used to illuminate the structure of the product. Figure 6.10 depicts the general reaction of the product.

Yield is 70%; Melting point 188-190 ^{0}C; FT-IR (KBr, cm^{-1}, υ): 2923–3081 (υAr-H), 1722 (υC=O), 1630-1384 (υC=C), 1346-1477 (υC-O), 751-831 (υC-S); ^{1}H-NMR (400 MHz, DMSO-d6, δ, ppm): 1.19 (t, 3H, N-CH2- CH$_3$), 2.51 (s, 3H, Ar-CH$_3$), 3.18 (s, 3H, Ar-CH$_3$), 4.08 (q, 2H, N-CH$_2$-CH$_3$), 4.62 (s, 2H, S-CH$_2$), 6.42 (s,1H, H-C-C=O), 7.26 (s, 1H, Ar-H), 7.35 (dd, 1H, thiophene H), 7.52 (d, 1H, thiophene-H), 7.56 (s, 1H, Ar-H), 7.80 (d, 1H, thiophene-H) ; ^{13}C-NMR (100 MHz, DMSO-d6, δ, ppm):15.26, 15.64, 20.87, 34.01, 40.57, 115.41, 117.57, 123.15, 125.79, 127.06, 127.01, 128.79, 129.63, 133.50, 134.82,   149.49, 150.31, 150.33, 151.70, 160.07. Molecular Weight (C$_{20}$H$_{19}$N$_3$O$_2$S$_2$): 397g/mol.

(8)
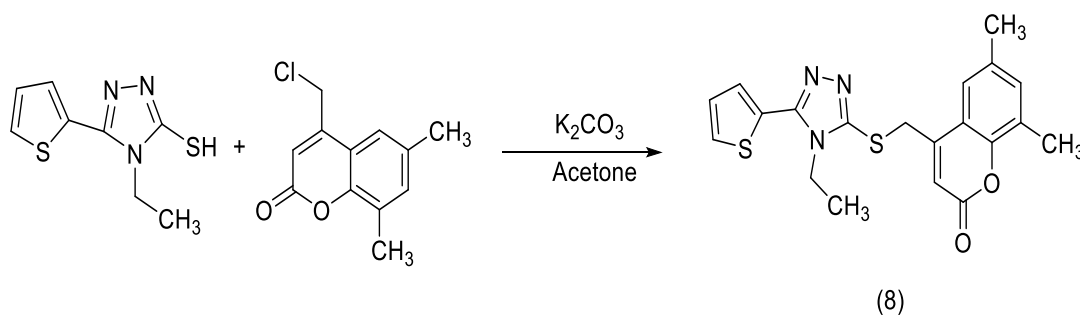
Figure 6.10. Reaction of synthesis 4-(((4-ethyl-5-(thiophen-2-yl)-4H-1,2,4-triazol-3-yl)thio)methyl)-6,8-dimethyl-2H-chromen-2-one (8)

6.3.7. 4-(((4-ethyl-5-(thiophen-2-yl)-4H-1,2,4-triazol-3-yl)thio)methyl)-6,7-dimethyl-2H-chromen-2-one (9)

In 30 ml of dry acetone, the potassium carbonate (K2CO3) (0.02 mol) was dissolved, added 4-(chloromethyl)-6,7-dimethyl-2H-chromen-2-one (0.02 mol). At room temperature, 4-Ethyl-5-(thiophene-2-yl)-4H-1,2,4-triazole-3-thiol (0.02 mol) was added dropwise to this solution for 6 hours. The solid product was filtrated and dried with recrystallized by ethyl alcohol. FT-IR, 1H-NMR, and 13C-NMR techniques were used to illuminate the structure of the product. Figure 6.11 depicts the general reaction of the product.

Yield is 75%; Melting point 165-167 ^{0}C; FT-IR (KBr, cm^{-1}, υ): 2922–3108 (υAr-H), 1722 (υC=O), 1621-1382 (υC=C), 1346-1477 (υC-O), 798 (υC-S); ^{1}H-NMR (400 MHz, DMSO-d6, δ, ppm): 1.18 (t, 3H, N-CH2- CH$_3$), 2.31 (s, 3H, Ar-CH$_3$), 3.12 (s, 3H, Ar-CH$_3$), 4.09 (q, 2H, N-CH$_2$-CH$_3$), 4.62 (s, 2H, S-CH$_2$), 6.36 (s,1H, H-C-C=O), 7.22 (s, 1H, Ar-H), 7.25 (t, 1H, thiophene H), 7.55 (d, 1H, thiophene-H), 7.63 (s, 1H, Ar-H), 7.81 (d, 1H, thiophene-H) ; ^{13}C-NMR (100 MHz,

DMSO-d6, δ, ppm):15.29, 19.31, 20.07, 30.85, 40.19, 114.52, 115.69, 117.60, 125.58, 128.05, 128.01, 128.78, 129.61, 133.37, 142.57, 149.51, 150.32, 151.56, 152.23, 160.28. Molecular Weight ($C_{20}H_{19}N_3O_2S_2$): 397g/mol.
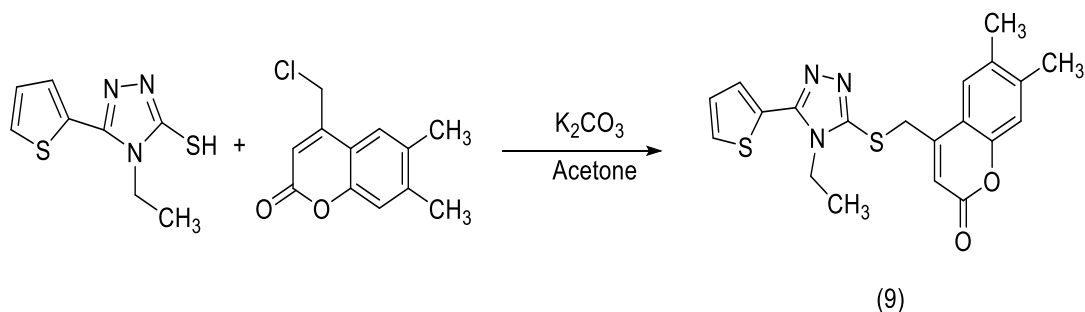
Figure 6.11. Reaction of synthesis 4-(((4-ethyl-5-(thiophen-2-yl)-4H-1,2,4-triazol-3-yl)thio)methyl)-6,7-dimethyl-2H-chromen-2-one (9)

6.3.8. 4-((((4-ethyl-5-(thiophen-2-yl)-4H-1,2,4-triazol-3-yl)thio)methyl)-7,8-dimethyl-2H-chromen-2-one (10)

In 30 ml of dry acetone, the potassium carbonate (K2CO3) (0.02 mol) was dissolved, added 4-(chloromethyl)-7,8-dimethyl-2H-chromen-2-one (0.02 mol). At room temperature, 4-Ethyl-5-(thiophene-2-yl)-4H-1,2,4-triazole-3-thiol (0.02 mol) was added dropwise to this solution for 6 hours. The solid product was filtrated and dried with recrystallized by ethyl alcohol. FT-IR, ^{1}H-NMR, and ^{13}C-NMR techniques were used to illuminate the structure of the product. Figure 6.12 depicts the general reaction of the product.

Yield is 75%; Melting point 175-177 [0]C; FT-IR (KBr, cm[-1], υ): 2920–3074 (υAr-H), 1723(υC=O), 1623-1382 (υC=C), 1346-1474 (υC-O), 753 (υC-S); ^{1}H-NMR (400 MHz, DMSO-d6, δ, ppm): 1.17 (t, 3H, N-CH2- CH3), 2.38 (s, 3H, Ar-CH3), 3.29 (s, 3H, Ar-CH3), 4.08 (q, 2H, N-CH2-CH3), 4.61 (s, 2H, S-CH2), 6.35 (s,1H, H-C-C=O), 7.27 (2H, Ar-H), 7.55 (t, 1H, thiophene H), 7.68 (d, 1H, thiophene-H), 7.81 (d, 1H, thiophene-H) ; ^{13}C-NMR (100 MHz, DMSO-d6, δ, ppm): 11.71, 15.31, 20.37, 33.83, 40.23, 114.29, 115.79, 122.51, 124.46, 126.07, 128.07, 128.80, 129.60, 142.15, 149.43, 150.32, 151.75, 151.93, 160.16, 160.16. Molecular Weight ($C_{20}H_{19}N_3O_2S_2$): 397g/mol.
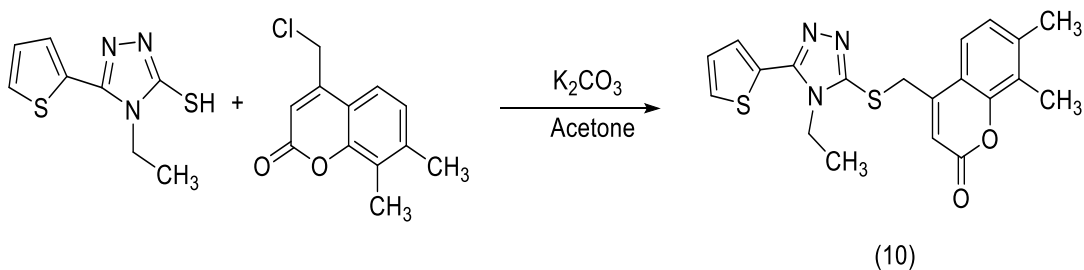
Figure 6.12. Reaction of synthesis 4-(((4-ethyl-5-(thiophen-2-yl)-4H-1,2,4-triazol-3-yl)thio)methyl)-7,8-dimethyl-2H-chromen-2-one (10)

6.4. Computational Study

The Gaussian 09W program's entire quantum chemical calculations at DFT B3LYP levels with a basis set cc-pVDZ were performed on a personal computer [74-76]. B3LYP with a cc-pVDZ [77] basis set is optimized for the molecular structures of the compound in the ground state (in vacuum). From optimization molecular structure founded Vibrational frequencies. On the optimal shape of the molecule, geometric parameters (bond lengths, bond angles, and torsion angles) of the compounds were calculated theoretically.

Because no imaginary frequency modes were obtained in the optimized geometry of the title molecule, a real minimum on the potential surface of energy was discovered. As a result, the measured upscale frequency, reduce mass, constant of power, infrared intensities, Raman operation and depolarization ratio were obtained. To calculate values of the frequency the harmonic was scaled down. The theoretical calculation for ^{1}H NMR and ^{13}C NMR were approached with GIAO computed. The theoretical NMR calculation of the solvent is greatly affected by it. The solvent DMSO has been used in nuclear magnetic resonance calculations as a solvent. The harmonic vibrational frequencies of the optimized structure were examined, and the theoretically obtained frequency values were scaled to 0.9588 for the theoretically derived frequency values.

The B3LYP/cc-pVDZ level was used for the molecular electrostatic potential (MEP) with the Millikan charge distribution [78-80] calculations for all the compounds. Based on vibrational analyses, using DFT/cc-pVDZ level, the thermodynamic properties of the compounds were determined at 25 ^{0}C temperatures. B3LYP is also suited for workstation capability in the Gaussian09W program at the cc-pVDZ basis set.

The Identifiers of electronic structure from all geometry structures the energy of the highest occupied molecular orbital (E$_{HOMO}$), the energy of the lowest unoccupied molecular orbital (E$_{LUMO}$), energy bandgap (ΔE = E$_{LUMO}$ - E$_{HOMO}$), and the dipole moment (μ), hardness (η), softness (σ), electronegativity (χ), electrophilicity (ω) index, nucleophilicity (ε) index, chemical potential (Pi)

and the fraction of transferred electrons (ΔN) related with corrosion inhibition activity were calculated [95-98].

7. RESULTS

7.1. 4-phenyl-5-(thiophen-2-yl)-2,4-dihydro-3H-1,2,4-triazole-3-thione (1)

The molecular was experimentally characterized by FT-IR and NMR spectroscopy. The melting point for compound (1) (Figure 7.1) is equal to 163-164 ^{0}C which was measured by Thomas Hoover melting point. The Yield is 75% and the color is white.

(1)
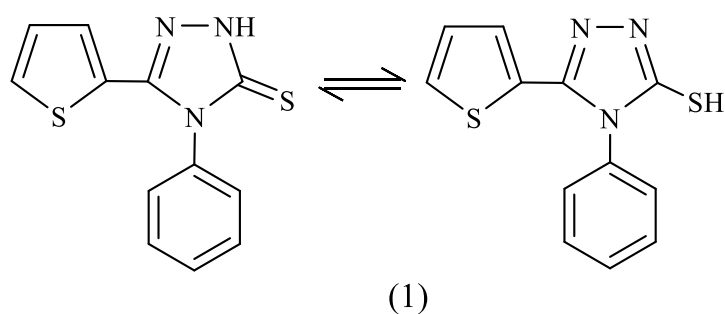
Figure 7.1. 4-phenyl-5-(thiophen-2-yl)-2,4-dihydro-3H-1,2,4-triazole-3-thione

The molecular structure of the compound (1) was determined using the Density Functional Theory (DFT/B3LYP) method in the ground state with the cc-pVDZ basis sets. Figure 7.2 shows molecular structures drawing by ChemBioDraw and GAUSVIEW. The optimized geometrical parameters (bond lengths, bond angles, and torsion angles) calculated using B3LYP/cc-pVDZ techniques are listed in Table 7.1.

A   B
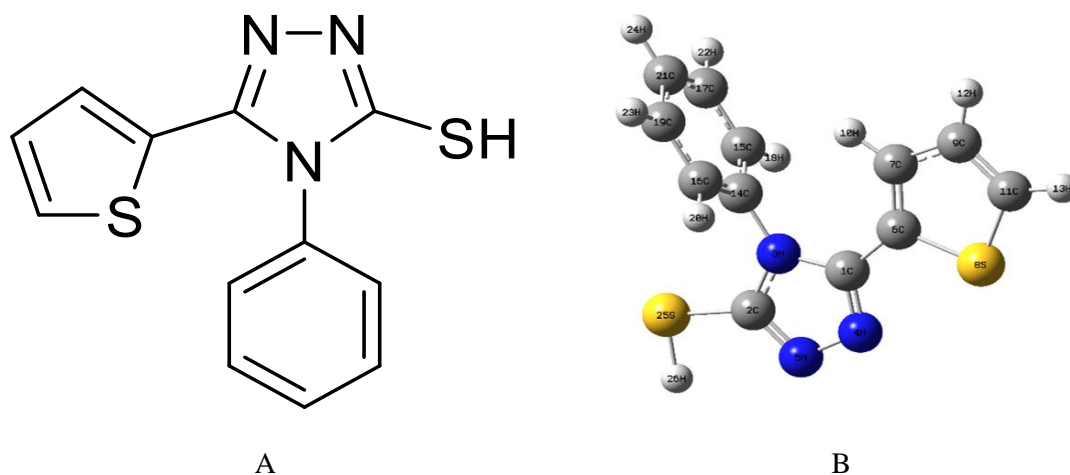
Figure 7.2. Structure of the compound (1) A) Drawing by ChemBioDraw Ultra B) Gaussian Optimized by B3LYP/cc-pVDZ

Table 7.1. In the ground state, geometrical optimization for compound (1)

Symbol	Bond Length	Symbol	Bond angle	Symbol	Dihedral angle
C2-C1	2.178	N3-C2-C1	38.385	N4-C1-N3-C2	0.004
N3-C2	1.379	N4-C1-N3	109.453	N5-C2-C1-N4	0.027
N4-C1	1.319	N5-C2-C1	72.838	C6-C1-N4-N5	-179.982
N5-C2	1.313	C6-C1-N4	123.617	C7-C6-C1-N4	177.369
C6-C1	1.452	C7-C6-C1	131.686	S8-C6-C1-N4	-2.283
C7-C6	1.381	S8-C6-C1	128.470	C9-C7-C6-C1	-179.704
S8-C6	1.756	C9-C7-C6	113.024	C11-C9-C7-C6	0.010
C9-C7	1.425	C11-C9-C7	112.731	C14-N3-C2-C1	-179.389
C11-C9	1.371	C14-N3-C2	126.173	C15-C14-N3-C2	-87.102
C14-N3	1.433	C15-C14-N3	119.627	C16-C14-N3-C2	92.295
C15-C14	1.399	C16-C14-N3	119.661	C17-C15-C14-N3	179.784
C16-C14	1.399	C17-C15-C14	119.466	C19-C16-C14-N3	-179.874
C17-C15	1.397	C19-C16-C14	119.451	C21-C17-C15-C14	-0.039
C19-C16	1.396	C21-C17-C15	120.135	S25-C2-C1-N4	179.903
C21-C17	1.398	S25-C2-C1	160.768		
S25-C2	1.769				

The FT-IR spectra are experimentally and theoretically shown in Figure 7.3 for compound (1). The experimental measurement used KBr pullet formed. Table 7.2 compared Experimentally and theoretically results with types of vibration was calculated B3LYB/cc-pVDZ. The correlation between Experimentally and theoretically results for FT-IR analysis was shown in Figure 7.4.

A   B
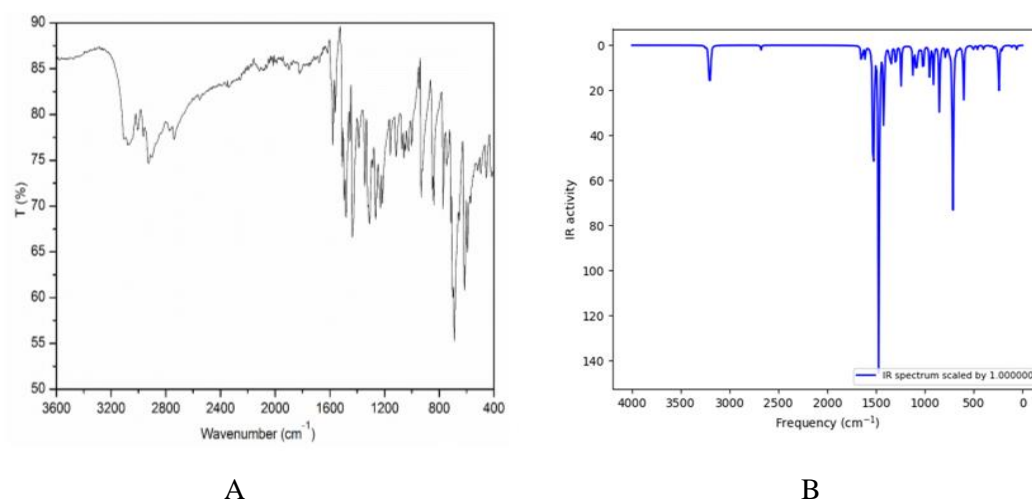
Figure 7.3. IR spectrum for compound (1). (A) Experimental (B) Theoretical results

Table 7.2. Theoretical and experimental vibrational for compound (1)

Assignments With TED	FT-IR (cm⁻¹) With KBr	Unscaled Frequencies B3LYP/cc-pVDZ
Sy, St C11-H13, C9-H12, C7-H10	3253	3250.08
an, St C7-H10, C11-H13	3244	3242.45
Sy, St C9-H12		3212.23
St, Ar-H	3039 - 3105	3212.12
St, Ar-H		3208.72
St, Ar-H		3200.34
St, S25-H16	2676	2677.58
Sy, St, C=C in ring	1673	1650.42
St, C1-N3 in triazole	1611	1611.48
St, C14-N3	1572	1529.95
St, C11=C9	1522	1520.88
St, C=C in ring	1478	1478.77
St, C2=N5		1472.92
St, C7-C9		1467.65
Sy, St, C2=N5-C	1415	1420.29
St, C=N in triazole	1464	1472.71
an, St, C11-H13, C7-H18, C9-H12		1366.20
an, St, C=C in ring		1355.10
an, St, triazole ring		1346.45
R, H in ring		1322.87
St, C2-S25	1259	1298.56
Sy, St, Ar-H		1183.68
St, N-N-H		1120.42
Sy, St, Ar-H		1095.21
Sic, St, C11-H13, C9-H12		1091.38
Sic, St, C11-H13, C7-H18	1076	1078.91
Sic, St, C9-H12, C7-H18		1061.40
T, Ar ring	1017	1020.72
an, St, C=C in ring		1015.75
An , ST, Ar-H		992.39
R, S25-H26		911.58
an, St, N3-C1-N4		719.57
R, St, C11-H13		709.63
St, Thiophene	681	656.61
R, S25-H26		243.00

St: Starching vibration, an: anti, Sy: Symmetrical, R: Rocking, Sic: Scissoring
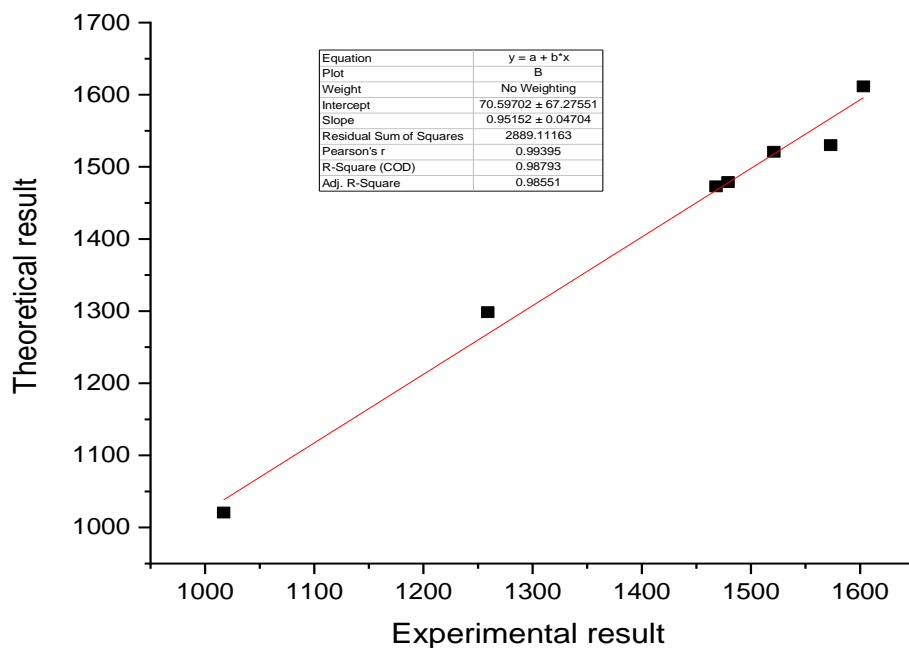
Figure 7.4. Relationship graphics for compound (1), between theoretical and experimental frequencies

The experimental Hydrogen ^{1}H NMR look Figure 7.5 and carbon ^{13}C NMR shown in Figure 7.6 chemical shifts for compound (1) were investigated in Dimethyl sulfoxide (DMSO-d6). Also in DMSO-d6 solvents, the theoretical ^{1}H and ^{13}C chemical shift values were determined using the DFT (B3LYP) method with the cc-pVDZ basis sets, all results were presents in Table 7.3.
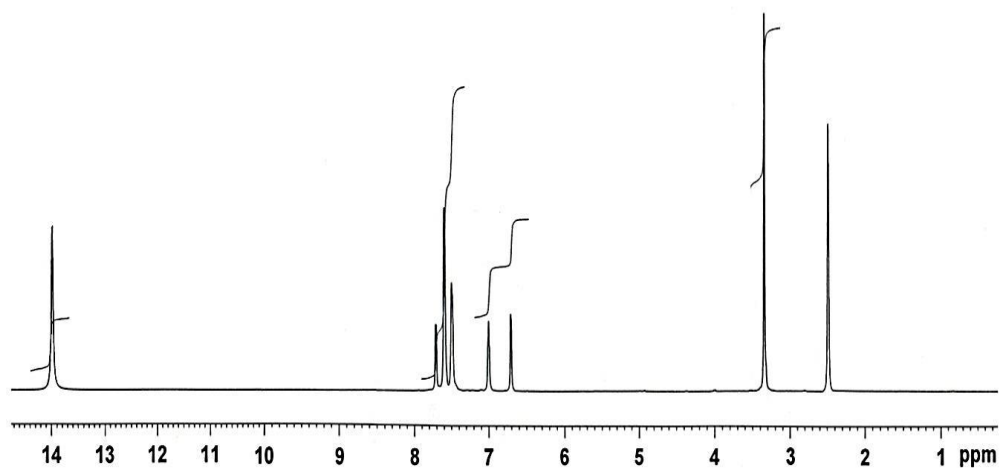
Figure 7.5. Experimental ^{1}H-NMR spectrum for compound (1) in DMSO-d6
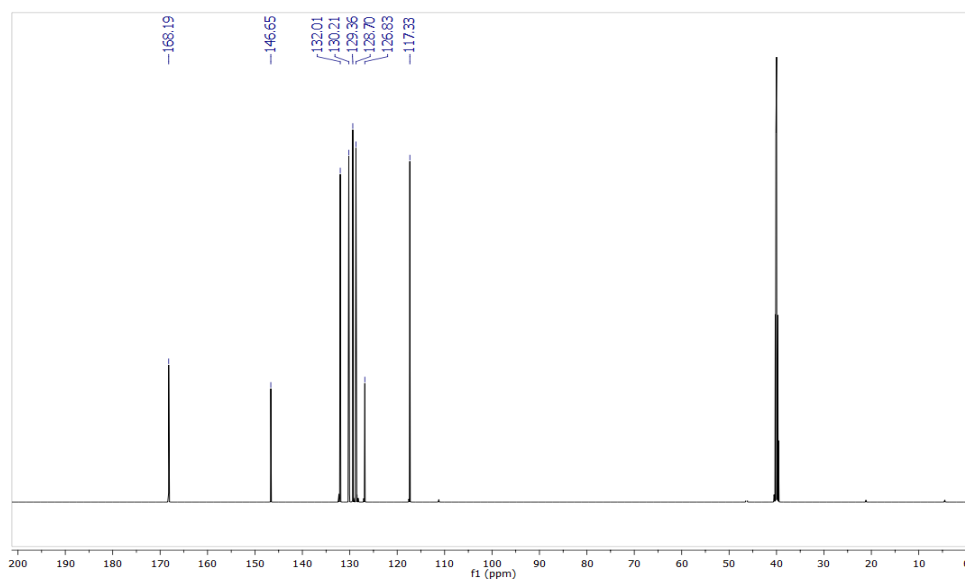
Figure 7.6. The experimental ^{13}C-NMR spectrum for compound (1) in DMSO-d6

Table 7.3. Theoretical and experimental ^{1}H and ^{13}C chemical shift (ppm) for compound (1).

Atom	Experimental in (DMSO-d6)	Theoretical by B3LYP/cc-pVDZ
C7,C9	117.34	130.44, 133.11
C15,C16	126.82	135.81
C17,C19	128.70	137.50
C21,C11	129.35	138.50,139.70
C14	130.22	142.50
C6	132.03	144.80
C1	146.64	158.50
C2	168.18	161.20
8H, Ar-H	6.64-7.72	7.14-8.97
1H, SH	13.98	5.51

B3LYP/cc-pVDZ was used to found Molecular electrostatic potential (MEP) for compound (1) shown in Figure 7.7. The negative region's red color was founded on nitrogens (N4, N5) of triazole and also founded a little on the S-H group, this indicates that the nitrogen (N4, N5) atoms and S-H groups attracted with more electrophiles.
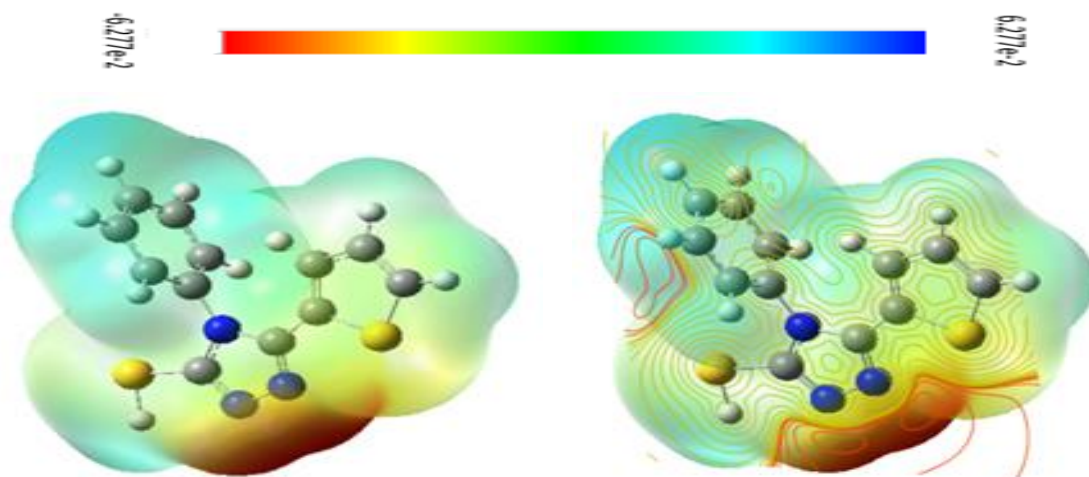
Figure 7.7. Molecular electrostatic potential for compound (1)

Mulliken population analysis for compound (1) shown in Figure 7.8. the more negative charges were distributed on the N3, N4, N5 and C11.
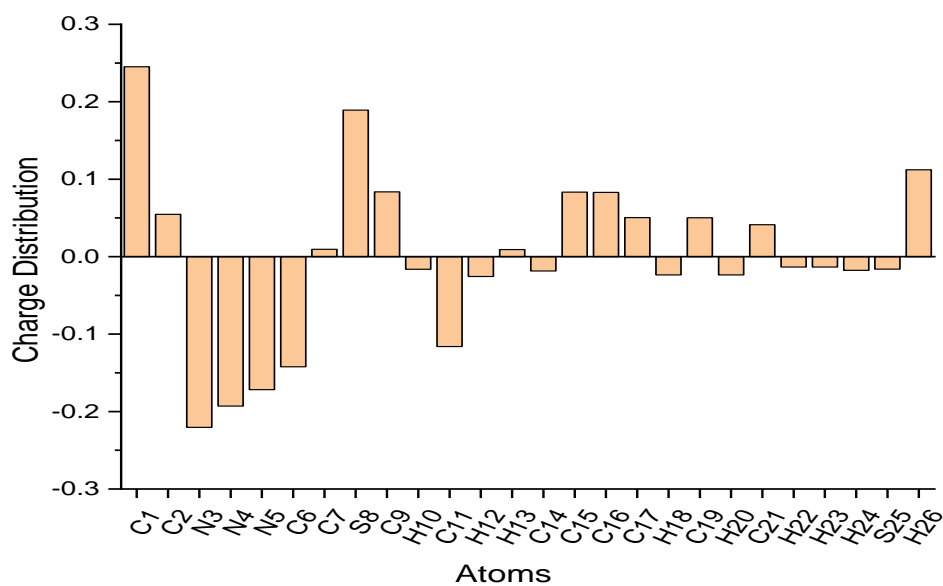
Figure 7.8. Millikan charge distribution on the compound (1)

Different parameters which is related to the inhibitor activity calculated for compound (1) used B3LYP/cc-pVDZ All parameters were shown in Table 7.4 including energy of the highest occupied molecular orbital (E_{HOMO}), energy of the lowest unoccupied molecular orbital (E_{LUMO}), energy bandgap ($\Delta E = E_{LUMO} - E_{HOMO}$), dipole moment ($\mu$), hardness ($\eta$), softness ($\sigma$), electronegativity ($\chi$), electrophilicity index (ω), nucleophilicity (ε) index and The fraction of transferred electrons (ΔN) which is related to transfer electron between inhibitor and metal surface.

Table 7.4. Calculation quantum chemical parameters for compound (1)

Parameters	Equations	Results
Total Energy (a.u)		-1423.372
μ (D)		5.515
E_{LUMO} (eV)		-1.205
E_{HOMO} (eV)		-5.7122
ΔE (eV)		4.506
I	$I = -E_{HOMO}$	5.712
A	$A = -E_{LUMO}$	1.205
χ (eV)	$\chi = (I + A) / 2$	3.458
η (eV)	$\eta = (I - A) / 2$	2.253
σ (eV)	$\sigma = I/\eta$	2.534
Pi (eV)	$Pi = -\chi$	-3.458
ω (eV)	$\omega = Pi^2/2\eta$	2.654
ε (eV)	$\varepsilon = Pi. \eta$	-7.794
ΔN	$\Delta N = (\chi_{metal} - \chi_{inhibitor}) / 2. (\eta_{metal} - \eta_{inhibitor})$	0.785

The Zero-point vibrational energy, Total energy, thermal energy, rotational constants, rotational temperatures and entropy of the molecules (1) were calculated using B3LYP/cc-pVDZ at a pressure of 1.00 atom and 298 K, Table 7.5 shows the results.

Table 7.5. Thermodynamic parameters for compound (1)

Parameters	B3LYP/cc-pVDZ
Zero-point vibrational energy(kcal/mol^{-1})	116.376
Total energy (a.u.)	-1423.372
Rotational constants (GHz)	
	0.54613
	0.32070
	0.21761
Rotational temperatures (K)	
	0.02621
	0.01539
	0.01044
Entropy (Kcal mol^{-1} K^{-1})	
Rotational	0.889
Translational	0.889
Vibrational	123.609
Total	125.386

7.2. 4-Ethyl-5-(thiophene-2-yl)-4H-1,2,4-triazole-3-thiol (2)

The molecular was experimentally characterized by FT-IR and NMR spectroscopy. The melting point for compound (2) (Figure 7.9) is equal to 178-188 0C which was measured by Thomas Hoover melting point. The Yield is 65% and the color is white.

(2)
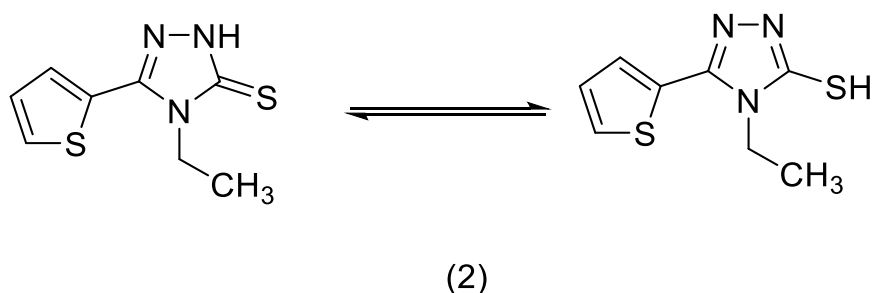
Figure 7.9. 4-Ethyl-5-(thiophene-2-yl)-4H-1,2,4-triazole-3-thiol

The molecular structure of the compound (2) was determined using the Density Functional Theory (DFT/B3LYP) method in the ground state with the cc-pVDZ basis sets. Figure 7.10 shows molecular structures drawing by ChemBioDraw and GAUSVIEW. The optimized geometrical parameters (bond lengths, bond angles, and torsion angles) calculated using B3LYP/cc-pVDZ techniques are listed in Table 7.6.

A   B

Figure 7.10. Structure of the compound (2) A) Drawing by ChemBioDraw Ultra B) Gaussian Optimized by B3LYP/cc-pVDZ

Table 7.6. In the ground state, geometrical optimization for compound (2)

Symbol	Bond Length	Symbol	Dihedral angle
C2-C1	2.168	N4-C1-C3-C2	-0.390
N3-C2	1.373	N5-C2-C1-C4	-0.080
N4-C1	1.321	C6-C1-C4-C5	178.486
N5-C2	1.315	C7-C6-C1-C4	160.296
C6-C1	1.453	S8-C6-C1-C4	-18.036
C7-C6	1.382	C9-C7-C6-C1	-178.675
S8-C6	1.755	C11-C9-C7-C6	0.165
C9-C7	1.426	C14-C3-C2-C1	-177.121
C11-C9	1.371	C15-C14-C3-C2	-88.238
C14-N3	1.463	S17-C2-C1-C4	179.291
C15-C14	1.528		

Symbol	Bond angle
N3-C2-C1	38.490
N4-C1-C3	109.760
N5-C2-C1	73.048
C6-C1-C4	123.132
C7-C6-C1	132.026
S8-C6-C1	117.345
C9-C7-C6	113.209
C11-C9-C7	112.648
C14-C3-C2	126.444
C15-C14-C3	113.324
S17-C2-C1	161.3180

The FT-IR spectra are experimentally and theoretically shown in Figure 7.11 for compound (2). The experimental measurement used KBr pullet formed. Table 7.7 compared Experimentally and theoretically results with types of vibration was calculated B3LYB/cc-pVDZ. The correlation between Experimentally and theoretically results for FT-IR analysis was shown in Figure 7.12.
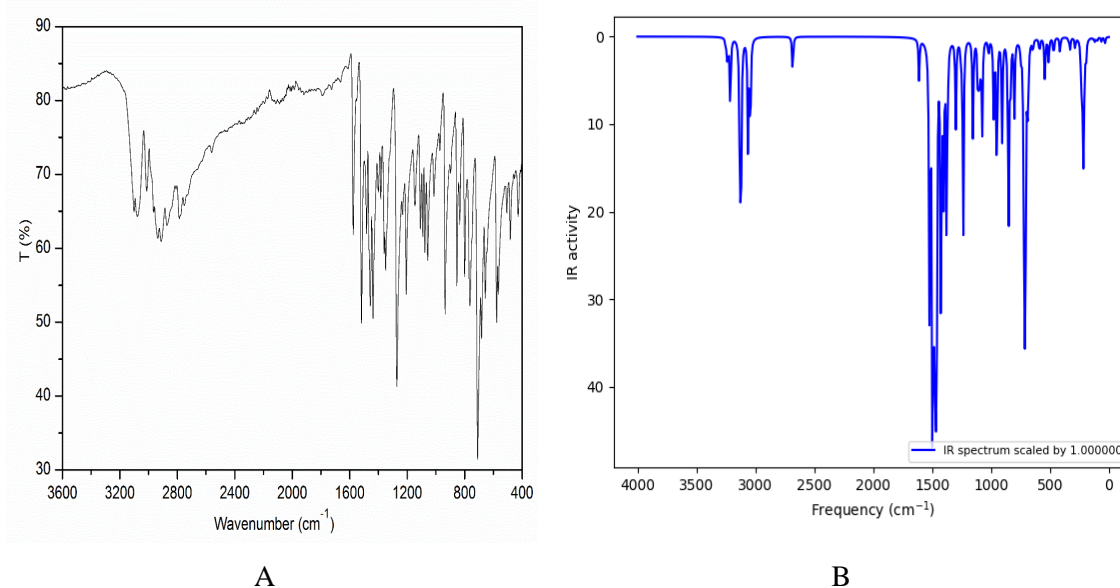
Figure 7.11. IR spectrum for compound (2). (A) Experimental (B) Theoretical results

Table 7.7. Theoretical and experimental vibrational for compound (2)

Assignments With TED	FT-IR (cm⁻¹) With KBr	Unscaled Frequencies B3LYP/cc-pVDZ
Sy, St, Vi C11-H13, C9-H12, C7-H10	2950	3250.10
an, St, Vi C7-H10, C11-H13		3235.18
Sy, St, Vi C11-H13, C9-H12, C7-H10		3211.85
Sy, St C15-H19,H16;C14-H22,H21		3130.57
an, St C15-H20,H16,H19		3121.31
St C14-H21,H22		3108.70
Sy, St C14-H21,H22		3061.59
Sy, St C15-H16,H19,H20	2870-2960	3042.25
St, Vi S17-H8	2765	2682.65
an, St, Vi C7=C6,C9=C11		1610.45
St, Vi C11=C9		1522.01
Sci, St, Vi C14-H21,H22		1496.03
Sci, St,Vi C15-H16,H19		1479.86
St,Vi C2=N5		1470.67
R, Vi C15-H16,H19,H20		1463.07
St, Vi C=N in Triazole	1570	1461.06
St, Vi C=N in Triazole		1424.50
an, St, Vi C15-H16,H19		1403.76
an, St, Vi Triazole ring	1290	1397.37
Sci, St, Vi C14-H21,H22		1379.73
St, Vi C14-H21,H22		1299.10
St H in Thiophene	1260	1235.92
St, Vi H in ethane group		1153.65
Si, Vi N4-N5		1110.75
R C15-H16,H19	1086	1099.33
Sci, St, Vi C11-H13,C9-H12		1089

Sci, St, Vi C11-H13, C7-H18		1075.17
St, Vi ethane group		977.35
Vi of All atoms		950.91
St, Vi S17-H18		905.82
St, Vi S8-C11	715	851.81
an, St, Vi N3-C1N4		721.77
R, St, C11-H13		710.6
St, Vi Thiophene		645.49
St,Vi S17-H18		234.74

St: Starching vibration, Vi: Vibration, an: anti, Sy: Symmetrical, R: Rocking, Sci: Scissoring

Equation	y = a + b*x
Plot	B
Weight	No Weighting
Intercept	31.39454 ± 81.5555
Slope	0.95433 ± 0.04262
Residual Sum of Squar	109919.53549
Pearson's r	0.99212
R-Square (COD)	0.9843
Adj. R-Square	0.98234
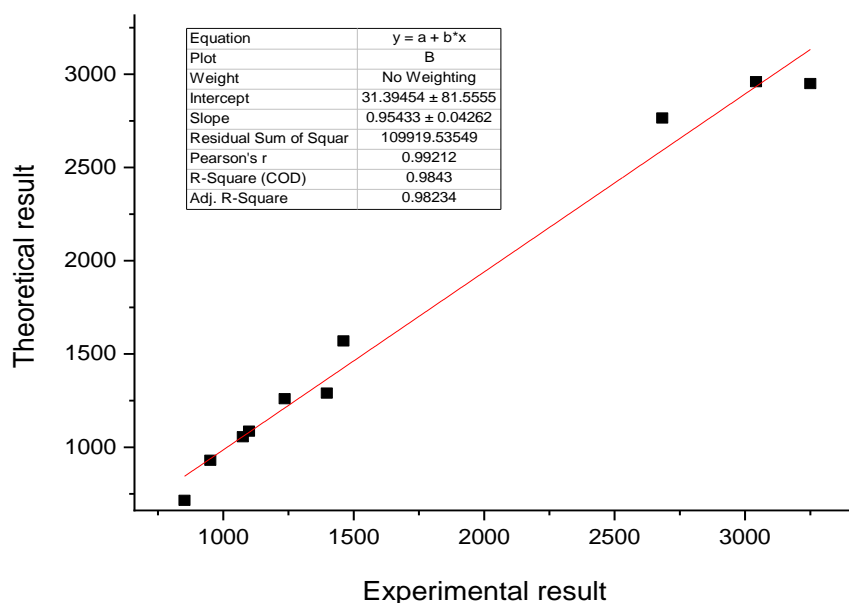
Figure 7.12. Relationship graphics for compound (2), between theoretical and experimental frequencies

The experimental Hydrogen ^{1}H NMR look Figure 7.13 and carbon ^{13}C NMR shown in Figure 7.14 chemical shifts for compound (2) were investigated in Dimethyl sulfoxide (DMSO-d6). Also in DMSO-d6 solvents, the theoretical ^{1}H and ^{13}C chemical shift values were determined using the DFT (B3LYP) method with the cc-pVDZ basis sets, all results were presents in Table 7.8.
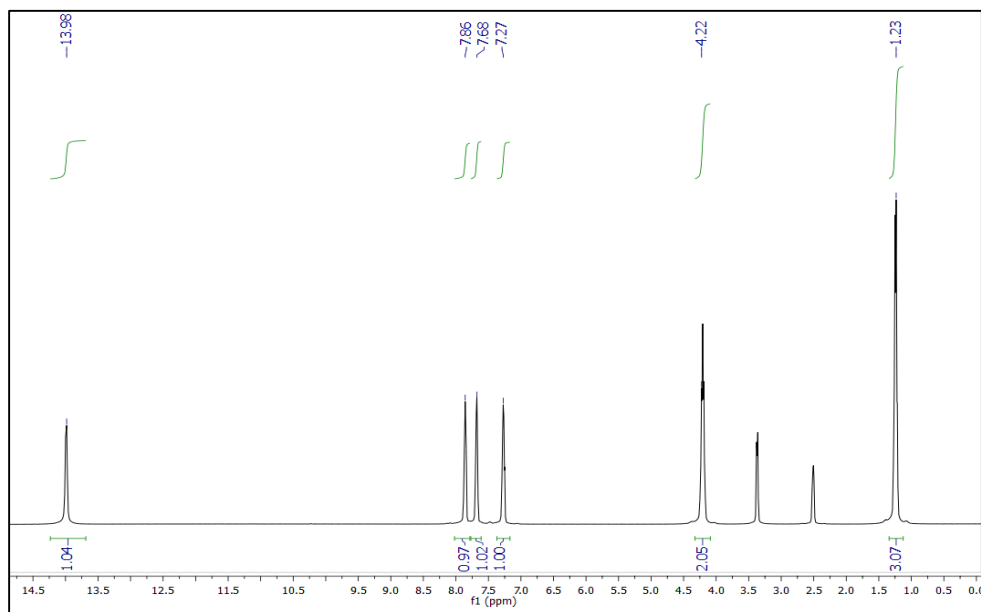
Figure 7.13. Experimental ^{1}H-NMR spectrum for compound (2) in DMSO-d6
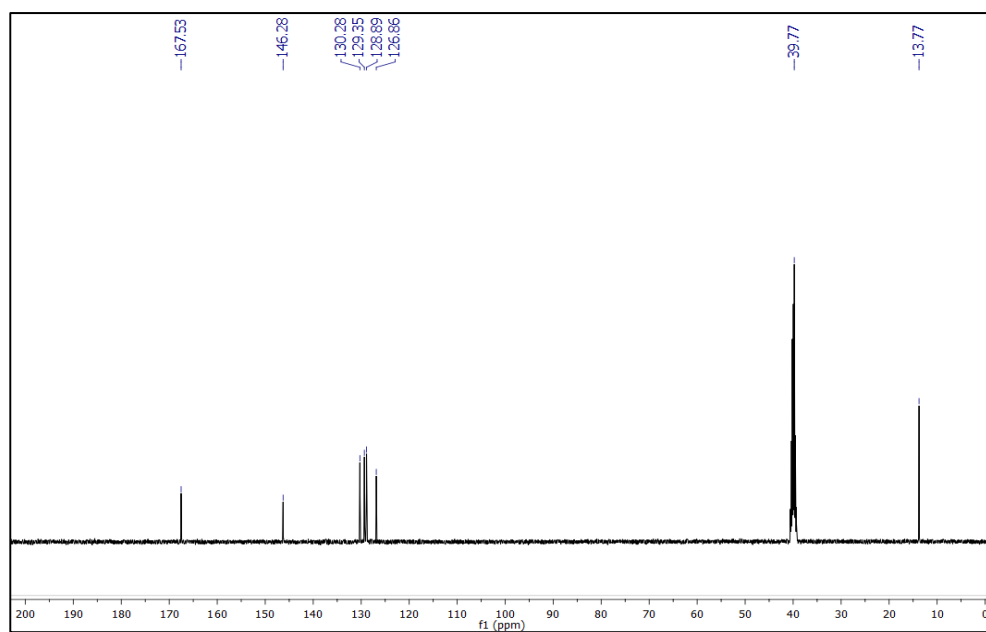
Figure 7.14. The experimental ^{13}C-NMR spectrum for compound (2) in DMSO-d6

Table 7.8. Theoretical and experimental ^{1}H and ^{13}C chemical shift (ppm) for compound (2).

Atom	Experimental in (DMSO-d6)	Calculated by B3LYP/cc-pVDZ
C15	13.70	25.00
C14	39.70	50.20

49

C7	126.80	130.10
C9	128.90	133.70
C11	130.30	140.20
C6	146.30	145.60
C1	168.50	159.33
C2	168.50	160.43
3H for CH3	1.23	2.6-2.8
2H for CH2	4.22	4.9-5.3
S-H	13.98	5.60
H for Thiophene group	7.27-7.86	8.4-8.5

B3LYP/cc-pVDZ was used to found Molecular electrostatic potential (MEP) for compound (2) shown in Figure 7.15. The negative region's red color was founded on nitrogens (N4, N5) of triazole and also founded a little on the S-H group, this indicates that the nitrogen (N4, N5) atoms and S-H groups attracted with more electrophiles.
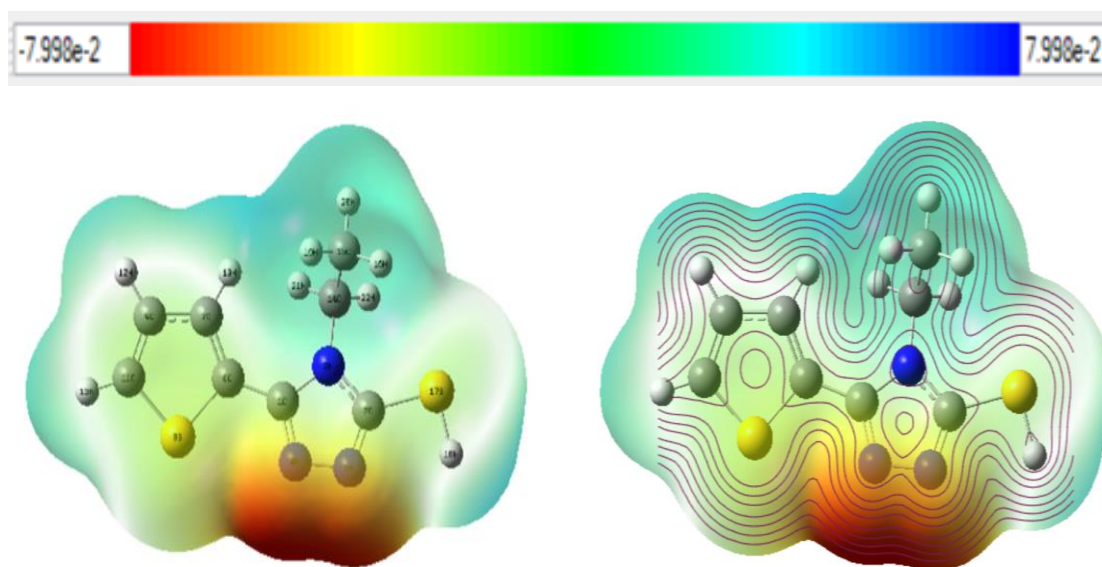
Figure 7.15. Molecular electrostatic potential for compound (2)

Mulliken population analysis for compound (2) is shown in Figure 7.16. the more negative charges were distributed on the N3, N4, N5, C6 and C11.
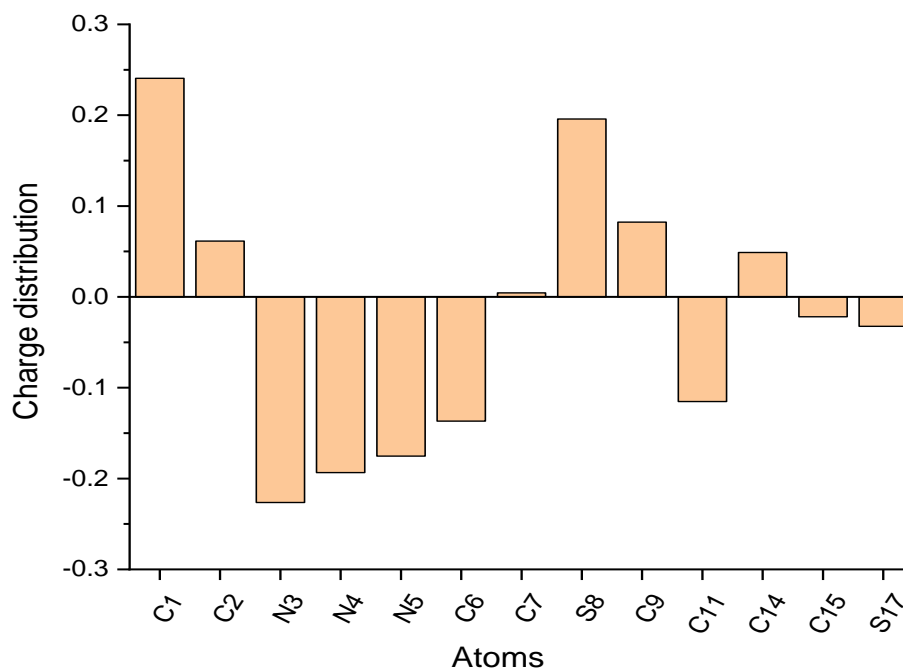
Figure 7.16. Millikan charge distribution on the compound (2)

Different parameters which are related to the inhibitor activity calculated for compound (2) used B3LYP/cc-pVDZ All parameters were shown in Table 7.9 including energy of the highest occupied molecular orbital (E_{HOMO}), energy of the lowest unoccupied molecular orbital (E_{LUMO}), energy bandgap (ΔE = E_{LUMO} - E_{HOMO}), dipole moment (μ), hardness (η), softness (σ), electronegativity (χ), electrophilicity index (ω), nucleophilicity (ε) index and The fraction of transferred electrons (ΔN) which is related to transfer electron between inhibitor and metal surface.

Table 7.9. Calculation quantum chemical parameters for compound (2)

Parameters	Equations	Results
Total Energy (a.u)		-1270.937
μ (D)		4.852
E_{LUMO} (eV)		-1.221
E_{HOMO} (eV)		-5.809
ΔE (eV)		4.587
I	$I = -E_{HOMO}$	5.809
A	$A = -E_{LUMO}$	1.221
χ (eV)	$\chi = (I + A) / 2$	3.515
η (eV)	$\eta = (I - A) / 2$	2.293
σ (eV)	$\sigma = I/\eta$	2.532
Pi (eV)	$Pi = -\chi$	-3.515
ω (eV)	$\omega = Pi^2/2\eta$	2.693
ε (eV)	$\varepsilon = Pi. \eta$	-8.063

ΔN	$\Delta N = (\chi_{metal} - \chi_{inhibitor}) / 2. (\eta_{metal} - \eta_{inhibitor})$	0.759

The Zero-point vibrational energy, Total energy, thermal energy, rotational constants, rotational temperatures and entropy of the molecules (2) were calculated using B3LYP/cc-pVDZ at a pressure of 1.00 atom and 298 K, Table 7.10 shows the results.

Table 7.10. Thermodynamic parameters for compound (2)

Parameters	B3LYP/cc-pVDZ
Zero-point vibrational energy(kcal/mol^{-1})	101.331
Total energy (a.u.)	-1157.799
Rotational constants (GHz)	
	1.386
	0.377
	0.303
Rotational temperatures (K)	
	0.06654
	0.01811
	0.01459
Entropy (Kcal mol^{-1} K^{-1})	
Rotational	0.889
Translational	0.889
Vibrational	107.353
Total	109.130

7.3. 2-chloro-1-(3-methyl-3-mesityl-cyclobutyl)–ethanone (5)

The molecular was experimentally characterized by FT-IR and NMR spectroscopy. The melting point for compound (5) (Figure 7.17) is equal to 97-98 ^{0}C which was measured by Thomas Hoover melting point. The Yield is 55% and the color are white.
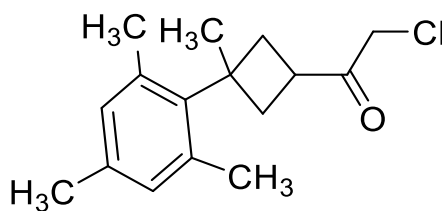
(5)

Figure 7.17. 2-chloro-1-(3-methyl-3-mesityl-cyclobutyl)–ethanone

The molecular structure of the compound (5) was determined using the Density Functional Theory (DFT/B3LYP) method in the ground state with the cc-pVDZ basis sets. Figure 7.18 show

molecular structures drawing by ChemBioDraw and GAUSVIEW. The optimized geometrical parameters (bond lengths, bond angles, and torsion angles) calculated using B3LYP/cc-pVDZ techniques are listed in Table 7.11.
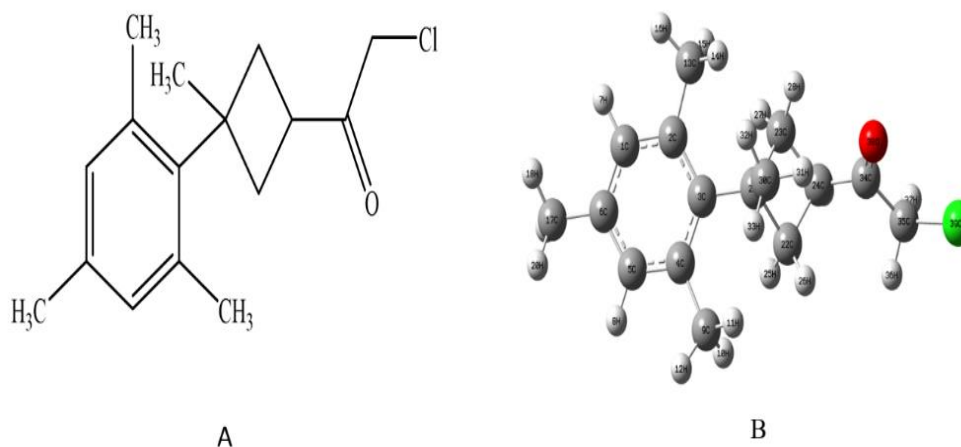
Figure 7.18. Structure of the compound (5) A) Drawing by ChemBioDraw Ultra B) Gaussian Optimized by B3LYP/cc-pVDZ

Table 7.11. In the ground state, geometrical optimization for compound (5)

Symbol	Bond Length	Symbol	Bond Angle	Symbol	Dihedral angle
C2-C1	1.402	C3-C2-C1	119.851	C4-C3-C2-C1	-5.287
C3-C2	1.421	C4-C3-C2	117.892	C5-C4-C3-C2	5.308
C4-C3	1.423	C5-C4-C3	119.883	C6-C1-C2-C3	1.384
C5-C4	1.405	C6-C1-C2	122.558	C9-C4-C3-C2	-172.763
C6-C1	1.397	C9-C4-C3	123.838	C13-C2-C1-C6	-176.945
C9-C4	1.514	C13-C2-C1	116.276	C17-C6-C1-C2	-178.076
C13-C2	1.513	C17-C6-C1	121.531	C21-C3-C2-C1	178.717
C17-C6	1.507	C21-C3-C2	120.873	C22-C21-C3-C2	-142.988
C21-C3	1.539	C22-C21-C3	116.962	C23-C21-C3-C2	-41.282
C22-C21	1.572	C23-C21-C3	117.281	C24-C21-C3-C2	-129.821
C23-C21	1.577	C24-C21-C3	91.342	C34-C24-C23-C21	-105.532
C24-C23	1.545	C34-C24-C23	116.323	C35-C34-C24-C23	-167.503
C34-C24	1.512	C35-C34-C24	113.275	O38-C34-C24-C23	13.165
C35-C34	1.531	O38-C34-C24	123.935	Cl39-C35-C34-C24	-171.276
O38-C34	1.214	Cl39-C35C34	114.107		
Cl39-C35	1.796				

The FT-IR spectra are experimentally and theoretically shown in Figure 7.19 for compound (5). The experimental measurement used KBr pullet formed. Table 7.12 compared Experimentally

and theoretically results with types of vibration was calculated B3LYB/cc-pVDZ. The correlation between Experimentally and theoretically results for FT-IR analysis was shown in Figure 7.20.
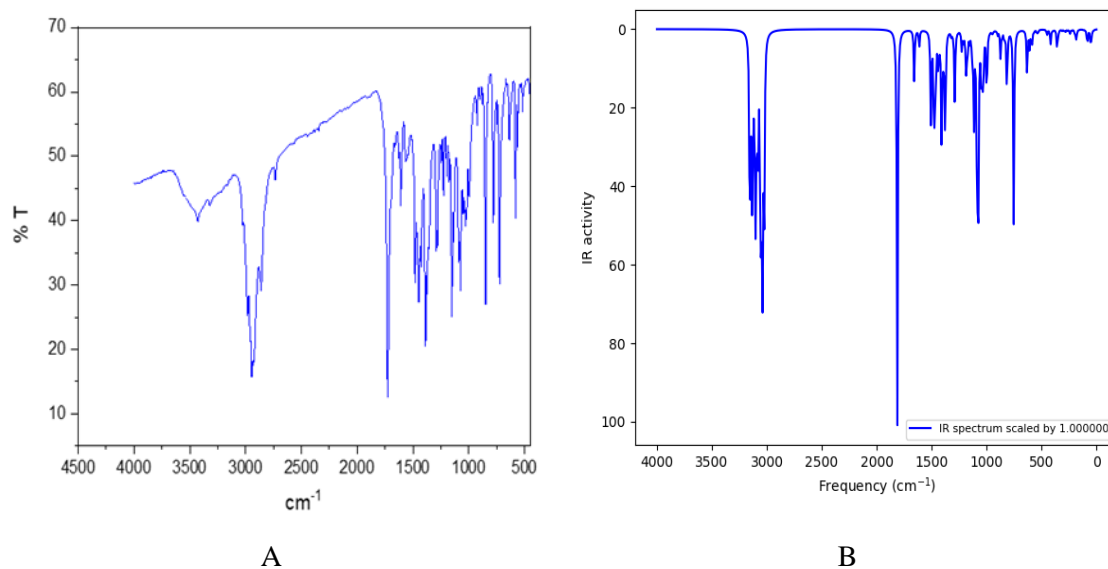
Figure 7.19. IR spectrum for compound (5). (A) Experimental (B) Theoretical results

Table 7.12. Theoretical and experimental vibrational for compound (5)

Assignments With TED	FT-IR (cm⁻¹) With KBr	Unscaled Frequencies B3LYP/cc-pVDZ	Assignments With TED	FT-IR (cm⁻¹) With KBr	Unscaled Frequencies B3LYP/cc-pVDZ
υsC1H7,C5H8	3156	3155	υsC-Hring	1508	1507
υasC23H27,H28	3148	3147	υCH3	1484-1460	1481-1463
υasC22H25, H26	3140	3134	ScC17,H18,H20	1452	1459,1049
υasC13H14,H16	3132	3133	υC35,H37	1412	1409
υasC9H11,H12	3124	3130	υsCH3	1404	1404
υasC30H31H32	3116	3126	υs-inCH3-ring	1396, 1036	1398,1046,1033
υasC35H36,H37	3108	3114	ro-inC24H29	1372	1376
υasC17H18,H20	3100	3112	υasC-ring	1324	1321,1316
υasC30H32,H33	3092	3102	roC35H36,H37	1284	1289
υasC13H15,H16	3084	3099	υs-ouC23H27,H28	1276	1274
υsC9H10,H12	3076	3098	υsouC1H7,C5H8	1268	1265
υsC17H18,H20	3068	3083	roC23H27,C24H29	1260	1261,1225
υsC23H27,H28	3060	3078	υC21C23	1156	1154

54

υsC35H36,H37	3052	3061	υsC21C22,C23C24	1132	1132
υsC22H25,H26	3044	3055	υasC22C2324	996, 988	999,996
υsC13H14,H15,H16	3036	3039	υasC1C5C6	972	974
υsC9H10,H11,H12	3028	3037	υasC21C23C30	940	943
υsC30H31,H32,H33	3020	3034	υasC21C22C23	908	909,883
υsC17H18,H19,H20	3012	3022	roC22H25H26	884	815
υC=O	1745	1812	υsC35Cl39	756	753
υsC=C-ring	1650	1658,1612			

υs: vibration Symmetrical, υ: vibration, υas: Vibration anti symmetrical, ro: Rocking, ou: ou of the plane, in: in a plane.

Equation	y = a + b*x
Plot	B
Weight	No Weighting
Intercept	8.13688 ± 6.017
Slope	0.99406 ± 0.002
Residual Sum of Squa	9789.08648
Pearson's r	0.99987
R-Square (COD)	0.99973
Adj. R-Square	0.99972
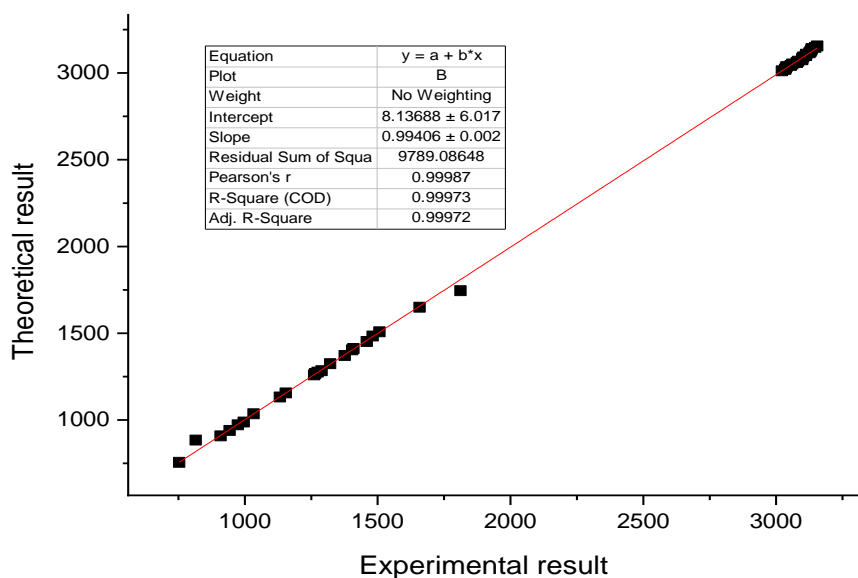
Figure 7.20. Relationship graphics for compound (5), between theoretical result and experimental frequencies

The experimental Hydrogen ^{1}H NMR look Figure 7.21 and carbon ^{13}C NMR shown in Figure 7.22 chemical shifts for compound (5) were investigated in Dimethyl sulfoxide (DMSO-d6). Also in DMSO-d6 solvents, the theoretical ^{1}H and ^{13}C chemical shift values were determined using the DFT (B3LYP) method with the cc-pVDZ basis sets, all results were presents in Table 7.13 and 7.14.
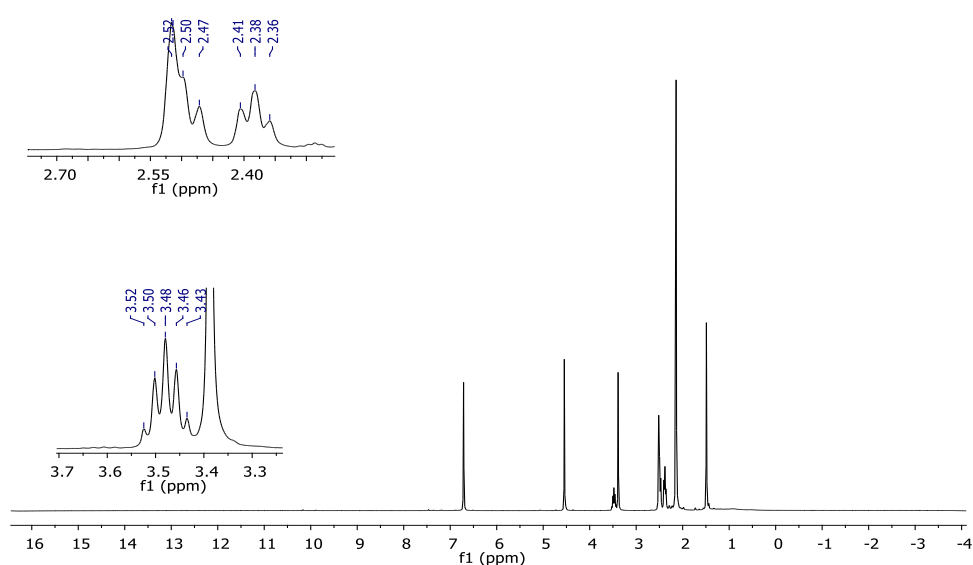
Figure 7.21. Experimental ^{1}H-NMR spectrum for compound (5) in DMSO-d6
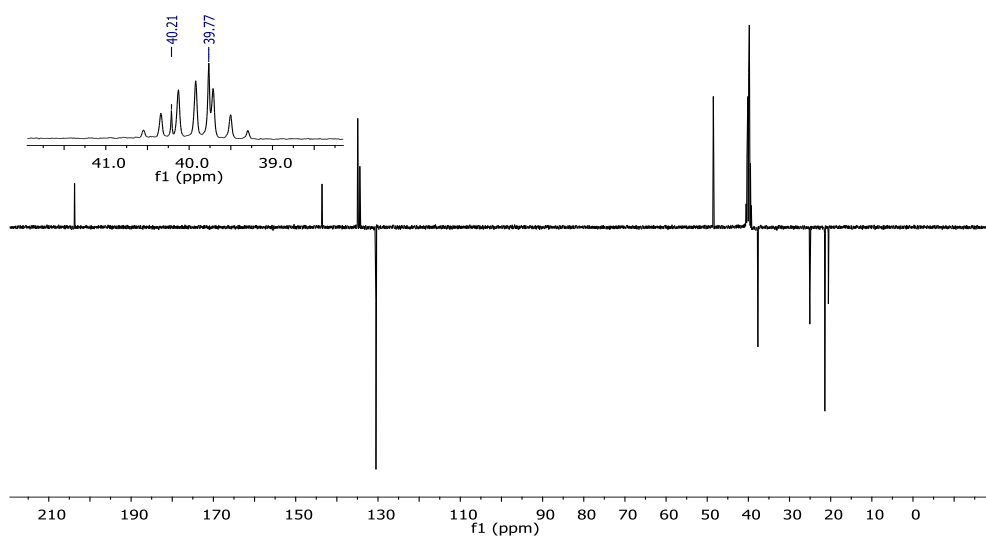
Figure 7.22. The experimental ^{13}C-NMR spectrum for compound (5) in DMSO-d6

Table 7.13. Experimental and theoretical chemical shifts (ppm) of ^{1}H-NMR of compound (5)

H number	Experimental Results	Theoretical Results
H7	6.75	7.945
H8	6.75	7.934
H36	4.55	5.629
H37	4.55	5.429
H25	3.52	4.190
H29	3.50	4.121
H28	3.48	3.770
H27	3.46	3.756

56

H15	2.52	3.726
H10	2.52	3.670
H19	2.52	3.619
H14	2.36	3.312
H20	2.41	3.296
H18	2.50	3.249
H11	2.47	3.194
H26	3.43	3.162
H31	2.41	3.137
H16	2.38	3.116
H12	2.37	3.070
H32	1.50	2.474
H33	1.50	2.418

Table 7.14. Experimental and theoretical chemical shifts (ppm) of ^{13}C-NMR of compound (5)

C number	Experimental Results	Theoretical results
C34	203.90	211.06
C3	143.94	152.64
C2	143.94	143.41
C4	143.94	143.31
C6	134.06	142.40
C1	130.29	135.81
C5	130.29	135.68
C35	48.42	64.38
C21	40.21	54.66
C22	39.77	49.08
C24	39.77	47.19
C23	37.68	44.68
C30	25.24	33.55
C13	20.75	30.47
C9	20.75	30.28
C17	20.45	28.91

B3LYP/cc-pVDZ was used to found Molecular electrostatic potential (MEP) for compound (5) shown in Figure 7.23. The negative region's red color is often above the atoms of two carbons (C34, C35) and oxygen with a little on the Cl atom, this indicates that the side of the chlorine atom is attached more electrophilic.
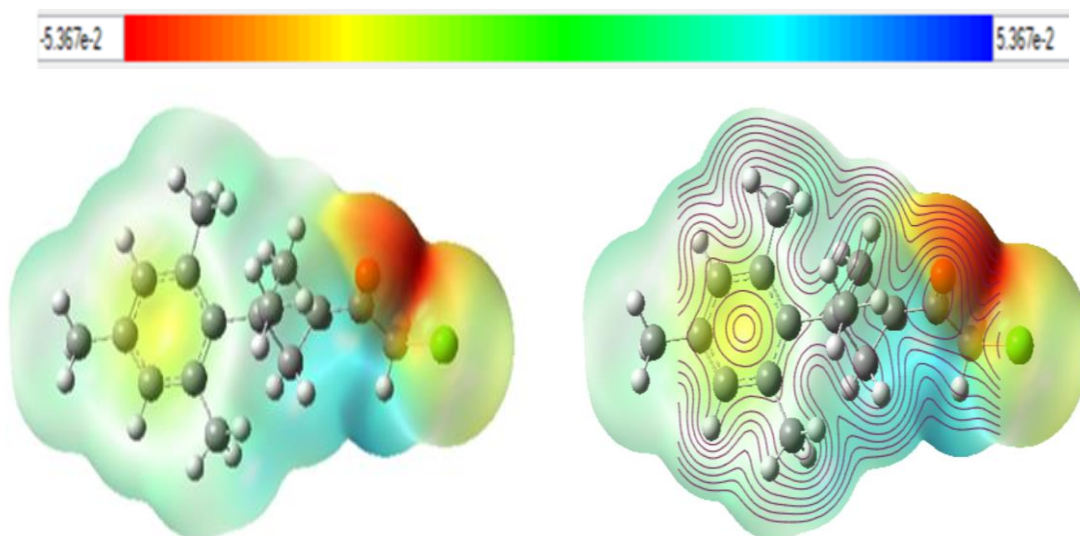
Figure 7.23. Molecular electrostatic potential for compound (5)

Mulliken population analysis for compound (5) shown in Figure 7.24 the more negative charges was distributed on the C2, C4, C24, C21, O38 and C11.
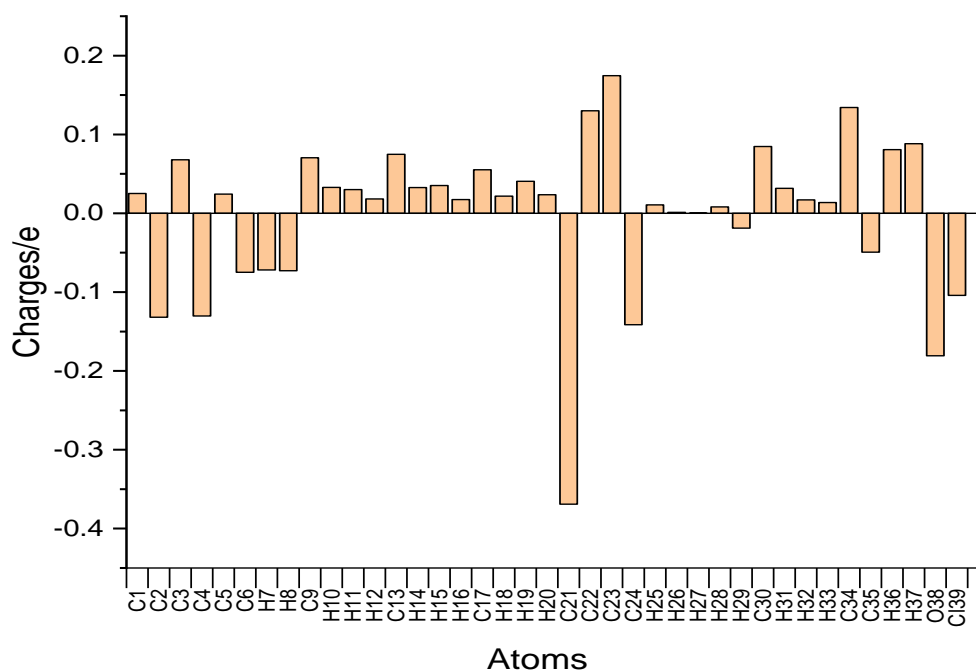
Figure 7.24. Millikan charge distribution on the compound (5)

Different parameters which are related to the inhibitor activity calculated for compound (5) used B3LYP/cc-pVDZ All parameters were shown in Table 7.15 including energy of the highest occupied molecular orbital (E_{HOMO}), energy of the lowest unoccupied molecular orbital (E_{LUMO}),

energy bandgap ($\Delta E = E_{LUMO} - E_{HOMO}$), dipole moment ($\mu$), hardness ($\eta$), softness ($\sigma$), electronegativity ($\chi$), electrophilicity index (ω), nucleophilicity (ε) index and The fraction of transferred electrons (ΔN) which is related to transfer electron between inhibitor and metal surface.

Table 7.15. Calculation quantum chemical parameters for compound (5)

| Parameters	Equations	Results
Total Energy (a.u)		-1157.799
μ (D)		3.7288
E_{LUMO} (eV)		-0.856
E_{HOMO} (eV)		-6.235
ΔE (eV)		5.379
I	I = -E_{HOMO}	6.235
A	A = -E_{LUMO}	0.856
χ (eV)	χ = (I + A) / 2	3.5455
η (eV)	η = (I – A) / 2	2.6895
σ (eV)	σ = I/η	2.318
Pi (eV)	Pi = -χ	-3.5455
ω (eV)	ω = Pi2/2η	2.336
ε (eV)	ε = Pi. η	4.673
ΔN	ΔN = (χmetal - χinhibitor) / 2. (ηmetal - ηinhibitor)	0.642

The Zero-point vibrational energy, Total energy, thermal energy, rotational constants, rotational temperatures and entropy of the molecules (5) were calculated using B3LYP/cc-pVDZ at a pressure of 1.00 atom and 298 K, Table 7.16 shows the results.

Table 7.16. Thermodynamic parameters for compound (5)

Parameters	B3LYP/cc-pVDZ
Zero-point vibrational energy(kcal/mol^{-1})	206.805
Total energy (a.u.)	-1157.799
Rotational constants (GHz)	
	1.020
	0.155
	0.144
Rotational temperatures (K)	
	0.048
	0.007
	0.0069
Entropy (Kcal mol^{-1} K^{-1})	
Rotational	0.889
Translational	0.889
Vibrational	217.045
Total	218.823

7.4. 1-(3-methyl-3-mesityl)-cyclobutyl-2–[[5-(thiophen-2-yl)-4-phenyl-4H-1,2,4 triazol-3- yl] sulfanyl]-ethanone (6)

The molecular was experimentally characterized by FT-IR and NMR spectroscopy. The melting point for compound (6) (Figure 7.25) is equal to 102-104 ^{0}C which was measured by Thomas Hoover melting point. The Yield is 55% and the color is white.

(6)
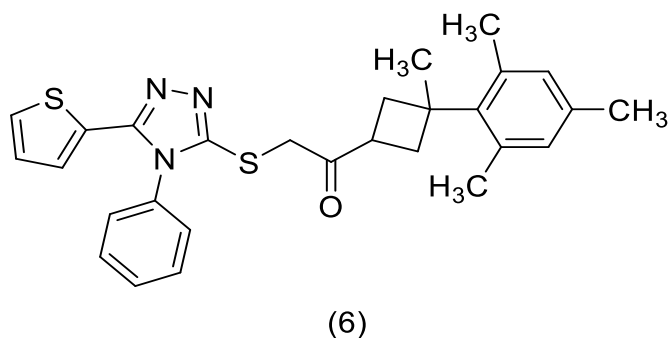
Figure 7.25. 1-(3-methyl-3-mesityl)-cyclobutyl-2–[[5-(thiophen-2-yl)-4-phenyl-4H-1,2,4 triazol-3- yl] sulfanyl]-ethanone

The molecular structure of the compound (6) was determined using the Density Functional Theory (DFT/B3LYP) method in the ground state with the cc-pVDZ basis sets. Figure 7.26 show molecular structures drawing by ChemBioDraw and GAUSVIEW. The optimized geometrical parameters (bond lengths, bond angles, and torsion angles) calculated using B3LYP/cc-pVDZ techniques are listed in Table 7.17.
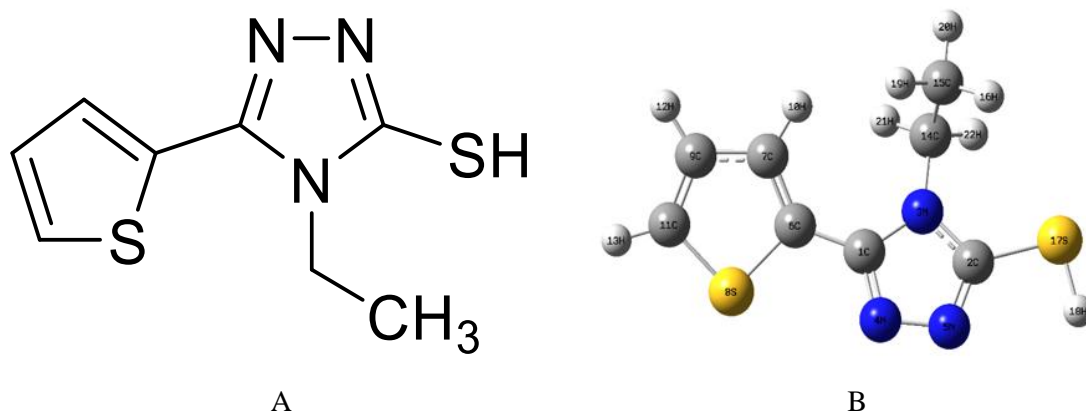

(A)
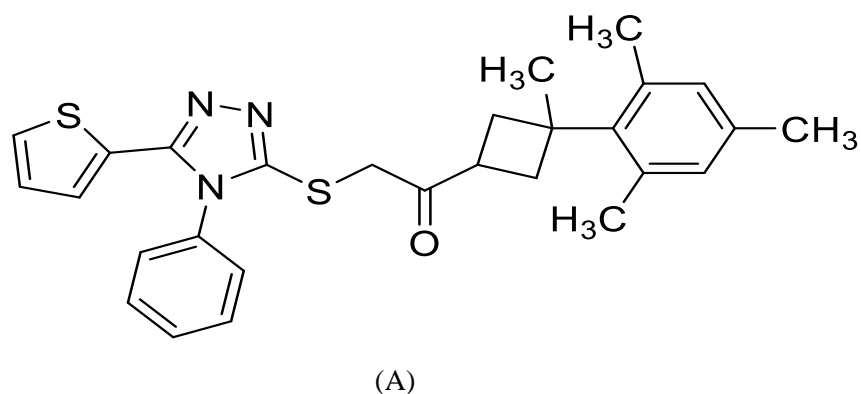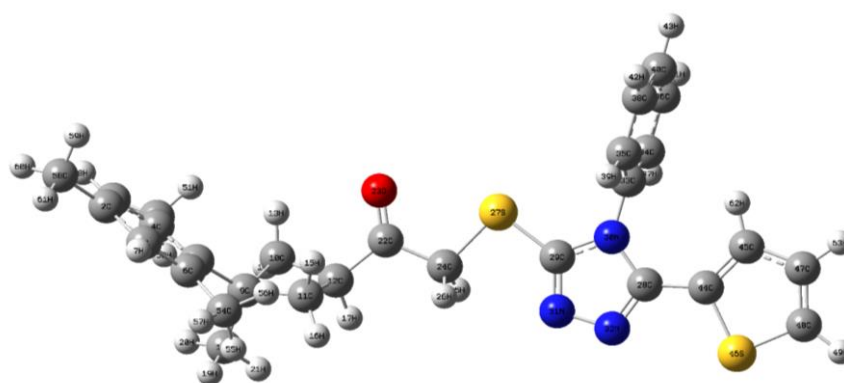
(B)

Figure 7.26. Structure of the compound (6) A) Drawing by ChemBioDraw Ultra B) Gaussian Optimized by B3LYP/cc-pVDZ

Table 7.17. In the ground state, geometrical optimization for compound (6)

Symbol	Bond Lengths	Symbol	Bond angle	Symbol	Dihedral angle
C2-C1	1.396	C2-C2-C1	117.062	C4-C3-C2-C1	-2.136
C2-C2	1.396	C4-C3-C2	122.538	C5-C4-C3-C2	-1.1562
C4-C3	1.402	C5-C4-C3	119.832	C6-C1-C2-C3	2.178
C5-C4	1.419	C6-C1-C2	122.489	C9-C5-C4-C3	-179.181
C6-C1	1.402	C9-C5-C4	120.999	C10-C9-C5-C4	40.280
C9-C5	1.534	C10-C9-C5	118.344	C11-C9-C5-C4	142.251
C10-C9	1.571	C11-C9-C5	117.730	C12-C10-C9-C5	137.351
C11-C9	1.572	C12-C10-C9	90.344	C18-C9-C5-C4	-89.023
C12-C10	1.540	C18-C9-C5	110.226	C22-C12-C10-C9	-134.993
C18-C9	1.540	C22-C12-C10	117.597	O23-C22-C12-C10	14.450
C22-C12	1.514	O23-C22-C12	122.720	C24-C22-C12-C10	-167.700
O23-C22	1.216	C24-C22-C12	115.617	S27-C24-C22-C12	-172.747
C24-C22	1.517	S27-C24-C22	109.612	C28-S27-C24-C22	175.916
S27-C24	1.835	C28-S27-C24	107.479	C29-S27-C24-C22	175.844
C28-S27	3.891	C29-S27-C24	96.471	N30-C29-S27-C24	179.16
C29-S27	1.766	N30-C29-S27	121.884	N31-C29-S27-C24	-1.084
N30-C29	1.381	N31-C29-S27	127.355	N32-C28-S27-C24	-0.966
N31-C29	1.316	N32-C28-S27	80.537	C33-N30-C29-S27	-0.403
N32-C28	1.318	C33-N30-C29	126.080	C34-C33-C30-C29	-89.185
C33-N30	1.434	C34-C33-C30	119.649	C35-C33-C30-C29	90.014
C34-C33	1.399	C35-C33-C30	119.667	C36-C34-C33-C30	179.737
C35-C33	1.399	C36-C34-C33	119.484	C38-C35-C33-C30	-179.747
C36-C34	1.396	C38-C35-C33	119.476	C40-C36-C34-C33	-0.175
C38-C35	1.396	C40-C36-C34	120.141	C44-C28-S27-C24	179.455
C40-C36	1.398	C44-C28-S27	155.972	C45-C44-C28-S27	-0.710
C44-C28	1.452	C45-C44-C28	131.765	S46-C44-C28-S27	179.211
C45-C44	1.381	S46-C44-C28	117.420	C47-C45-C44-C28	179.912

S46-C44	1.756	C47-C45-C44	113.040	C48-C47-C45-C44	0.006
C47-C45	1.426	C48-C47-C45	112.744	C50-C4-C3-C2	177.594
C48-C47	1.371	C50-C4-C3	116.501	C54-C6-C1-C2	-177.697
C50-C4	1.516	C54-C6-C1	116.444	C58-C2-C1-C6	-178.031
C54-C6	1.517	C58-C2-C1	121.445		
C58-C2	1.509				

The FT-IR spectra are experimentally and theoretically shown in Figure 7.27 for compound (6). The experimental measurement used KBr pullet formed. Table 7.18 compared Experimentally and theoretically results with types of vibration was calculated B3LYB/cc-pVDZ. The correlation between Experimentally and theoretically results for FT-IR analysis was shown in Figure 7.28.

A	B
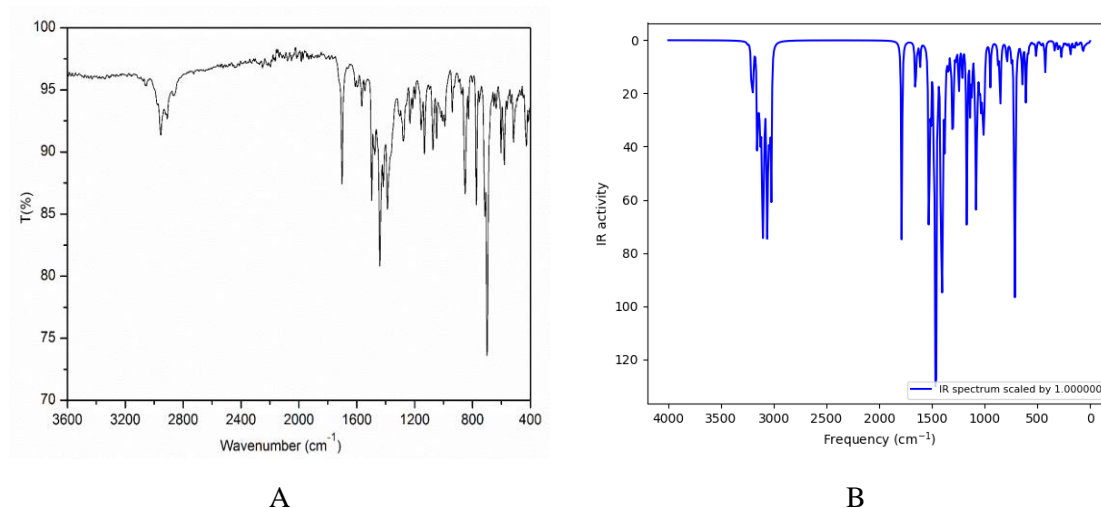
Figure 7.27. IR spectrum for compound (6). (A) Experimental (B) Theoretical results

Table 7.18. Theoretical and experimental vibrational for compound (6)

Assignments With TED	FT-IR (cm⁻¹) With KBr	Unscaled Frequencies B3LYP/cc-pVDZ	Assignments With TED	FT-IR (cm⁻¹) With KBr	Unscaled Frequencies B3LYP/cc-pVDZ
ST C45H62, C47H53, C48H49		3244.98	ST C44=C45		1611.53
UNST C45H62, C48H49		3244.16	ST C47=C48		1521.40
ST H-phenyl	3059	3212.11	ST C-phenyl		1478.81
ST C47H53		3211.85	ST C45C47, C28-N32		1469.42
ST H-phenyl		3208.76	ST C29=N31	1498	1461.86
ST H-phenyl		3200.20	SCI C58H60H61		1459.51
ST H-phenyl		3191.17	SCI C11H15H16		1442.21

ST H- mesityl	3156.67	ST C28N29C30	1414.26
UNST H- mesityl	3154.58	SCI CH3- mesityl	1404.85
UNST C10H13H14	3140.17	SCI C24H25H26	1400.16
UNST C11H15H16	3129.85	RO C12H17	1376.99
UNST C54H55H57	3123.96	ST C=C-phenyl	1355.21
UNST C50H52H53	3121.55	ST C-N	1342.67
UNST C58H60H61	3112.35	UNST C-Mesityl	1323.12
UNST C18H19H20	3107.23	WA C-Mesityl	1318.29
UNST C50H51H52H53	3105.47	RO C-H in phenyl	1183.21
UNST C24H25H26	3102.14	ST N31-N32	1131	1120.24
UNST C54H55H56H57	3101.77	SCI C48H49, C47H63		1091
UNST C18H19H20H21	3096.65	SCI CH2-cyclobutan		1064.72
UNST C58H59H60H61	3083.82	WA phenyl		1021.88
ST C12H17	3071.59	UNTS C-phenyl		1016.42
ST C11H15H16	3061.17	UNST C10C11C12		1009.92
ST C24H25H26	3051.54	ST C27-S24	1045	1000.50
ST C50H51H52H53	3043.14	ST CH3-Mestiyl		977.53
ST C54H55H56H57	3040.74	RO C45H62C47H63C48		916.67
ST C18H19H20H21	3026.06	ST CH2	854	872.65
ST C58H59H60H61	2910	3022.46	ST C48-S46		852.39
ST C22=O23	1697	1786.23	ST C24S27		797.43
ST C=C-mesityl	1658.88	ST C48-S46-C44	774	746.59
ST C=C-phenyl	1650.84	ST C24-S27		715.70
ST C=C-phenyl	1638.02	UNST C-Phenyl		711.20
ST C=C-mesityl	1614.17		

T: Starching vibration, UN: anti, S: Symmetrical, RO: Rocking, SCI: Scissoring
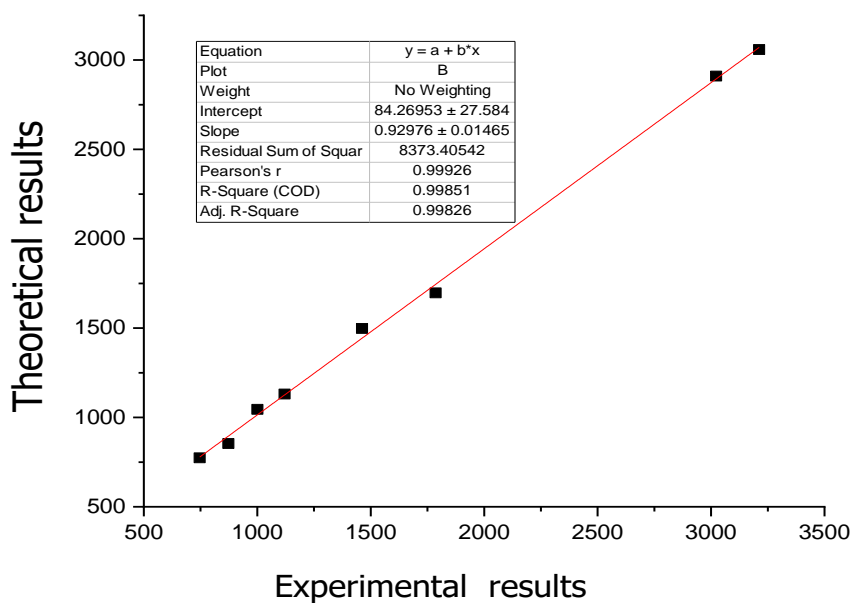
Figure 7.28. Relationship graphics for compound (6), between theoretical result and experimental frequencies

The experimental Hydrogen ^{1}H NMR look Figure 7.29 and carbon ^{13}C NMR shown in Figure 7.30 chemical shifts for compound (6) were investigated in Dimethyl sulfoxide (DMSO-d6). Also in DMSO-d6 solvents, the theoretical ^{1}H and ^{13}C chemical shift values were determined using the DFT (B3LYP) method with the cc-pVDZ basis sets, all results were presents in Table 7.19 and 7.20.
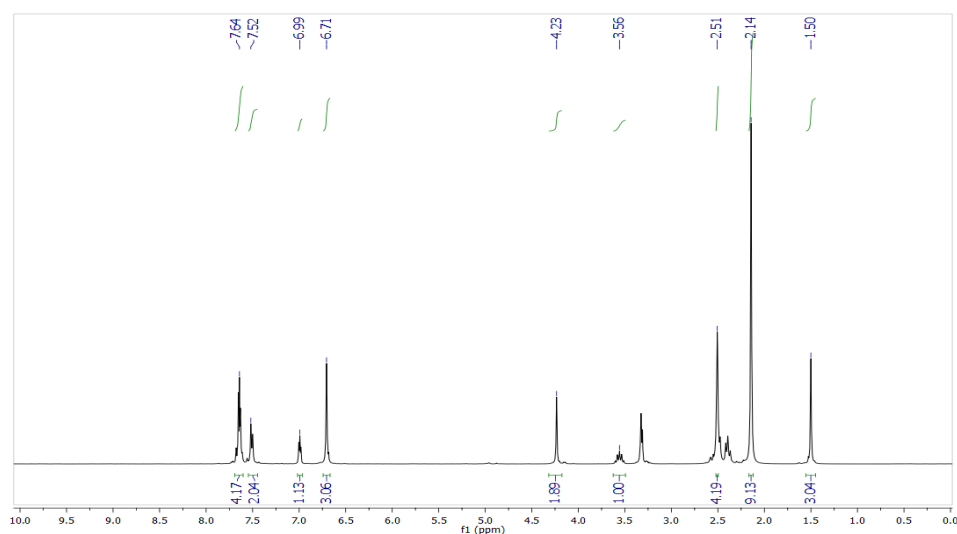
Figure 7.29. Experimental ^{1}H-NMR spectrum for compound (6) in DMSO-d6
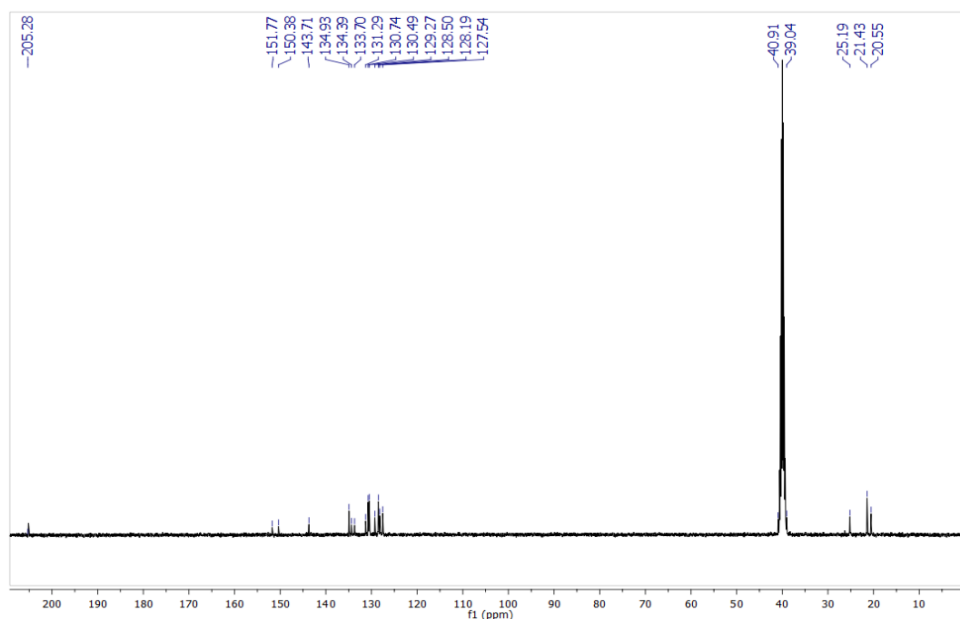
Figure 7.30. The experimental ^{13}C-NMR spectrum for compound (6) in DMSO-d6

Table 7.19. Experimental and theoretical chemical shifts (ppm) of ^{1}H-NMR of compound (6)

H number	Experimental Results	Theoretical Results
H43	6.99	8.27
H41	7.64	8.20
H42	7.64	8.19
H39	7.64	7.84
H37	7.64	7.83
H49	6.69	7.68
H8	7.51	7.21
H7	7.51	7.20
H63	6.69	7.16
H62	6.69	6.43
H26	4.23	4.99
H25	4.23	4.73
H17	3.56	3.76
H13	2.50	3.48
H51	2.14	3.04
H16	2.50	3.02
H59	2.14	2.90
H56	2.14	2.85
H15	2.50	2.73
H52	2.14	2.62
H55	2.14	2.59
H61	2.14	2.56
H60	2.14	2.55
H53	2.14	2.38
H57	2.14	2.35
H14	2.50	2.34
H21	1.50	2.17
H19	1.50	1.95

	H20	1.50	1.92

Table 7.20. Experimental and theoretical chemical shifts (ppm) of ^{13}C-NMR of compound (6)

C number	Experimental Results	Theoretical results
C22	205.3	211.84
C29	151.8	164.58
C28	150.4	157.63
C5	143.7	151.43
C44	134.9	144.03
C4	133.7	143.51
C6	133.7	143.5
C2	131.3	142.43
C33	130.7	141.42
C48	130.5	138.69
C40	130.5	137.45
C38	129.3	136.87
C36	129.3	136.76
C1	128.5	135.80
C3	128.5	135.62
C35	128.2	135.31
C34	128.2	135.21
C47	127.5	131.49
C45	127.5	129.47
C24	40.90	59.60
C11	25.20	53.11
C9	39.00	52.87
C12	39.00	49.15
C10	25.20	44.22
C18	21.40	32.56
C50	20.50	30.61
C54	20.50	30.30
C58	20.50	28.82

B3LYP/cc-pVDZ was used to found Molecular electrostatic potential (MEP) for compound (6) shown in Figure 7.31. The negative region's red color is often above the atoms of two nitrogens (N31, N32) and oxygen.
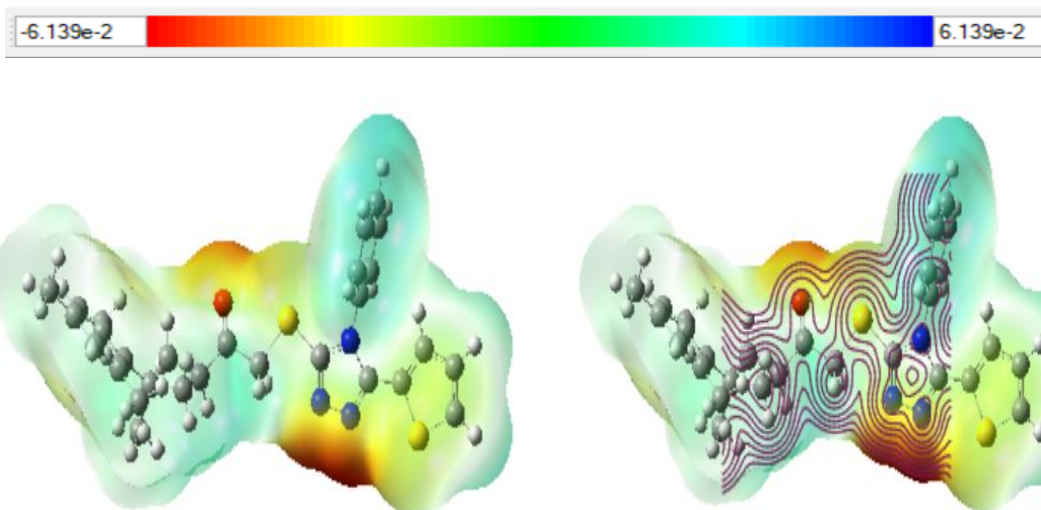
Figure 7.31. Molecular electrostatic potential for compound (6)

Mulliken population analysis for compound (6) shown in Figure 7.32 the more negative charges were distributed on the C9, C44, N30, N31.
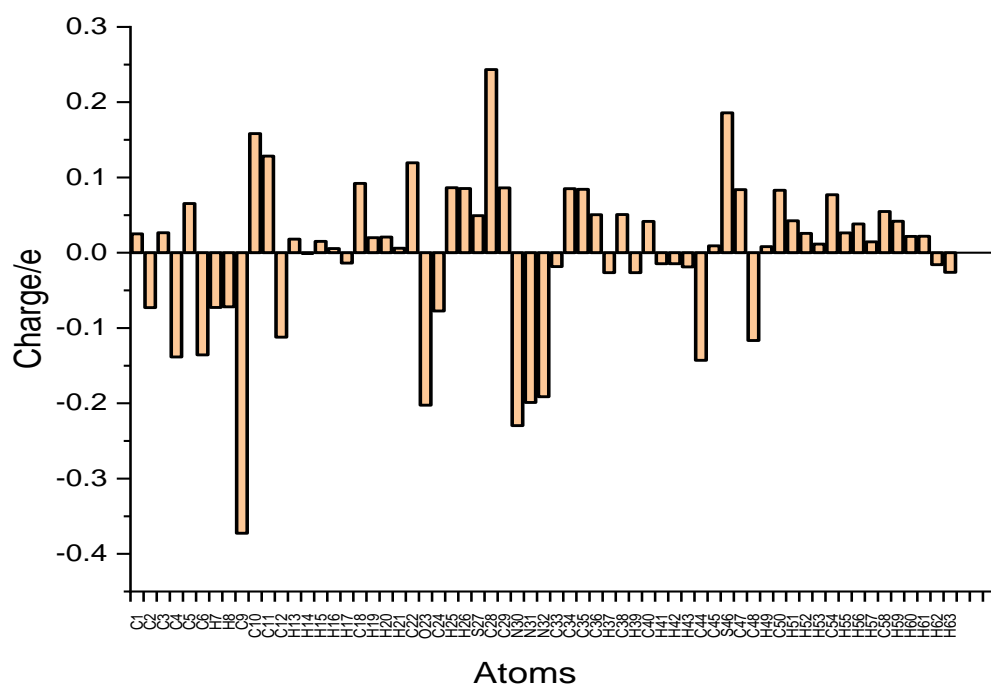
Figure 7.32. Millikan charge distribution on the compound (6)

Different parameters which are related to the inhibitor activity calculated for compound (6) used B3LYP/cc-pVDZ All parameters were shown in Table 7.21 including energy of the highest occupied molecular orbital (E_{HOMO}), energy of the lowest unoccupied molecular orbital (E_{LUMO}), energy bandgap ($\Delta E = E_{LUMO} - E_{HOMO}$), dipole moment ($\mu$), hardness ($\eta$), softness ($\sigma$), electronegativity ($\chi$), electrophilicity index (ω), nucleophilicity (ε) index and The fraction of transferred electrons (ΔN) which is related to transfer electron between inhibitor and metal surface.

Table 7.21. Calculation quantum chemical parameters for compound (6)

Parameters	Equations	Results
Total Energy (a.u)		-2120.361
μ (D)		2.646
E_{LUMO} (eV)		-1.344
E_{HOMO} (eV)		-5.764
ΔE (eV)		4.419
I	$I = -E_{HOMO}$	5.764
A	$A = -E_{LUMO}$	1.344
χ (eV)	$\chi = (I + A) / 2$	3.554
η (eV)	$\eta = (I - A) / 2$	2.209
σ (eV)	$\sigma = I/\eta$	2.608
Pi (eV)	$Pi = -\chi$	-3.554
ω (eV)	$\omega = Pi2/2\eta$	2.858
ε (eV)	$\varepsilon = Pi. \eta$	7.854
ΔN	$\Delta N = (\chi metal - \chi inhibitor) / 2. (\eta metal - \eta inhibitor)$	0.779

The Zero-point vibrational energy, Total energy, thermal energy, rotational constants, rotational temperatures and entropy of the molecules (6) were calculated using B3LYP/cc-pVDZ at a pressure of 1.00 atom and 298 K, Table 7.22 shows the results.

Table 7.22. Thermodynamic parameters for compound (6)

Parameters	B3LYP/cc-pVDZ
Zero-point vibrational energy(kcal/mol^{-1})	206.805
Total energy (a.u.)	-1157.799
Rotational constants (GHz)	
	1.020
	0.155
	0.144
Rotational temperatures (K)	
	0.048
	0.007
	0.0069
Entropy (Kcal mol^{-1} K^{-1})	

Rotational	0.889
Translational	0.889
Vibrational	217.045
Total	218.823

7.5. 4-(((4-ethyl-5-(thiophen-2-yl)-4H-1,2,4-triazol-3-yl)thio)methyl)-7-methyl-2H-chromen-2-one (7)

The molecular was experimentally characterized by FT-IR and NMR spectroscopy. The melting point for compound (7) (Figure 7.33) is equal to 145-147 ^{0}C which was measured by Thomas Hoover melting point. The Yield is 65% and the color is light brown.

(7)
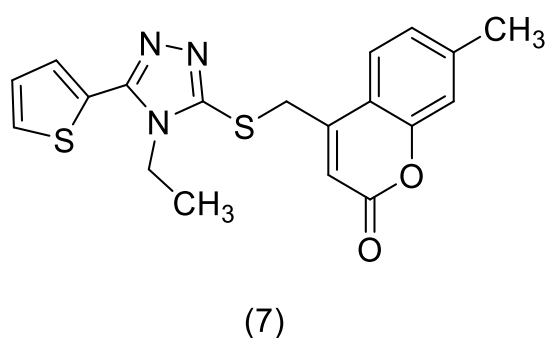
Figure 7.33. 4-(((4-ethyl-5-(thiophen-2-yl)-4H-1,2,4-triazol-3-yl)thio)methyl)-7-methyl-2H-chromen-2-one

The molecular structure of the compound (7) was determined using the Density Functional Theory (DFT/B3LYP) method in the ground state with the cc-pVDZ basis sets. Figure 7.34 show molecular structures drawing by ChemBioDraw and GAUSVIEW. The optimized geometrical parameters (bond lengths, bond angles, and torsion angles) calculated using B3LYP/cc-pVDZ techniques are listed in Table 7.23.

(A) (B)
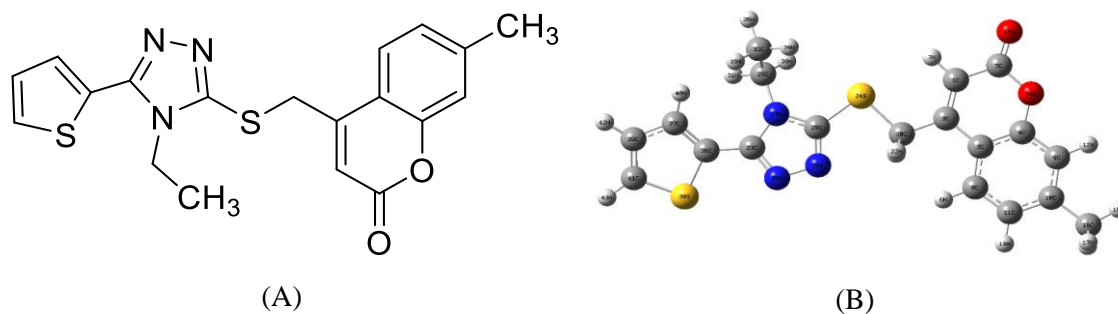
Figure 7.34. Structure of the compound (7) A) Drawing by ChemBioDraw Ultra B) Gaussian Optimized by B3LYP/cc-pVDZ

Table 7.23. In the ground state, geometrical optimization for compound (7)

Symbol	Bond lengths	Symbol	Angle angle	Symbol	Dihedral angle
C2-C1	1.358	C3-C2-C1	118.616	C4-C3-C2-C1	-0.084
C3-C2	1.458	C4-C3-C2	117.853	C5-C1-C2-C3	0.020
C4-C3	1.409	C5-C1-C2	123.121	C8-C3-C2-C1	179.899
C5-C1	1.458	C8-C3-C2	124.697	C9-C4-C3-C2	-179.983
C8-C3	1.412	C9-C4-C3	121.464	C10-C9-C4-C3	-0.031
C9-C4	1.399	C10-C9-C4	120.539	C11-C8-C3-C3	179.998
C10-C9	1.395	C11-C8-C3	121.076	O14-C4-C3-C2	0.041
C11-C8	1.387	O14-C4-C3	122.137	O15-C5-C1-C2	-179.965
O14-C4	1.364	O15-C5-C1	125.956	C16-C10-C9-C4	-179.937
O15-C5	1.206	C16-C10-C9	121.159	C20-C2-C1-C5	-179.827
C16-C10	1.508	C20-C2-C1	123.892	C23-C20-C2-C1	-2.178
C20-C2	1.505	C23-C20-C2	164.774	S24-C20-C2-C1	-1.287
C23-C20	4.767	S24-C20-C2	113.708	N25-C23-C20-C2	-173.197
S24-C20	1.840	N25-C23-C20	58.954	N26-N25-C23-C20	2.213
N25-C23	1.321	N26-N25-C23	108.229	N27-C23-C20-C2	4.487
N26-N25	1.372	N27-C23-C20	50.948	C28-N26-N25-C23	-0.066
N27-C23	1.387	C28-N26-N25	107.010	C29-N27-C23-C20	174.477
C28-N26	1.316	C29-N27-C23	129.957	C32-C29-N27-C23	96.002
C29-N27	1.463	C32-C29-N27	113.336	C36-C23-C20-C2	63.001
C32-C29	1.528	C36-C23-C20	176.178	C37-C36-C23-C20	-78.819
C36-C23	1.454	C37-C36-C23	131.915	S38-C36-C23-C20	102.978
C37-C36	1.382	S38-C36-C23	117.434	C39-C37-C36-C23	-178.553
S38-C36	1.754	C39-C37-C36	113.199	C41-C39-C37-C36	0.155
C39-C37	1.425	C41-C39-C37	112.644		
C41-C39	1.371				

The FT-IR spectra are experimentally and theoretically shown in Figure 7.35 for compound (7). The experimental measurement used KBr pullet formed. Table 7.24 compared Experimentally and theoretically results with types of vibration was calculated B3LYB/cc-pVDZ. The correlation between Experimentally and theoretically results for FT-IR analysis was shown in Figure 7.36.

(A)

(B)
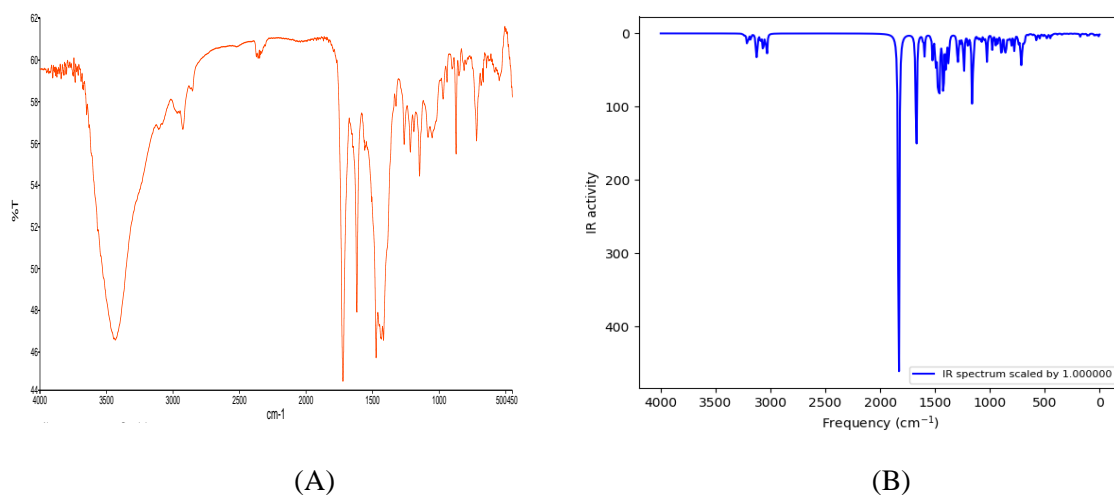
Figure 7.35. IR spectrum for compound (7). (A) Experimental (B) Theoretical results

Table 7.24. Theoretical and experimental vibrational for compound (7)

Assignments With TED	FT-IR (cm⁻¹) With KBr	Unscaled Frequencies B3LYP/cc-pVDZ	Assignments With TED	FT-IR (cm⁻¹) With KBr	Unscaled Frequencies B3LYP/cc-pVDZ
ST-CH in thiophene		3250.50	SCI-C29H30H31	1366	1374.78
STV-C37H40	3231	3235.55	STV-C37-C39		1364.93
STV-C1H7		3217.06	RO-C20H21H22	1217	1173.70
UNST-CH in thiophene		3213.00	STV-C5-O14	1266	1161.52
STV-C8H6,C11H13,C9H12	3201	3205.10	STV-N26-C28-N27	1155	1150.58
V-C9H12		3199.87	STV-N25-N26	1134	1111.95
UNSTV-C8H6,C11H13	3165	3179.73	RO-C32H33,34,35		1099.12
UNSTV-ethylene group		3131.29	SCI-C39H42,C41H43	1086	1089.58
UNSTV-C16H17,18,19		3125.38	STV-C2-C28		1056.91
UNSTV-C32H33,35		3121.66	STV-C23-N27		1022.01
UNSTV-C20H21,22		3115.53	STV-C29-C32		976.70
UNSTV-ethylene group	3081	3110.06	STV-C23-N25-N26		947.73
STV-C20H21,22	3069	3069.79	STV-C5-O14	938	893.77
STV-C32H33,H35		3042	STV-C41-S38		853.09
STV-C15H17,18,19	2937	3031.27	STV-C20-S24	808	805.35
STV-C5=O15	1717	1830.76	STV-C20-S24		777.82
VC1=C2	1705	1675.95	UNSTV-C41-S38-C36	740	747.80

71

STV-C=C in ring		1668.32	RO-N25-C23-N27	722.91
STV-C=C in thiophene	1605	1611.13	STV-triazole	693.91
STV- C in ring		1595.81	STV-N25-N26	685.51
STV-C-H in ring	1501	1538.33	RO-C36-C37-C39	587	590.49
STV-CH3		1472.91-1454.99	STV-C2-C3		542.24
SCI-C20H21,H22		1424.08	STV-C23-C36		515.80
SCI-C32H33H34H35		1401.43	STV-CH in ring		451
SCI-C16H17,18,19		1396.17	STV- C in thophen		340.16
STV-C28-N26	1439	1394.43	STV-ethylene group		306.97
UNSTV-C in ring		1378.70			

TV: Starching vibration, UN: anti, S: Symmetrical, RO: Rocking, SCI: Scissoring

Equation	y = a + b*x
Plot	B
Weight	No Weighting
Intercept	31.96263 ± 20.529
Slope	0.98094 ± 0.01033
Residual Sum of Squa	36093.39905
Pearson's r	0.99895
R-Square (COD)	0.9979
Adj. R-Square	0.99779
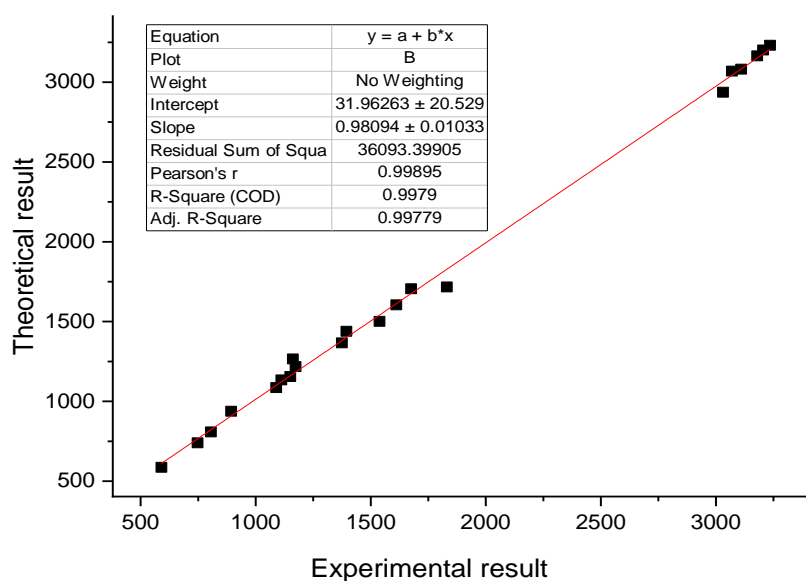
Figure 7.36. Relationship graphics for compound (7), between theoretical and experimental frequencies

The experimental Hydrogen ^{1}H NMR look Figure 7.37 and carbon ^{13}C NMR shown in Figure 7.38 chemical shifts for compound (7) were investigated in Dimethyl sulfoxide (DMSO-d6). Also in DMSO-d6 solvents, the theoretical ^{1}H and ^{13}C chemical shift values were determined using the DFT (B3LYP) method with the cc-pVDZ basis sets, all results were presents in Table 7.25 and 7.26.

Figure 7.37. Experimental ^{1}H-NMR spectrum for compound (7) in DMSO-d6
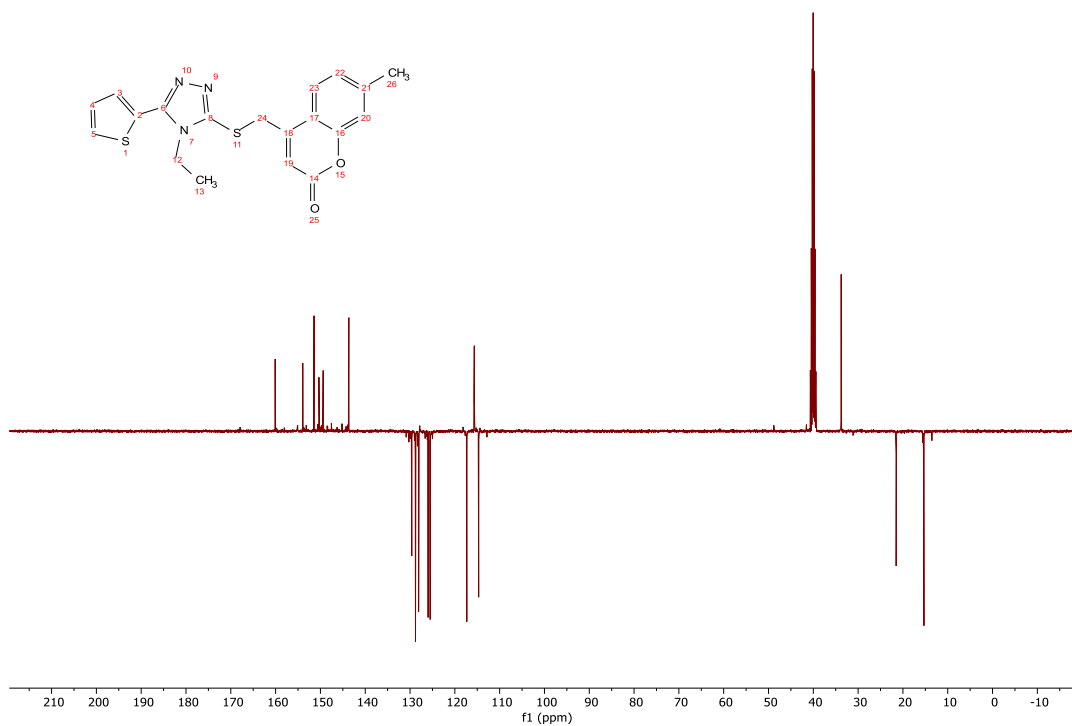
Figure 7.38. The experimental ^{13}C-NMR spectrum for compound (7) in DMSO-d6

73

Table 7.25. Experimental and theoretical chemical shifts (ppm) of ^{1}H-NMR of compound (7)

H number	Experimental Results	Theoretical Results
H6	7.85	8.73
H43	7.85	8.59
H13	7.57	8.44
H40	7.27	8.43
H42	7.27	8.32
H12	7.27	8.27
H7	6.32	7.11
H22	4.62	5.88
H21	4.62	5.62
H31	4.09	5.34
H30	4.09	5.13
H17	3.39	3.87
H18	3.39	3.87
H19	3.39	3.27
H34	1.17	2.87
H33	1.17	2.72
H35	1.17	2.66

Table 7.26. Experimental and theoretical chemical shifts (ppm) of ^{13}C-NMR of compound (7)

C number	Experimental Results	Theoretical Results
C28	160.10	161.93
C5	160.10	161.88
C4	153.90	160.71
C23	151.40	158.01
C2	150.30	157.81
C10	149.40	152.17
C36	143.50	143.92
C41	129.60	139.58
C39	128.70	132.15
C11	128.00	131.43
C8	125.90	130.12
C37	125.40	129.24
C3	117.20	124.1
C9	115.60	123.39
C1	114.40	118.05
C29	40.20	48.77
C20	33.80	48.15
C16	21.20	30.06
C32	15.30	23.21

B3LYP/cc-pVDZ was used to found Molecular electrostatic potential (MEP) for compound (7) shown in Figure 7.39. The negative region's red color is often above the atoms of two nitrogens (N25, N26) and oxygen (O15).
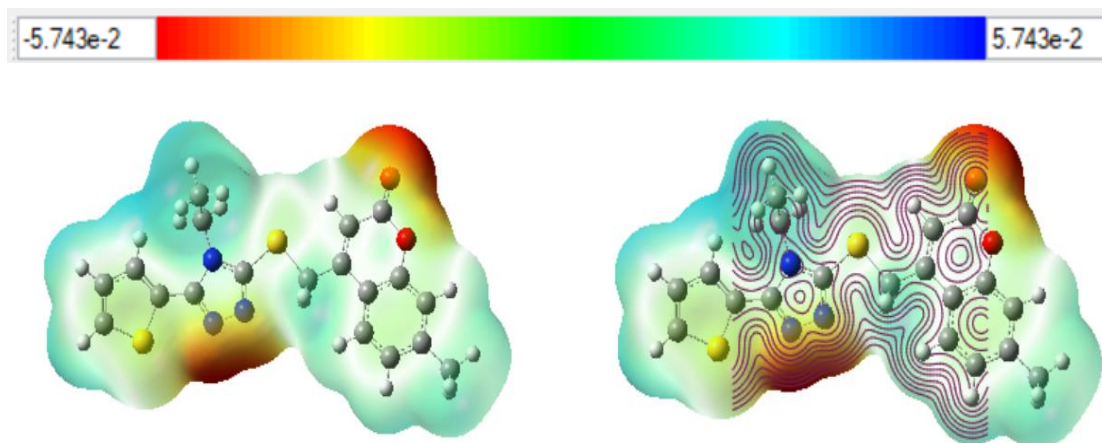
Figure 7.39. Molecular electrostatic potential for compound (7)

Mulliken population analysis for compound (7) shown in Figure 7.40 the more negative charges were distributed on the N25, N26, N27, O14 and O15.
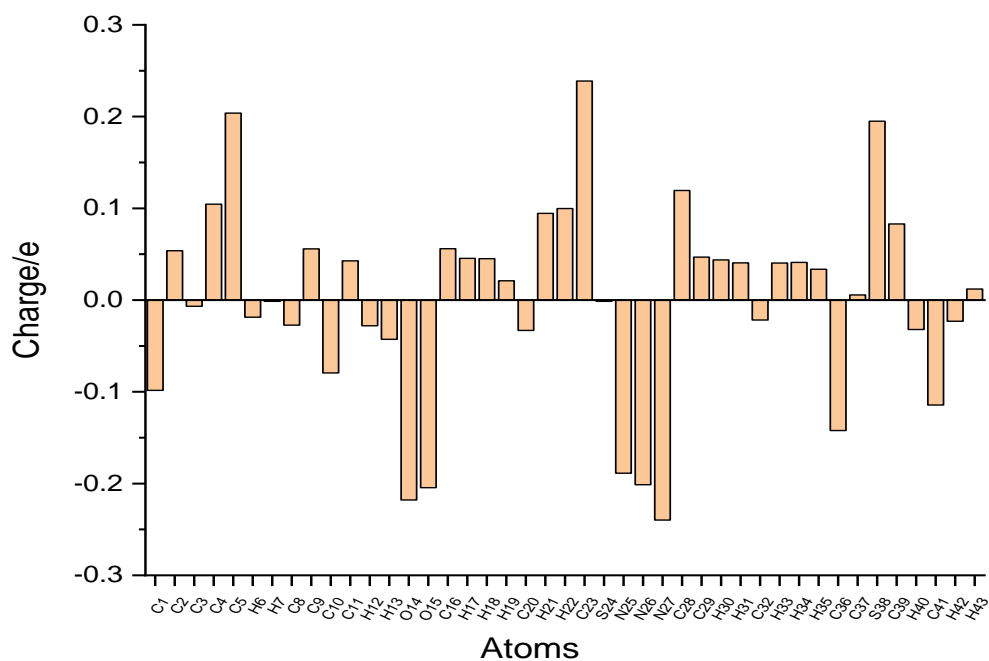
Figure 7.40. Millikan charge distribution on the compound (7)

Different parameters which are related to the inhibitor activity calculated for compound (7) used B3LYP/cc-pVDZ All parameters were shown in Table 7.27 including energy of the highest occupied molecular orbital (E_{HOMO}), energy of the lowest unoccupied molecular orbital (E_{LUMO}),

energy bandgap ($\Delta E = E_{LUMO} - E_{HOMO}$), dipole moment ($\mu$), hardness ($\eta$), softness ($\sigma$), electronegativity ($\chi$), electrophilicity index (ω), nucleophilicity (ε) index and The fraction of transferred electrons (ΔN) which is related to transfer electron between inhibitor and metal surface

Table 7.27. Calculation quantum chemical parameters for compound (7)

Parameters	Equations	Results
Total Energy (a.u)		-1845.426
μ (D)		3.277
E_{LUMO} (eV)		-1.909
E_{HOMO} (eV)		-5.886
ΔE (eV)		3.976
I	$I = -E_{HOMO}$	5.886
A	$A = -E_{LUMO}$	1.909
χ (eV)	$\chi = (I + A) / 2$	3.897
η (eV)	$\eta = (I - A) / 2$	1.988
σ (eV)	$\sigma = I/\eta$	2.960
Pi (eV)	$Pi = -\chi$	-3.897
ω (eV)	$\omega = Pi2/2\eta$	3.820
ε (eV)	$\varepsilon = Pi.\ \eta$	7.640
ΔN	$\Delta N = (\chi metal - \chi inhibitor) / 2. (\eta metal - \eta inhibitor)$	0.780

The Zero-point vibrational energy, Total energy, thermal energy, rotational constants, rotational temperatures and entropy of the molecules (7) were calculated using B3LYP/cc-pVDZ at a pressure of 1.00 atom and 298 K, Table 7.28 shows the results.

Table 7.28. Thermodynamic parameters for compound (7)

Parameters	B3LYP/cc-pVDZ
Zero-point vibrational energy(kcal/mol^{-1})	204.612
Total energy (a.u.)	-1845.426
Rotational constants (GHz)	
	0.409
	0.064
	0.056
Rotational temperatures (K)	
	0.019
	0.003
	0.0027
Entropy (Kcal mol^{-1} K^{-1})	
Rotational	0.889
Translational	0.889
Vibrational	217.832
Total	219.610

7.6. 4-(((4-ethyl-5-(thiophen-2-yl)-4H-1,2,4-triazol-3-yl)thio)methyl)-6,8-dimethyl-2H-chromen-2-one (8)

The molecular was experimentally characterized by FT-IR and NMR spectroscopy. The melting point for compound (8) (Figure 7.41) is equal to 188-190 ^{0}C which was measured by Thomas Hoover melting point. The Yield is 70% and the color is light brown.
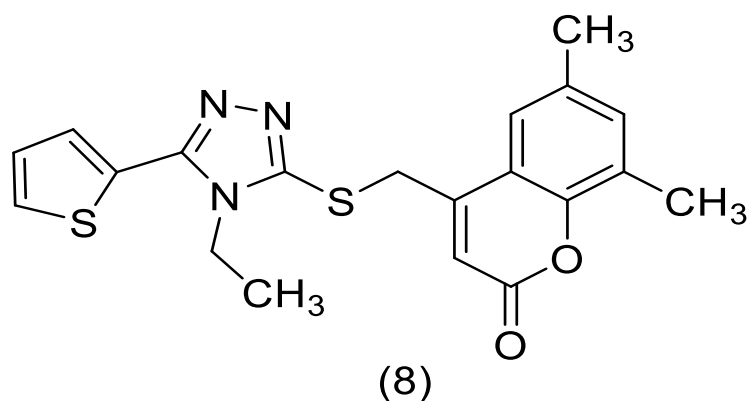
Figure 7.41. 4-(((4-ethyl-5-(thiophen-2-yl)-4H-1,2,4-triazol-3-yl)thio)methyl)-6,8-dimethyl-2H-chromen-2-one

The molecular structure of the compound (8) was determined using the Density Functional Theory (DFT/B3LYP) method in the ground state with the cc-pVDZ basis sets. Figure 7.42 show molecular structures drawing by ChemBioDraw and GAUSVIEW. The optimized geometrical parameters (bond lengths, bond angles, and torsion angles) calculated using B3LYP/cc-pVDZ techniques are listed in Table 7.29.

(A)   (B)

Figure 7.42. Structure of the compound (8) A) Drawing by ChemBioDraw Ultra B) Gaussian Optimized by B3LYP/cc-pVDZ

Table 7.29. In the ground state, geometrical optimization for compound (8)

Symbol	Bond Length	Symbol	Bond angle	Symbol	Dihedral angle
C2-C1	1.358	C3-C2-C1	118.830	C4-C3-C2-C1	-0.091
C3-C2	1.460	C4-C3-C2	117.650	C5-C1-C2-C3	0.059
C4-C3	1.406	C5-C1-C2	123.099	C8-C3-C2-C1	179.854
C5-C1	1.457	C8-C3-C2	123.999	C9-C4-C3-C2	179.994
C8-C3	1.412	C9-C4-C3	121.918	C10-C9-C4-C3	-0.024
C9-C4	1.408	C10-C9-C4	117.411	C11-C8-C3-C2	-179.989
C10-C9	1.393	C11-C8-C3	121.352	O12-C4-C3-C2	0.013
C11-C8	1.391	O12-C4-C3	122.056	O13-C5-C1-C2	179.991
O12-C4	1.367	O13-C5-C1	126.030	C14-C2-C1-C5	-179.815
O13-C5	1.206	C14-C2-C1	123.729	C17-C14-C2-C1	-6.995
C14-C2	1.505	C17-C14-C2	164.749	S18-C14-C2-C1	-0.854
C17-C14	4.767	S18-C14-C2	113.784	N19-C17-C14-C2	-166.469
S18-C14	1.841	N19-C17-C14	58.977	N20-N19-C17-C14	2.385
N19-C17	1.321	N20-N19-C17	108.227	N21-C17-C14-C2	11.011
N20-N19	1.372	N21-C17-C14	50.932	C22-N20-N19-C17	-0.052
N21-C17	1.387	C22-N20-N19	107.018	C23-N21-C17-C14	174.221
C22-N20	1.316	C23-N21-C17	129.946	C26-C23-N21-C17	96.086
C23-N21	1.463	C26-C23-N21	113.339	C30-C17-C14-C2	70.458
C26-C23	1.528	C30-C17-C14	176.067	C31-C30-C17-C14	-79.640
C30-C17	1.454	C31-C30-C17	131.920	S32-C30-C17-C14	102.161
C31-C30	1.382	S32-C30-C17	117.429	C33-C31-C30-C17	-178.547
S32-C30	1.754	C33-C31-C30	113.199	C35-C33-C31-C30	0.155
C33-C31	1.425	C35-C33-C31	112.644	C38-C9-C4-C3	179.992
C35-C33	1.371	C38-C9-C4	120.089	C42-C11-C8-C3	179.988
C38-C9	1.506	C42-C11-C8	121.521		
C42-C11	1.509				

The FT-IR spectra are experimentally and theoretically shown in Figure 7.43 for compound (8). The experimental measurement used KBr pullet formed. Table 7.30 compared Experimentally and theoretically results with types of vibration was calculated B3LYB/cc-pVDZ. The correlation between Experimentally and theoretically results for FT-IR analysis was shown in Figure 7.44.

(A)

(B)

Figure 7.43. IR spectrum for compound (8). (A) Experimental (B) Theoretical results

Table 7.30. Theoretical and experimental vibrational for compound (8)

Assignments With TED	FT-IR (cm⁻¹) With KBr	Unscaled Frequencies B3LYP/cc-pVDZ	Assignments With TED	FT-IR (cm⁻¹) With KBr	Unscaled Frequencies B3LYP/cc-pVDZ
ST-CH in thiophene	3434	3250.47	SCI-C26H27H28H29	1384	1396.18
STV-C31H34	3231	3235.32	STV-C17N21		1394.49
STV-C1H7		3216.21	RO-C23H24H25	1346	1374.95
UNST-CH in thiophene		3212.91	STV-C31-C33		1364.90
STV-C8H5	3201	3196.50	STV-C4-O12	1266	1280.49
V-C10H45		3164.47	STV-C5-O12	1115	1177.38
UNSTV-ethylene group	3165	3131.17	RO-C14H15H1		1173.74
UNSTV-C38H39H40H41		3128.74	UNSTV-ethylene group		1150.65
UNSTV-C26H27H28H29		3121.49	STV-N19-N20	1084	1112.01
UNSTV-C42H43H44H45		3119.50	RO-C26H27H28H29		1099.15
UNSTV-C14H15H16		3115.53	STV-C33H36-C35H37		1089.52
UNSTV-ethylene group	3081	3109.98	STV-C31-C33		1076.77
UNSTV-C38H39H40	3071	3098.49	UNSTV-CH3 in ring group		1054.91-1029.36
UNSTV-C42H43H44		3086.07	STV-C17-N21		1022.10
STV-C14H15H16	2923	3070.42	STV-C11-C42		988.23
STV-C23H24H25		3062.26	STV-C23-C26		976.76
STV-C26H27H28H29		3042.19	STV-C5-O12	940	945.15, 922.29

STV-C38H30H40H41		3038.72	RO-C33H36	925	913.56
STV-C42H43H44H45		3028.29	RO-S-C35	831	853.15
STV-C5=O13	1722	1828.34	STV-C31H34		836.04
STVC1=C2	1705	1678.54	STV-ethylene group		803.52
STV-C=C in ring	1630	1657.43	RO-C4-C3-C9		789.38
STV-C=C in thiophene	1589	1611.115-1521.73	STV-S18-C14	798	784.38
STV- C in ring		1503.18	STV-S32-C30	751	747.78
SCI-C23H24H25	1501	1493.81	RO-N21-C17-N10		722.93
RO-C26H27H28	1477	1478.77	STV-O13=C5-O12	712	719.88
STV-C22=N20		1467.95	STV-ethylene group		306.97
UNSTV-C26H27H28H29		1461.59	STV-N19-N20		694.32-685.45
UNSTV-C42H43H44H45		1455.71	STV-C in thiophen ring		590.38
UNSTV-C38H39H40H41	1441	1452.35-1448.41	STV-C in a ring		580.58,539.73
SCI-C14H15H16		1424.74	STV-C in thiophen ring		510.70
STV-C22-N21	1417	1420.00	STV-C17-C30		484.03
SCI-C14H15H16		1412.46	STV-S32-C35	531	339.86
SCI-C26H27H28H29		1401.59	STV-ethylene group		314.19

TV: Starching vibration, UN: anti, S: Symmetrical, RO: Rocking, SCI: Scissoring

Equation	y = a + b*x
Plot	B
Weight	No Weighting
Intercept	-16.10122 ± 29.74289
Slope	1.00545 ± 0.01437
Residual Sum of Square	79684.28591
Pearson's r	0.99786
R-Square (COD)	0.99573
Adj. R-Square	0.99553

Figure 7.44. Relationship graphics for compound (8), between theoretical and experimental frequencies

The experimental Hydrogen ¹H NMR look Figure 7.45 and carbon ¹³C NMR shown in Figure 7.46 chemical shifts for compound (8) were investigated in Dimethyl sulfoxide (DMSO-d6). Also in DMSO-d6 solvents, the theoretical ¹H and ¹³C chemical shift values were determined using the DFT (B3LYP) method with the cc-pVDZ basis sets, all results were presents in Table 7.31 and 7.32.

Figure 7.45. Experimental ¹H-NMR spectrum for compound (8) in DMSO-d6

Figure 7.46. The experimental ¹³C-NMR spectrum for compound (8) in DMSO-d6

81

Table 7.31. Experimental and theoretical chemical shifts (ppm) of ^{1}H-NMR of compound (8)

H number	Experimental Results	Theoretical Results
H37	7.80	7.88
H46	7.56	7.87
H6	7.52	7.75
H34	7.35	7.71
H36	7.26	7.60
H7	6.42	6.43
H16	4.62	5.21
H15	4.62	4.90
H25	4.08	4.63
H24	4.08	4.42
H39	3.18	3.10
H40	3.18	3.09
H44	3.18	3.08
H43	2.51	3.07
H41	2.51	2.56
H45	2.51	2.54
H28	1.19	2.16
H27	1.19	2.01
H29	1.19	1.94

Table 7.32. Experimental and theoretical chemical shifts (ppm) of ^{13}C-NMR of compound (8)

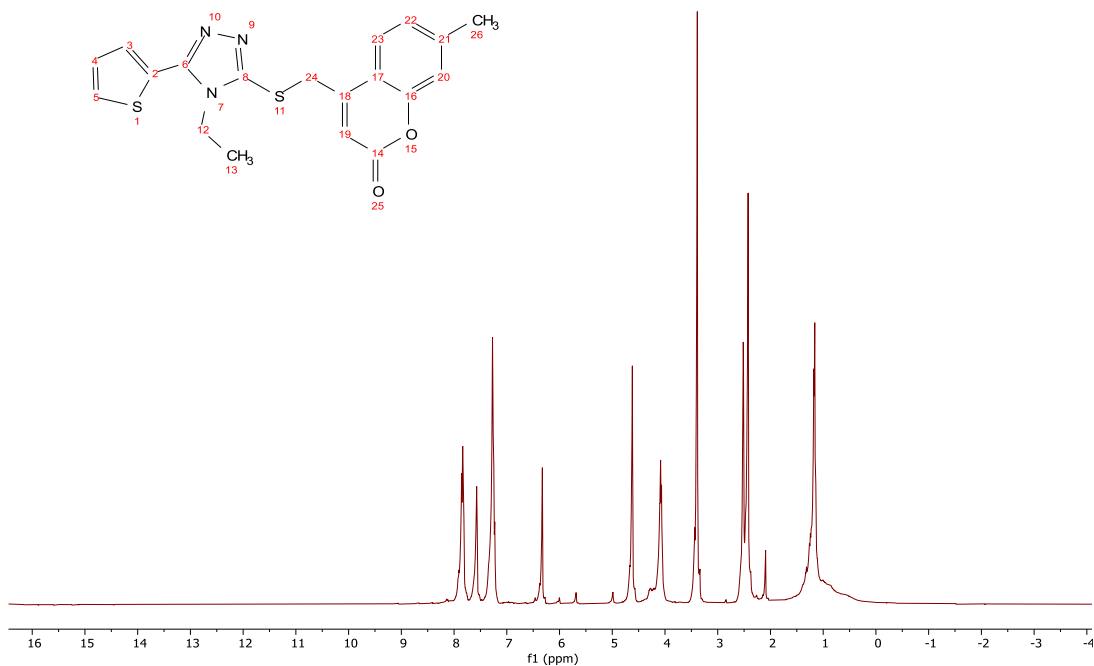| C number	Experimental Results	Theoretical Results
C22	160.07	161.95
C5	151.7	161.79
C2	150.33	158.11
C17	150.31	158.01
C4	149.49	157.57
C30	134.82	143.94
C11	133.50	142.17
C10	129.63	140.07
C35	128.79	139.57
C9	127.10	135.15
C33	127.06	132.12
C31	125.79	129.24
C8	123.15	127.73
C3	117.59	126.06
C1	115.41	118.62
C23	40.57	48.77
C14	34.01	48.61
C42	20.87	29.16
C38	15.64	25.60
C26	15.26	23.22

B3LYP/cc-pVDZ was used to found Molecular electrostatic potential (MEP) for compound (8) shown in Figure 7.47. The negative region's red color is often above the atoms of two nitrogens (N19, N20) and oxygen (O13, O12).

Figure 7.47. Molecular electrostatic potential for compound (8)

Mulliken population analysis for compound (8) shown in Figure 7.48 the more negative charges was distributed on the N19, N20, N21, O12 and O13, C1, C30.

Figure 7.48. Millikan charge distribution on the compound (8)

Different parameters which are related to the inhibitor activity calculated for compound (8) used B3LYP/cc-pVDZ All parameters were shown in Table 7.33 including energy of the highest

occupied molecular orbital (E_{HOMO}), energy of the lowest unoccupied molecular orbital (E_{LUMO}), energy bandgap ($\Delta E = E_{LUMO} - E_{HOMO}$), dipole moment ($\mu$), hardness ($\eta$), softness ($\sigma$), electronegativity ($\chi$), electrophilicity index (ω), nucleophilicity (ε) index and The fraction of transferred electrons (ΔN) which is related to transfer electron between inhibitor and metal surface

Table 7.33. Calculation quantum chemical parameters for compound (8)

| Parameters	Equations	Results
Total Energy (a.u)		-1884.745
μ (D)		3.172
E_{LUMO} (eV)		-1.883
E_{HOMO} (eV)		-5.877
ΔE (eV)		3.993
I	$I = -E_{HOMO}$	5.877
A	$A = -E_{LUMO}$	1.883
χ (eV)	$\chi = (I + A) / 2$	3.880
η (eV)	$\eta = (I - A) / 2$	1.996
σ (eV)	$\sigma = I/\eta$	2.943
Pi (eV)	$Pi = -\chi$	-3.880
ω (eV)	$\omega = Pi2/2\eta$	3.770
ε (eV)	$\varepsilon = Pi. \eta$	7.749
ΔN	$\Delta N = (\chi_{metal} - \chi_{inhibitor}) / 2. (\eta_{metal} - \eta_{inhibitor})$	0.781

The Zero-point vibrational energy, Total energy, thermal energy, rotational constants, rotational temperatures and entropy of the molecules (8) were calculated using B3LYP/cc-pVDZ at a pressure of 1.00 atom and 298 K, Table 7.34 shows the results.

Table 7.34. Thermodynamic parameters for compound (8)

Parameters	B3LYP/cc-pVDZ
Zero-point vibrational energy(kcal/mol^{-1})	221.842
Total energy (a.u.)	-1884.745
Rotational constants (GHz)	
	0.373
	0.062
	0.053
Rotational temperatures (K)	
	0.0179
	0.0029
	0.0025
Entropy (Kcal mol^{-1} K^{-1})	
Rotational	0.889
Translational	0.889
Vibrational	236.127
Total	237.904

7.7. 4-(((4-ethyl-5-(thiophen-2-yl)-4H-1,2,4-triazol-3-yl)thio)methyl)-6,7-dimethyl-2H-chromen-2-one (9)

The molecular was experimentally characterized by FT-IR and NMR spectroscopy. The melting point for compound (9) (Figure 7.49) is equal to 165-167 ^{0}C which was measured by Thomas Hoover melting point. The Yield is 75% and the color is white.

(9)

Figure 7.49. 4-(((4-ethyl-5-(thiophen-2-yl)-4H-1,2,4-triazol-3-yl)thio)methyl)-6,7-dimethyl-2H-chromen-2-one

The molecular structure of the compound (9) was determined using the Density Functional Theory (DFT/B3LYP) method in the ground state with the cc-pVDZ basis sets. Figure 7.50 shows molecular structures drawing by ChemBioDraw and GAUSVIEW. The optimized geometrical parameters (bond lengths, bond angles, and torsion angles) calculated using B3LYP/cc-pVDZ techniques are listed in Table 7.35.

(A)   (B)

Figure 7.50. Structure of the compound (9) A) Drawing by ChemBioDraw Ultra B) Gaussian Optimized by B3LYP/cc-pVDZ

Table 7.35. In the ground state, geometrical optimization for compound (9)

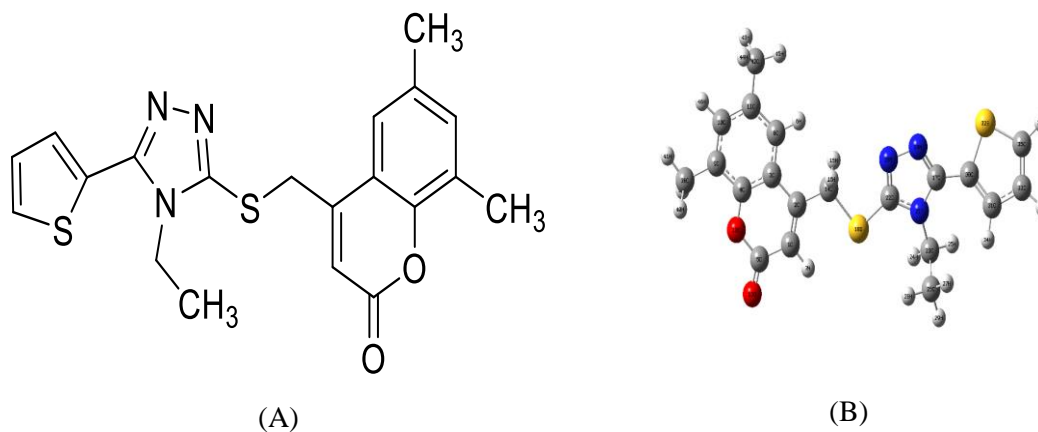| Symbol	Bond Length	Symbol	Bond angle	Symbol	Dihedral angle
C2-C1	1.358	C3-C2-C1	118.557	C4-C3-C2-C1	-0.110
C3-C2	1.458	C4-C3-C2	117.769	C5-C1-C2-C3	0.000
C4-C3	1.406	C5-C1-C2	123.183	C8-C3-C2-C1	179.966
C5-C1	1.458	C8-C3-C2	124.701	C9-C8-C3-C2	179.912
C8-C3	1.411	C9-C8-C3	91.522	C10-C8-C3-C2	179.903
C9-C8	2.423	C10-C8-C3	122.402	O11-C4-C3-C2	0.100
C10-C8	1.392	O11-C4-C3	122.372	O12-C5-C1-C2	-179.934
O11-C4	1.365	O12-C5-C1	125.868	C13-C2-C1-C5	-179.795
O12-C5	1.206	C13-C2-C1	123.839	C16-C13-C2-C1	4.433
C13-C2	1.505	C16-C13-C2	164.567	S17-C13-C2-C1	-1.110
C16-C13	4.769	S17-C13-C2	113.652	N18-C16-C13-C2	179.530
S17-C13	1.840	N18-C16-C13	59.002	N19-N18-C16-C13	2.376
N18-C16	1.321	N19-N18-C16	108.234	N20-C16-C13-C2	-2.983
N19-N18	1.372	N20-C16-C13	50.903	C21-N19-N18-C16	-0.085
N20-C16	1.387	C21-N19-N18	107.007	C22-N20-C16-C13	174.227
C21-N19	1.316	C22-N20-C16	129.953	C25-C22-N20-C16	95.856
C22-N20	1.463	C25-C22-N20	113.337	C29-C16-C22-C2	56.271
C25-C22	1.528	C29-C16-C22	176.018	C30-C29-C16-C13	-79.305
C29-C16	1.454	C30-C29-C16	131.929	S31-C29-C16-C13	102.442
C30-C29	1.382	S31-C29-C16	117.427	C32-C30-C29-C16	-178.606
S31-C29	1.755	C32-C30-C29	113.201	C34-C32-C30-C29	0.162
C32-C30	1.425	C34-C32-C30	112.649	C37-C10-C8-C3	-179.953
C34-C32	1.371	C37-C10-C8	120.413	C41-C9-C10-C3	179.944
C37-C10	1.509	C41-C9-C10	150.850	C45-C9-C8-C3	-0.009
C41-C9	1.507	C45-C9-C8	89.101		
C45-C9	1.394				

The FT-IR spectra are experimentally and theoretically shown in Figure 7.51 for compound (9). The experimental measurement used KBr pullet formed. Table 7.36 compared between Experimentally and theoretically results with types of vibration was calculated B3LYB/cc-pVDZ. The correlation between Experimentally and theoretically results for FT-IR analysis was shown in Figure 7.52.
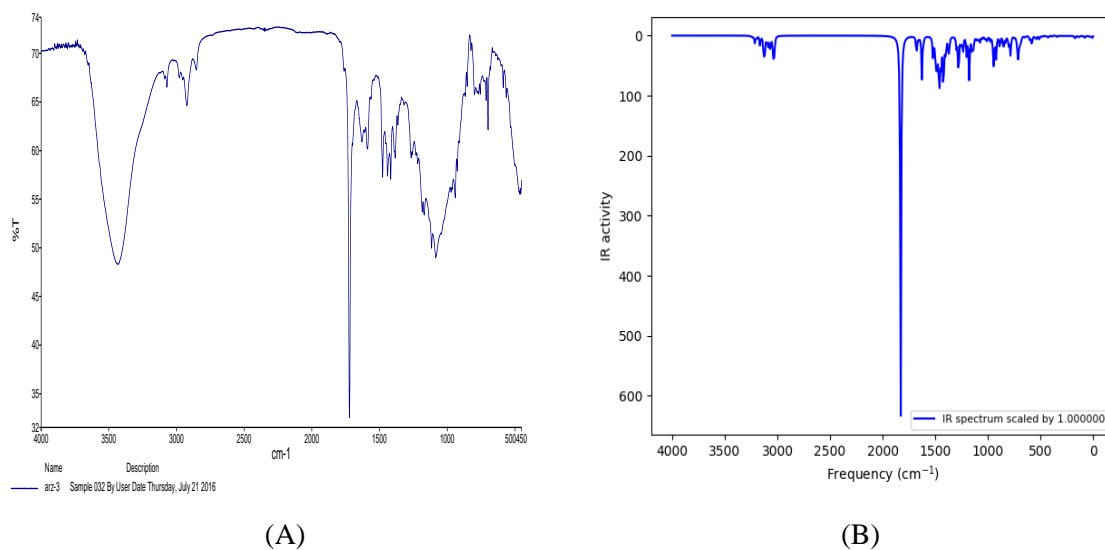
(A)

(B)

Figure 7.51. IR spectrum for compound (9). (A) Experimental (B) Theoretical results

Table 7.36. Theoretical and experimental vibrational for compound (9)

Assignments With TED	FT-IR (cm⁻¹) With KBr	Unscaled Frequencies B3LYP/cc-pVDZ	Assignments With TED	FT-IR (cm⁻¹) With KBr	Unscaled Frequencies B3LYP/cc-pVDZ
ST-CH in thiophene	3435	3250.46	UNSTV-CH3 in ring	1434	1447.59
STV-C30H33	3105	3235.82	STV-C21-N20	1417	1420.19
STV-C1H7		3217.09	STV-C16-N20, C21=N19		1394.45
UNST-CH in thiophene		3213.00	RO-ethylene group		1375.13
STV-C45H46		3198.20	STV-C=C in thiophene	1382	1365.04
STV-C8H6		3189.42	STV-C in ring		1364.43
UNSTV-ethylene group		3131.56	RO-C13H14H15		1267.78
UNSTV-C41H42H43H44		3124.80	STV-CH in thiophene	1212	1237.06
UNSTV-C25H26H27H28		3121.64	STV-C1-C5	1126	1217.71
UNSTV-C37H38H39H40		3120.34	RO-C13H14H15	1115	1172.45
UNSTV-C13H14H15		3115.93	STV-C5-O10		1167.11
UNSTV-ethylene group		3110.19	UNSTV-C in ring		1149.18
UNSTV-C41H43H44		3080.40	STV-N18-N19	1084	1111.57
STV-C13H14H15		3070.35	RO-C25H26H27H28		1099.19
STV-C22H23H24	2922	3062.43	STV-C32H35-C34H36		1089.84
STV-C25H26H27H28		3042.44	STV-C30-C31		1076.71
STV-C41H42H43H44		3026.13	UNSTV-CH3 in ring group	1026	1061.04-1024.68

STV-C37H38H39H40		3023.89	STV-C16-N20		1021.76
STV-C5=O12	1722	1828.52	STV-C22-C25		976.89
STVC1=C2	1704	1675.72	STV-C5-O10		930.73
STV-C=C in ring	1621	1670.13	STV-C in thiophene	940	852.85
STV-C=C in thiophene	1556	1610.89	STV-C13-S17	798	783.47
STV- C=C in ring		1594.06, 1529.50	STV-C29-S31	770	747.59
STV-C32=C34	1501	1521.55	STV-C in ring		735.20
SCI-C22H23H24		1493.54	RO-C16-N18-N20	720	723.03
SCI-C25H26H27	1468	1478.48	RO-C21-N19-N20		685.49
STV-C21=N19, C16=N18		1467.71	RO-C29-C30-C32		590.08
SCI-C25H26H27H28		1461.81	RO-C13-H14H15		541.00
UNSTV-CH3 in ring		1461.12	RO-C29-S31-C34		484.37
STV-C21=N19	1441	1458.55			

TV: Starching vibration, UN: anti, S: Symmetrical, RO: Rocking, SCI: Scissoring

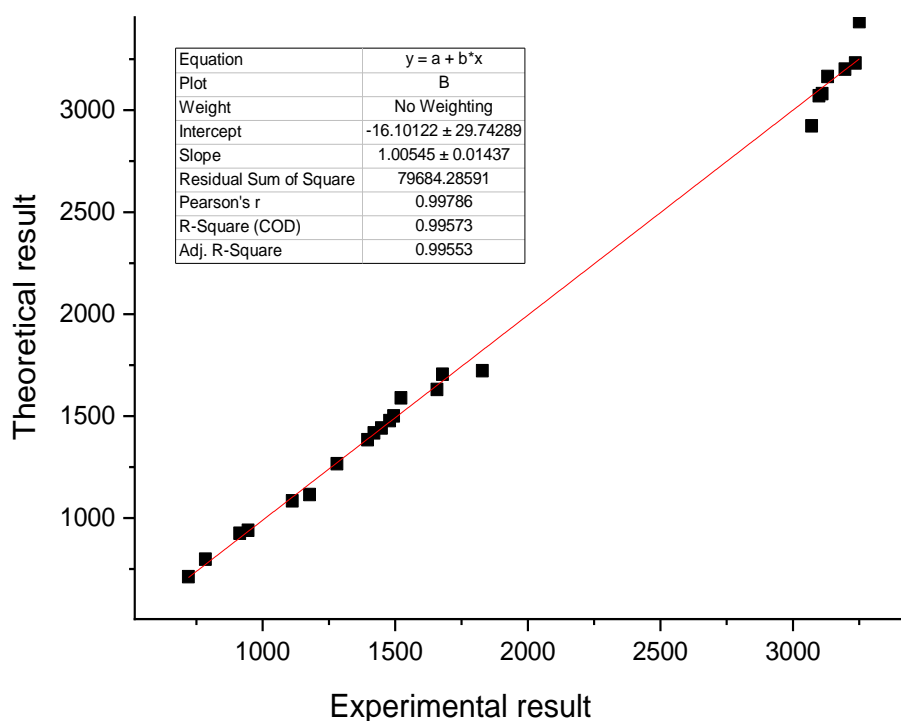| Equation	y = a + b*x
Plot	B
Weight	No Weighting
Intercept	5.22705 ± 35.836
Slope	0.9849 ± 0.02107
Residual Sum of Squar	101442.73423
Pearson's r	0.99546
R-Square (COD)	0.99093
Adj. R-Square	0.99048
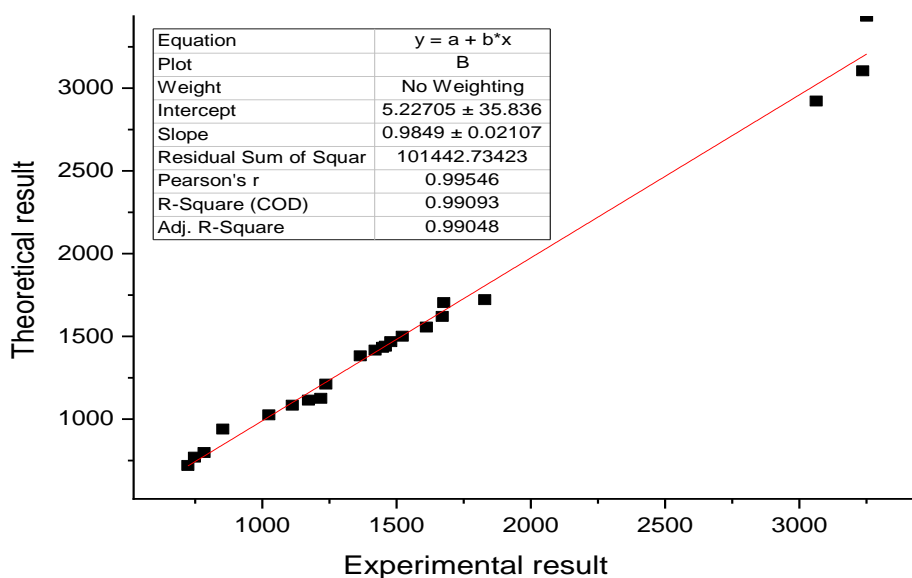
Figure 7.52. Relationship graphics for compound (9), between theoretical and experimental frequencies

The experimental Hydrogen ^{1}H-NMR look Figure 7.53 and carbon ^{13}C NMR shown in Figure 7.54 chemical shifts for compound (9) were investigated in Dimethyl sulfoxide (DMSO-d6). Also in DMSO-d6 solvents, the theoretical ^{1}H and ^{13}C chemical shift values were determined using the DFT (B3LYP) method with the cc-pVDZ basis sets, all results were presents in Table 7.37 and 7.38.
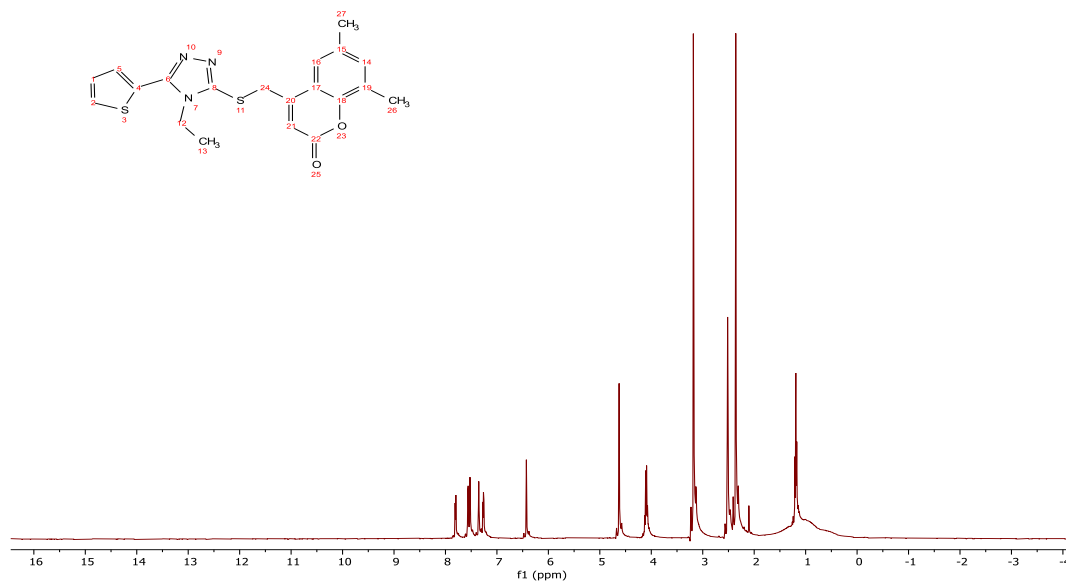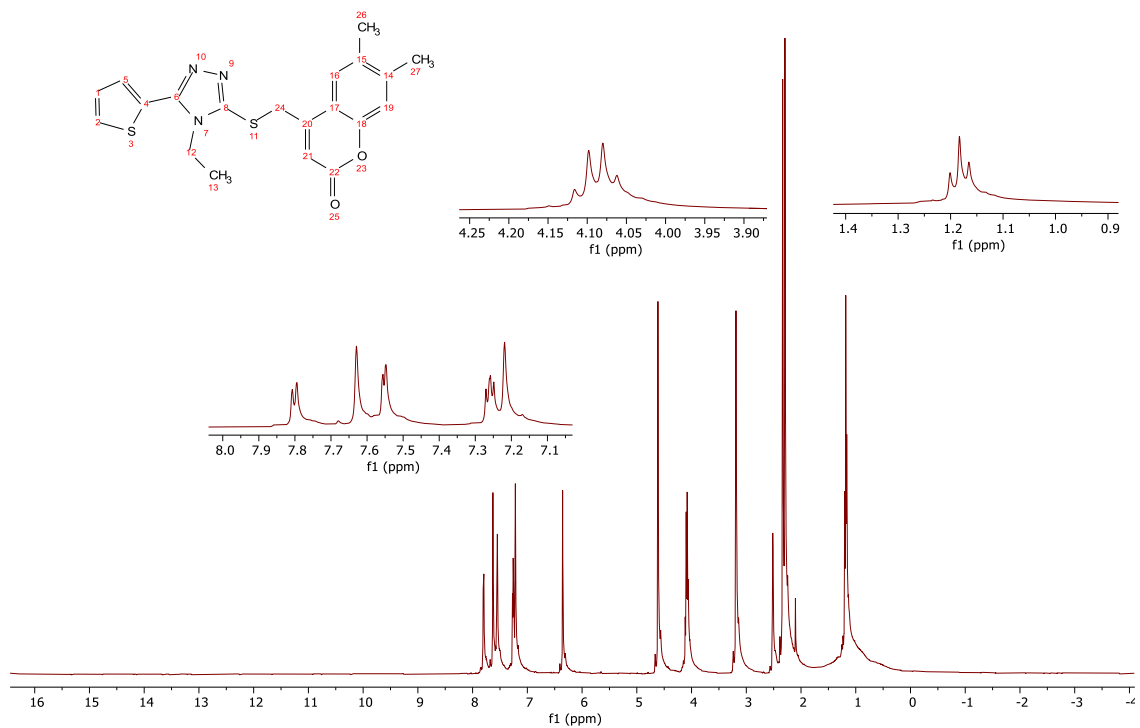
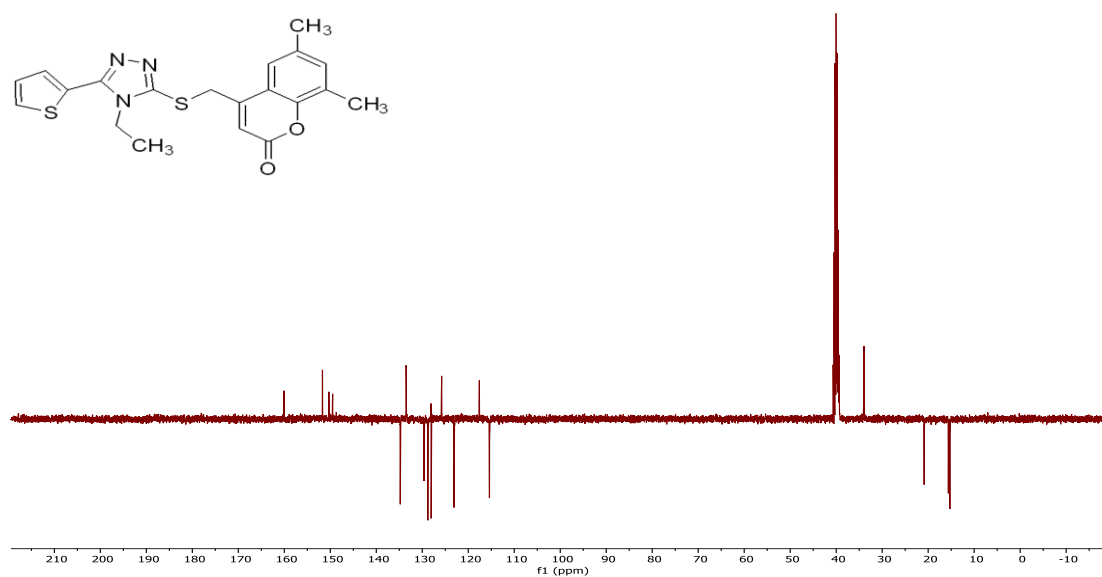**Figure 7.53.** Experimental ^{1}H-NMR spectrum for compound (9) in DMSO-d6
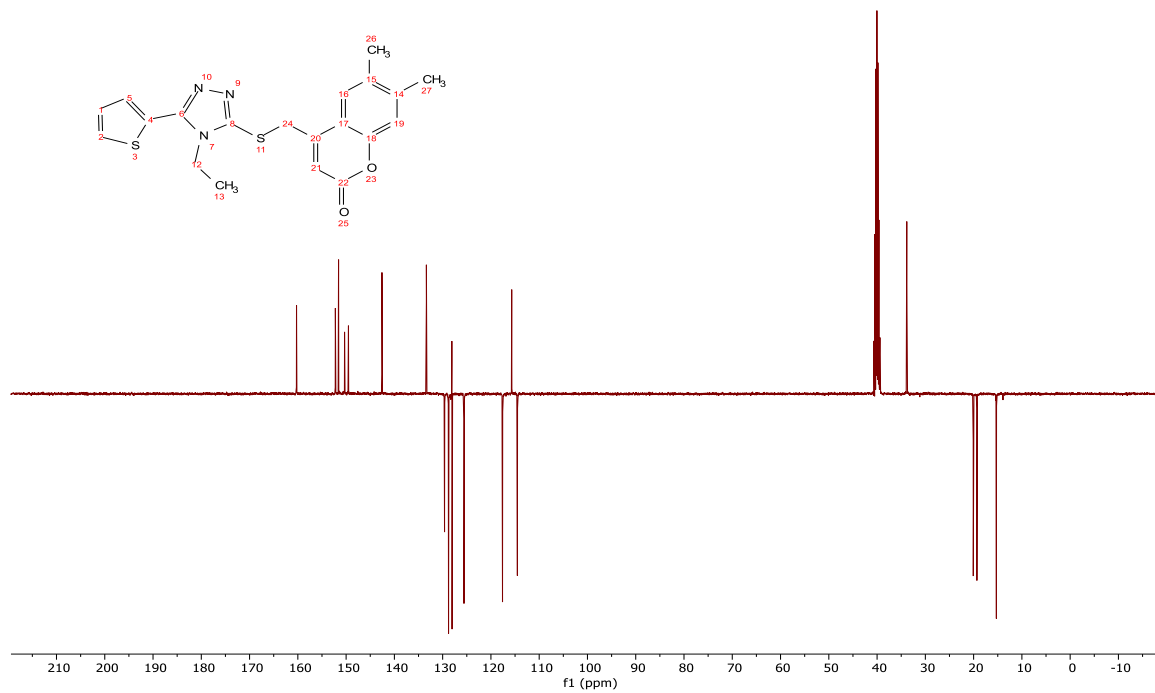
Figure 7.54. The experimental ^{13}C-NMR spectrum for compound (9) in DMSO-d6

Table 7.37. Experimental and theoretical chemical shifts (ppm) of ^{1}H-NMR of compound (9)

H number	Experimental Results	Theoretical Results
H36	7.81	7.67
H6	7.63	7.66
H46	7.55	7.46
H33	7.25	7.36
H35	7.22	7.35
H7	6.36	6.31
H15	4.62	5.09
H14	4.62	4.84
H24	4.09	4.46
H23	4.09	4.28
H43	3.12	2.81
H44	3.12	2.8
H39	3.12	2.75
H38	2.31	2.74
H40	2.31	2.62
H42	2.31	2.58
H27	1.18	2.22
H26	1.18	1.95
H28	1.18	1.73

Table 7.38. Experimental and theoretical chemical shifts (ppm) of ^{13}C-NMR of compound (9)

C number	Experimental Results	Theoretical Results
C4	160.28	160.13
C21	152.23	159.98
C5	151.56	159.86
C16	150.32	156.76
C2	149.51	154.55
C9	142.57	148.79
C29	133.37	146.31
C10	129.61	139.71
C34	128.78	138.9
C32	128.10	130.42
C8	128.05	129.93
C30	125.58	125.67
C3	117.60	124.7
C45	115.69	124.48
C1	114.52	119.92
C13	40.19	48.38
C22	30.85	48.15
C41	20.07	29.29
C37	19.31	28.66
C25	15.29	23.41

B3LYP/cc-pVDZ was used to found Molecular electrostatic potential (MEP) for compound (9) shown in Figure 7.55. The negative region's red color is often above the atoms of two nitrogens (N18, N19) and oxygen (O11, O12).
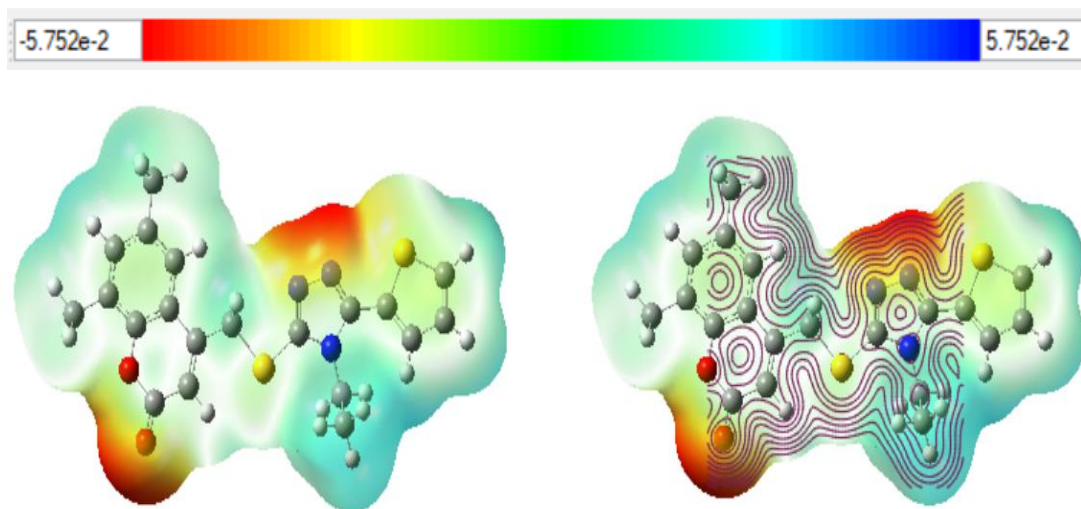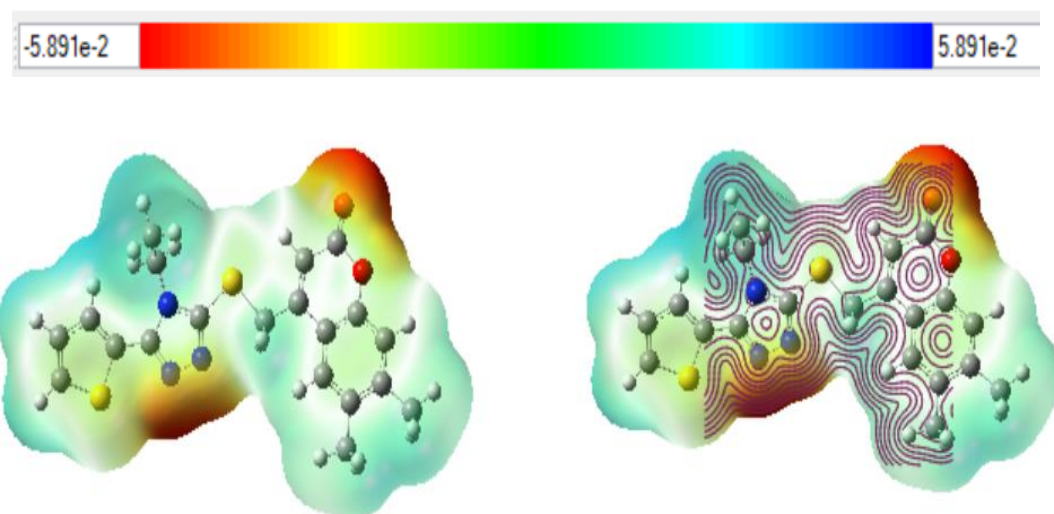
Figure 7.55. Molecular electrostatic potential for compound (9)

Mulliken population analysis for compound (9) shown in Figure 7.56 the more negative charges were distributed on the N18, N19, N20, O11, O12, C9, C10 and C28.
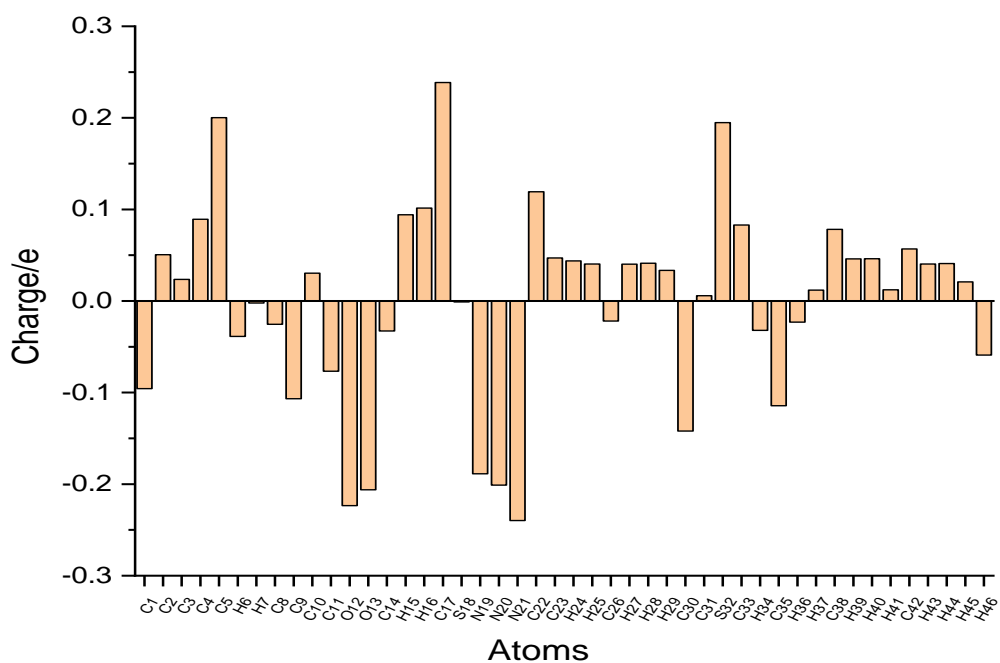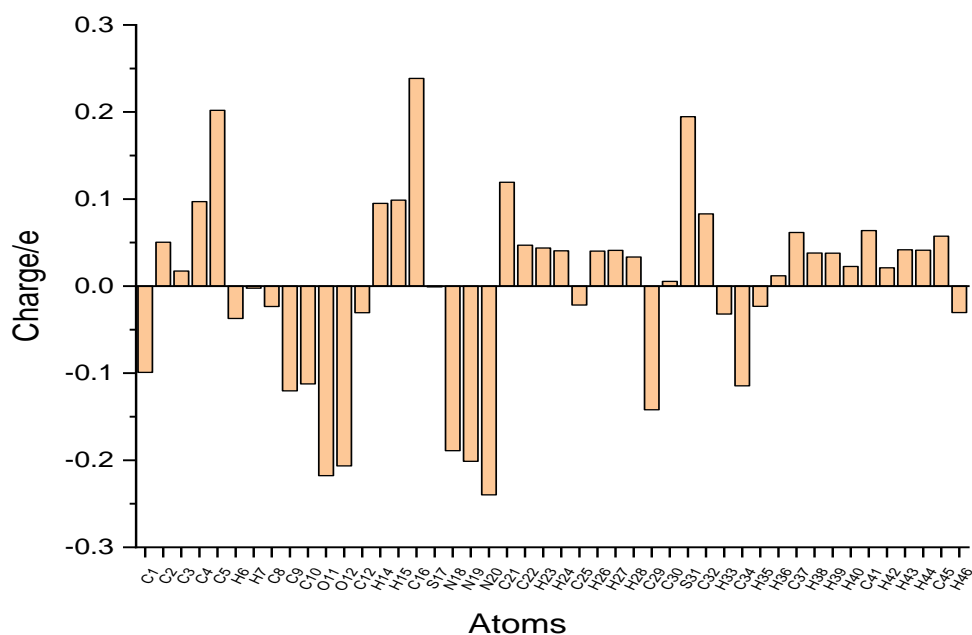

Figure 7.56. Millikan charge distribution on the compound (9)

Different parameters which are related to the inhibitor activity calculated for compound (9) used B3LYP/cc-pVDZ All parameters were shown in Table 7.39 including energy of the highest occupied molecular orbital (E_{HOMO}), energy of the lowest unoccupied molecular orbital (E_{LUMO}),

energy bandgap ($\Delta E = E_{LUMO} - E_{HOMO}$), dipole moment ($\mu$), hardness ($\eta$), softness ($\sigma$), electronegativity ($\chi$), electrophilicity index (ω), nucleophilicity (ε) index and The fraction of transferred electrons (ΔN) which is related to transfer electron between inhibitor and metal surface

Table 7.39. Calculation quantum chemical parameters for compound (9)

Parameters	Equations	Results
Total Energy (a.u)		-1884.744
μ (D)		3.343
E_{LUMO} (eV)		-1.855
E_{HOMO} (eV)		-5.870
ΔE (eV)		4.014
I	$I = -E_{HOMO}$	5.870
A	$A = -E_{LUMO}$	1.855
χ (eV)	$\chi = (I + A) / 2$	3.863
η (eV)	$\eta = (I - A) / 2$	2.007
σ (eV)	$\sigma = I/\eta$	2.924
Pi (eV)	$Pi = -\chi$	-3.863
ω (eV)	$\omega = Pi2/2\eta$	3.717
ε (eV)	$\varepsilon = Pi. \eta$	7.755
ΔN	$\Delta N = (\chi metal - \chi inhibitor) / 2. (\eta metal - \eta inhibitor)$	0.781

The Zero-point vibrational energy, Total energy, thermal energy, rotational constants, rotational temperatures and entropy of the molecules (9) were calculated using B3LYP/cc-pVDZ at a pressure of 1.00 atom and 298 K, Table 7.40 shows the results.

Table 7.40. Thermodynamic parameters for compound (9)

Parameters	B3LYP/cc-pVDZ
Zero-point vibrational energy(kcal/mol^{-1})	221.912
Total energy (a.u.)	-1884.744
Rotational constants (GHz)	
	0.340
	0.062
	0.053
Rotational temperatures (K)	
	0.0163
	0.0030
	0.0025
Entropy (Kcal mol^{-1} K^{-1})	
Rotational	0.889
Translational	0.889
Vibrational	236.049
Total	237.826

7.8. 4-(((4-ethyl-5-(thiophen-2-yl)-4H-1,2,4-triazol-3-yl)thio)methyl)-7,8-dimethyl-2H-chromen-2-one (10)

The molecular was experimentally characterized by FT-IR and NMR spectroscopy. The melting point for compound (10) (Figure 7.57) is equal to 175-177 ^{0}C which was measured by Thomas Hoover melting point. The Yield is 75% and the color is Brown.
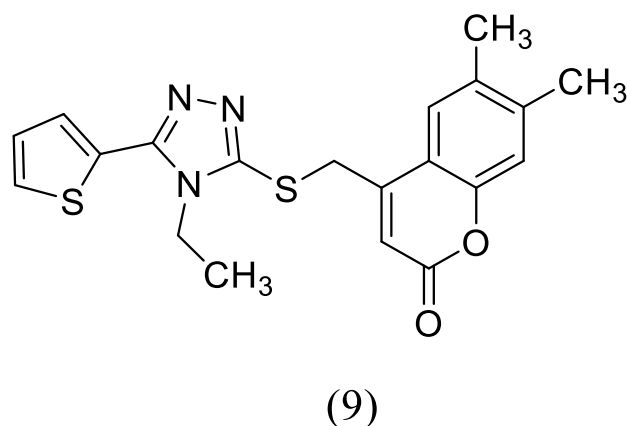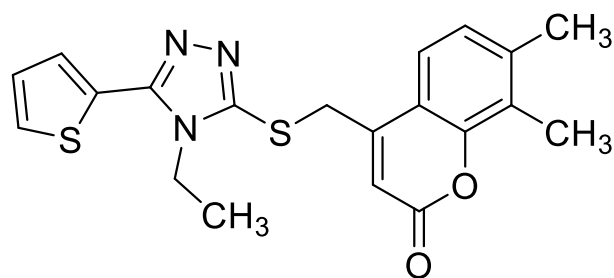

(10)

Figure 7.57. 4-((((4-ethyl-5-(thiophen-2-yl)-4H-1,2,4-triazol-3-yl)thio)methyl)-7,8-dimethyl-2H-chromen-2-one

The molecular structure of the compound (10) was determined using the Density Functional Theory (DFT/B3LYP) method in the ground state with the cc-pVDZ basis sets. Figure 7.58 show molecular structures drawing by ChemBioDraw and GAUSVIEW. The optimized geometrical parameters (bond lengths, bond angles, and torsion angles) calculated using B3LYP/cc-pVDZ techniques are listed in Table 7.41.
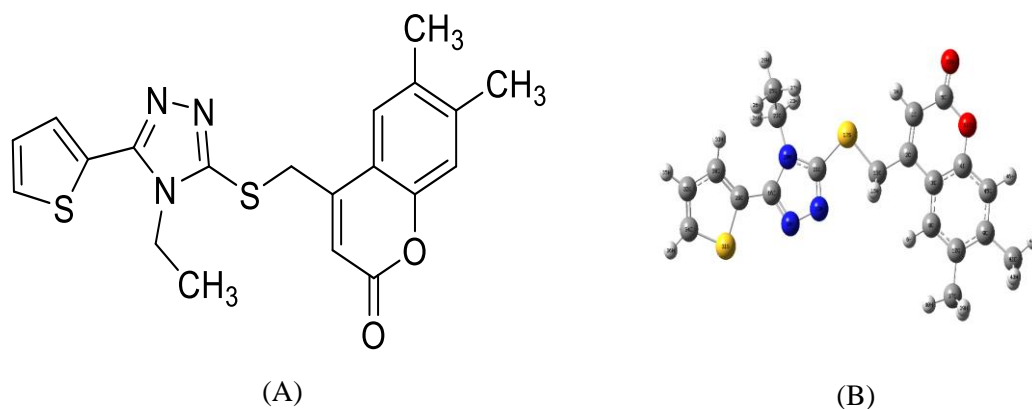

(A)   (B)
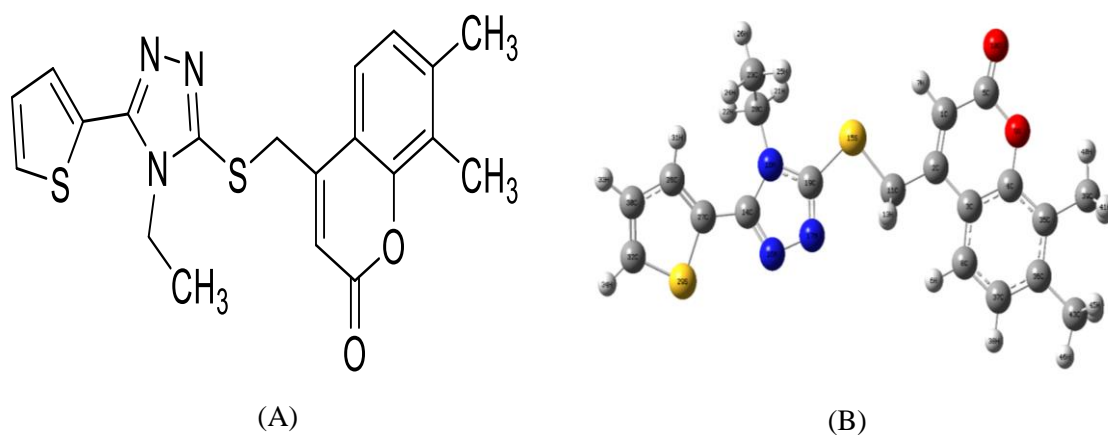
Figure 7.58. Structure of the compound (10) A) Drawing by ChemBioDraw Ultra B) Gaussian Optimized by B3LYP/cc-pVDZ

Table 7.41. In the ground state, geometrical optimization for compound (10)

Symbol	Bond Length	Symbol	Bond angle	Symbol	Dihedral angle
C2-C1	1.357	C3-C2-C1	118.945	C4-C3-C2-C1	-0.070
C3-C2	1.459	C4-C3-C2	118.104	C5-C1-C2-C3	0.016
C4-C3	1.411	C5-C1-C2	122.840	C8-C3-C2-C1	179.900
C5-C1	1.456	C8-C3-C2	124.071	O9-C4-C3-C2	0.025
C8-C3	1.408	O9-C4-C3	121.082	O10-C5-C1-C2	-179.964
O9-C4	1.368	O10-C5-C1	126.079	C11-C2-C1-C5	-179.836
O10-C5	1.207	C11-C2-C1	123.678	C14-C11-C2-C1	-2.263
C11-C2	1.506	C14-C11-C2	164.731	S15-C11-C2-C1	-1.336
C14-C11	4.768	S15-C11-C2	113.702	N16-C14-C11-C2	-173.209
S15-C11	1.841	N16-C14-C11	58.971	N17-N16-C14-C11	2.191
N16-C14	1.321	N17-N16-C14	108.231	N18-C14-C11-C2	4.500
N17-N16	1.372	N18-C14-C11	50.930	C19-N17-N16-C14	-0.068
N18-C14	1.387	C19-N17-N16	107.013	C20-N18-C14-C11	174.510
C19-N17	1.316	C20-N18-C14	129.957	C23-C20-N18-C14	96.000
C20-N18	1.463	C23-C20-N18	113.334	C27-C14-C11-C2	62.642
C23-C20	1.528	C27-C14-C11	176.185	C28-C27-C14-C11	-78.472
C27-C14	1.454	C28-C27-C14	131.917	S29-C27-C14-C11	103.324
C28-C27	1.382	S29-C27-C14	117.434	C30-C28-C27-C14	-178.554
S29-C27	1.754	C30-C28-C27	113.200	C32-C30-C28-C27	0.155
C30-C28	1.425	C32-C30-C28	112.645	C35-C4-C3-C2	179.986
C32-C30	1.371	C35-C4-C3	122.521	C36-C35-C4-C3	-0.020
C35-C4	1.407	C36-C35-C4	118.202	C37-C8-C3-C2	-179.970
C36-C35	1.408	C37-C8-C3	120.408	C39-C35-C4-C3	-179.987
C37-C8	1.387	C39-C35-C4	120.622	C43-C36-C35-C4	-179.936
C39-C35	1.508	C43-C36-C35	120.216		
C43-C36	1.507				

The FT-IR spectra are experimentally and theoretically shown in Figure 7.59 for compound (10). The experimental measurement used KBr pullet formed. Table 7.42 compared Experimentally and theoretically results with types of vibration was calculated B3LYB/cc-pVDZ. The correlation between Experimentally and theoretically results for FT-IR analysis was shown in Figure 7.60.
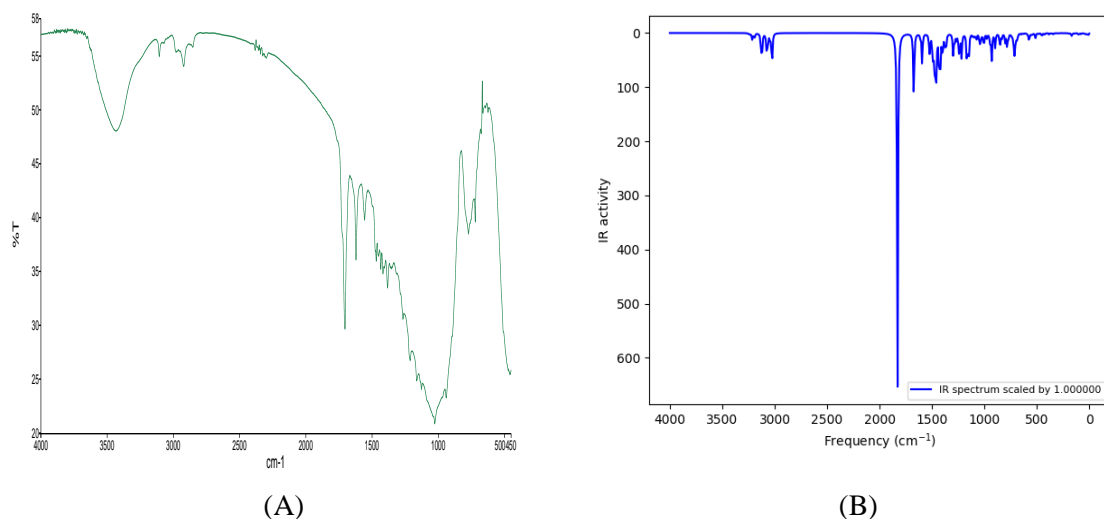
(A)

(B)
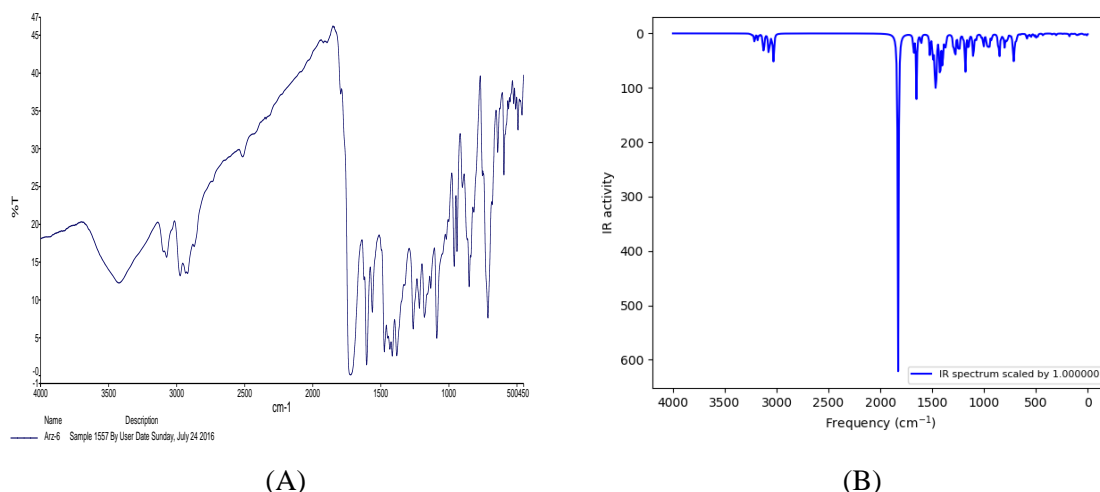
Figure 7.59. IR spectrum for compound (10). (A) Experimental (B) Theoretical results

Table 7.42. Theoretical and experimental vibrational for compound (10)

Assignments With TED	FT-IR (cm⁻¹) With KBr	Unscaled Frequencies B3LYP/cc-pVDZ	Assignments With TED	FT-IR (cm⁻¹) With KBr	Unscaled Frequencies B3LYP/cc-pVDZ
ST-CH in thiophene	3423	3250.46	UNSTV-CH3 in ring	1474	1450.90
STV-C28H31		3235.56	STV-C19-N18	1449	1420.16
STV-C1H7		3217.56	STV-C19=N17, C14-N18	1382	1394.37
UNST-CH in thiophene		3212.91	RO-ethylene group		1374.77
STV-C8H6		3208.86	STV-C=C in ring		1365.36
STV-C37H38		3182.11	STV-C in thiophene		1364.89
STV-C39H48		3165.37	STV-C4-O9	1262	1293.64
UNSTV-ethylene group		3131.27	RO-C11H12H13		1278.11
UNSTV-C43H44H45H46		3123.67	STV-CH in thiophene		1237.26
UNSTV-C23H24H25H26		3121.52	SCI-CH in ring	1216	1200.97
UNSTV-ethylene group		3110.01	STV-C5-O9	1180	1180.65
USTV-CH3 in ring		3081.75	RO-C11H12H13		1173.91
USTV-CH3 in ring	3074	3078.97	STV-ethylene group	1133	1150.66
STV-C11H12H13		3071.04	STV-N16-N17		1111.83
STV-C20H21H22		3062.17	RO-CH3 in ethylene		1099.13
STV-C23H24H25H26		3042.23	SCI-CH in thiophene	1088	1089.56
STV-C39H40H41H42	2974	3030.32	STV-C28-C30		1077.02
STV-C43H44H45H46	2920	3026.26	UNSTV-CH3 in ring group		1060.14, 1027.79,
STV-C5=O10	1723	1827.79	STV-C14-N18	1019	1022.03
STVC1=C2	1623	1678.7	STV-C20-C23	960	976.78
STV-C=C in ring	1604	1651.18	STV-C5-O9	940	953.41

95

STV-C=C in thiophene	1611.10	RO-C11H12H13	927.34
STV- C=C in ring	1604.61, 1524.79	UNSTV-CH in thiophene	900 913.48
STV-C30=C32 in thiophene	1521.68	STV-C32-S29	851 853.11
SCI-C20H21H22	1493.90	STV-C11-S15	816 798.06
SCI-C23H24H25	1478.66	STV-C11-S15	753 773.57
RO-C39H40H41H42	1471.30	STV-N16-C14-N18	712 722.85
STV-C19=N17, C14=N16	1467.90	STV-C11-S15	716.10
RO-CH3 in ring	1465.72	STV-CH in thiophene	710.74
STV-C23H24H25H26	1461.52	STV-N16-N17	693.79
STV-C19=N17	1458.93	STV-C19-N18	685.47

TV: Starching vibration, UN: anti, S: Symmetrical, RO: Rocking, SCI: Scissoring
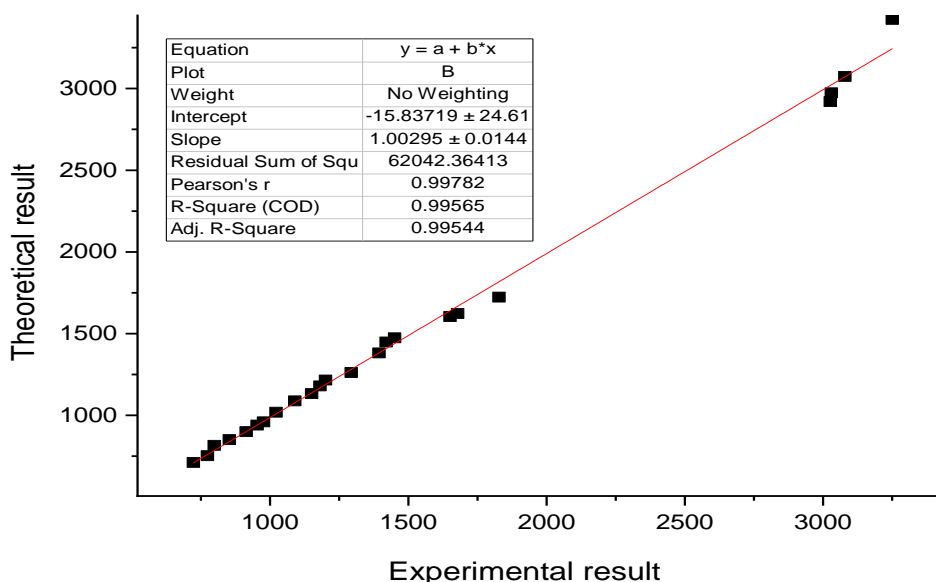
Figure 7.60. Relationship graphics for compound (10), between theoretical and experimental frequencies

The experimental Hydrogen ^{1}H NMR look Figure 7.61 and carbon ^{13}C NMR shown in Figure 7.62 chemical shifts for compound (10) were investigated in Dimethyl sulfoxide (DMSO-d6). Also in DMSO-d6 solvents, the theoretical ^{1}H and ^{13}C chemical shift values were determined using the DFT (B3LYP) method with the cc-pVDZ basis sets, all results were presents in Table 7.43 and 7.44.
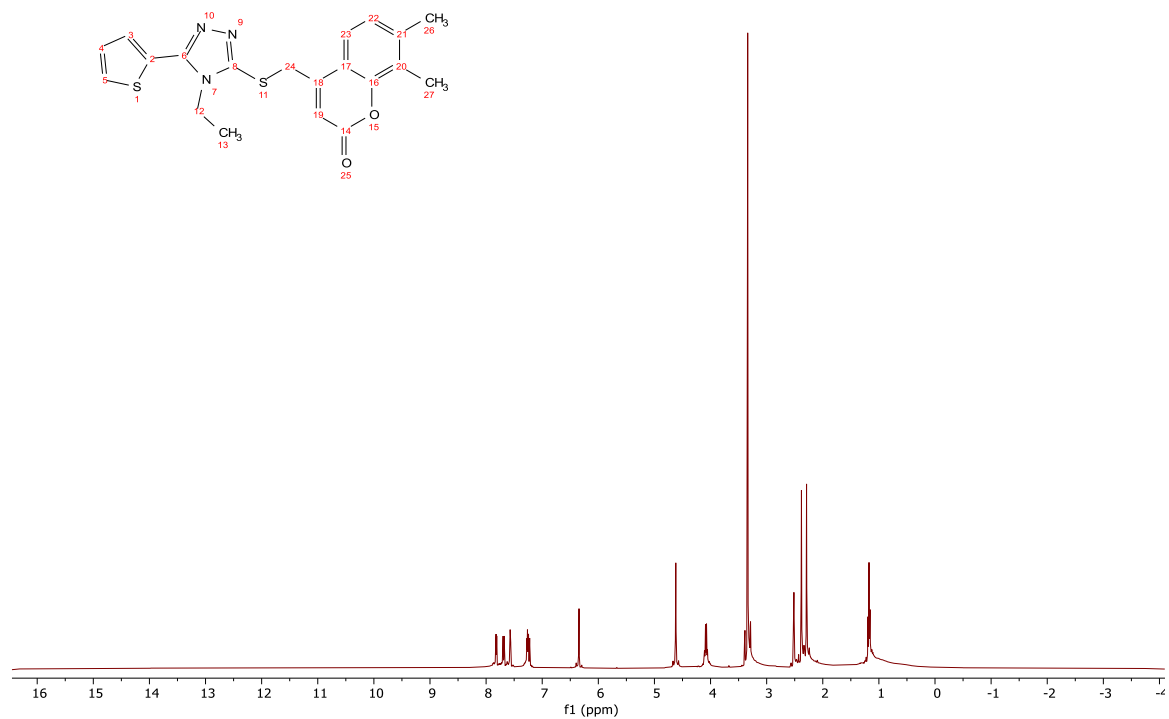
Figure 7.61. Experimental ^{1}H-NMR spectrum for compound (10) in DMSO-d6
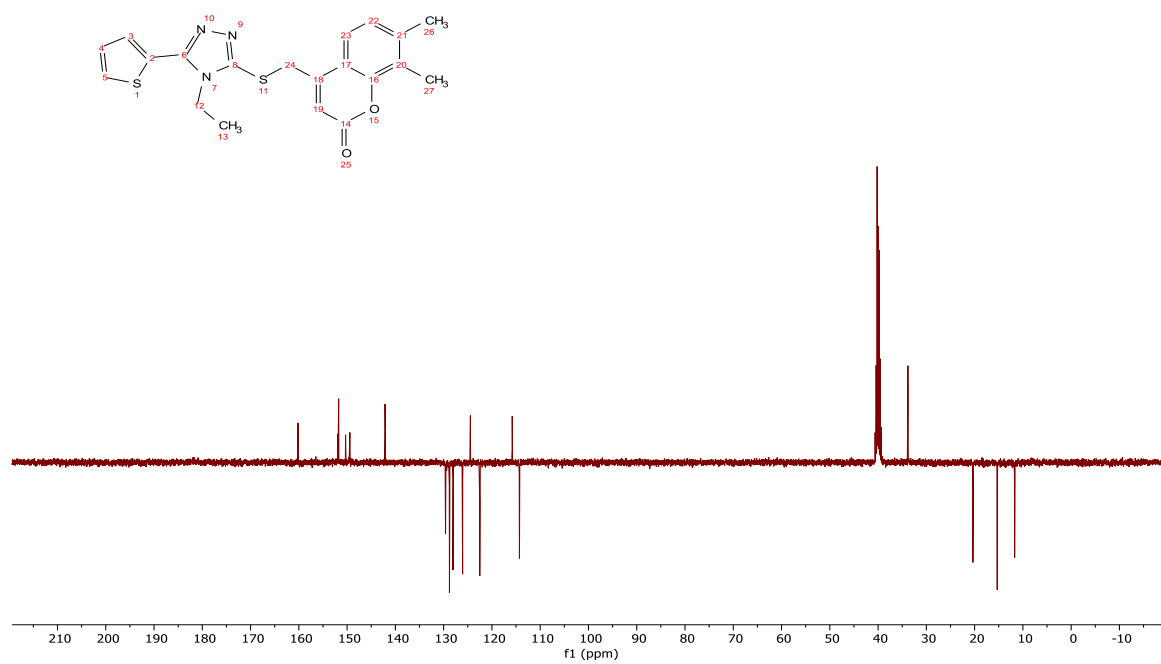
Figure 7.62. The experimental ^{13}C-NMR spectrum for compound (10) in DMSO-d6

97

Table 7.43. Experimental and theoretical chemical shifts (ppm) of ^{1}H-NMR of compound (10)

H number	Experimental Results	Theoretical Results
H34	7.81	7.66
H31	7.68	7.36
H6	7.27	7.72
H38	7.27	7.46
H33	7.55	7.35
H7	6.35	6.34
H13	4.61	5.14
H12	4.61	4.83
H22	4.08	4.47
H21	4.08	4.28
H40	3.29	3.87
H45	3.29	2.82
H44	3.29	2.81
H46	2.38	2.55
H41	2.38	2.31
H42	2.38	2.3
H25	1.17	2.22
H24	1.17	1.95
H26	1.17	1.74

Table 7.44. Experimental and theoretical chemical shifts (ppm) of ^{13}C-NMR of compound (10)

C number	Experimental Results	Theoretical Results
C19	160.16	160.78
C5	160.16	160.61
C4	151.93	160.11
C14	151.75	157.62
C2	150.32	156.3
C36	149.43	150.26
C27	142.15	147.21
C32	129.60	139.71
C35	128.80	134.69
C37	128.07	131.73
C30	126.07	131.19
C8	124.46	127.51
C28	122.51	126.52
C3	115.79	125.97
C1	114.29	120.24
C11	40.23	49.51
C20	33.83	49
C43	20.37	30.4
C23	15.31	24.28
C39	11.71	20.55

B3LYP/cc-pVDZ was used to found Molecular electrostatic potential (MEP) for compound (10) shown in Figure 7.63 The negative region's red color is often above the atoms of two nitrogens (N116, N17) and oxygen (O9, O10).
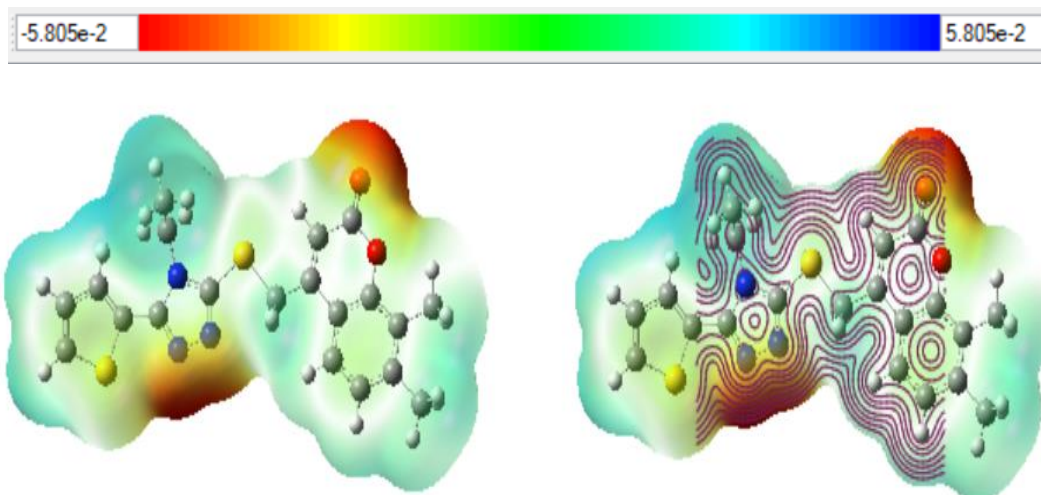
Figure 7.63. Molecular electrostatic potential for compound (10)

Mulliken population analysis for compound (10) shown in Figure 7.64 the more negative charges were distributed on the N16, N17, N18, O9, O10, C27, C35 and C36.
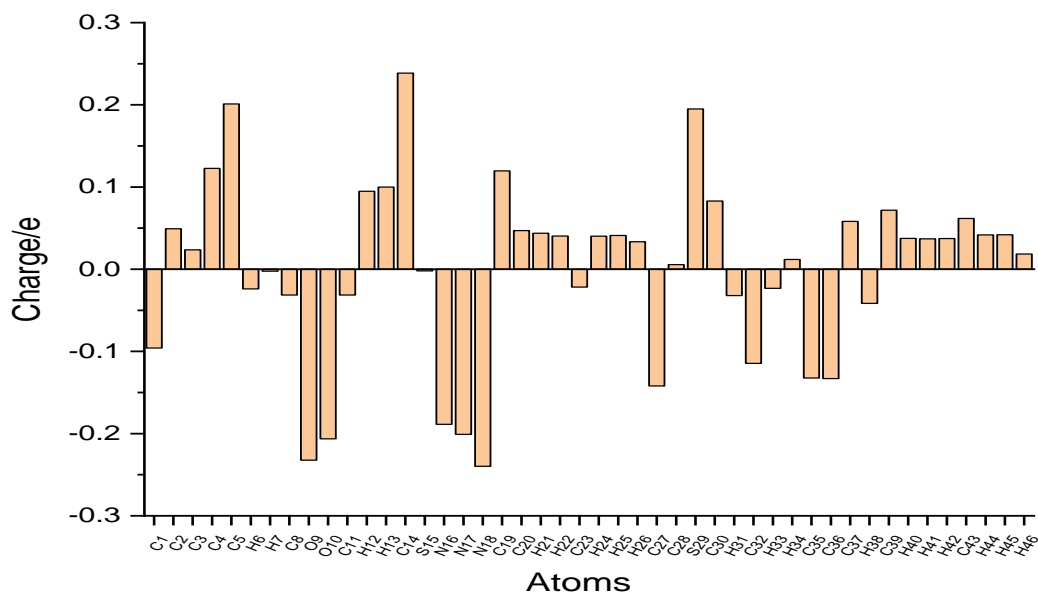
Figure 7.64. Millikan charge distribution on the compound (10)

Different parameters which are related to the inhibitor activity calculated for compound (10) used B3LYP/cc-pVDZ All parameters were shown in Table 7.45 including energy of the highest occupied molecular orbital (E_{HOMO}), energy of the lowest unoccupied molecular orbital (E_{LUMO}), energy bandgap ($\Delta E = E_{LUMO} - E_{HOMO}$), dipole moment ($\mu$), hardness ($\eta$), softness ($\sigma$), electronegativity ($\chi$), electrophilicity index (ω), nucleophilicity (ε) index and The fraction of transferred electrons (ΔN) which is related to transfer electron between inhibitor and metal surface

Table 7.45. Calculation quantum chemical parameters for compound (10)

Parameters	Equations	Results
Total Energy (a.u)		-1884.743
μ (D)		2.703
E_{LUMO} (eV)		-1.870
E_{HOMO} (eV)		-5.866
ΔE (eV)		3.996
I	$I = -E_{HOMO}$	5.866
A	$A = -E_{LUMO}$	1.870
χ (eV)	$\chi = (I + A) / 2$	3.868
η (eV)	$\eta = (I - A) / 2$	1.998
σ (eV)	$\sigma = I/\eta$	2.935
Pi (eV)	$Pi = -\chi$	-3.868
ω (eV)	$\omega = Pi2/2\eta$	3.744
ε (eV)	$\varepsilon = Pi. \eta$	7.729
ΔN	$\Delta N = (\chi_{metal} - \chi_{inhibitor}) / 2. (\eta_{metal} - \eta_{inhibitor})$	0.783

The Zero-point vibrational energy, Total energy, thermal energy, rotational constants, rotational temperatures and entropy of the molecules (10) were calculated using B3LYP/cc-pVDZ at a pressure of 1.00 atom and 298 K, Table 7.46 shows the results.

Table 7.46. Thermodynamic parameters for compound (10)

Parameters	B3LYP/cc-pVDZ
Zero-point vibrational energy(kcal/mol^{-1})	221.945
Total energy (a.u.)	-1884.743
Rotational constants (GHz)	
	0.470
	0.058
	0.051
Rotational temperatures (K)	
	0.0195
	0.0028
	0.0024
Entropy (Kcal mol^{-1} K^{-1})	
Rotational	0.889
Translational	0.889

Vibrational	236.135
Total	237.912

8. DISCUSSION

8.1. Reaction Analysis of Synthesized 1,2,4-triazole Compounds

In the first part of the study, two types of thiosemicarbazides were obtained by interacting carboxylic acid hydrazides with two different types of isothiocyanate, adding KOH subsequently to the reaction medium aliphatic and aromatic substituted 1,2,4-triazoles were obtained.

High yield (70-90 %) thiosemicarbazide derivatives were formed from carboxylic acid hydrazide derivatives and isothiocyanates. Figure 8.1 depicts the reaction pathways of 1,2,4-triazole derivatives.
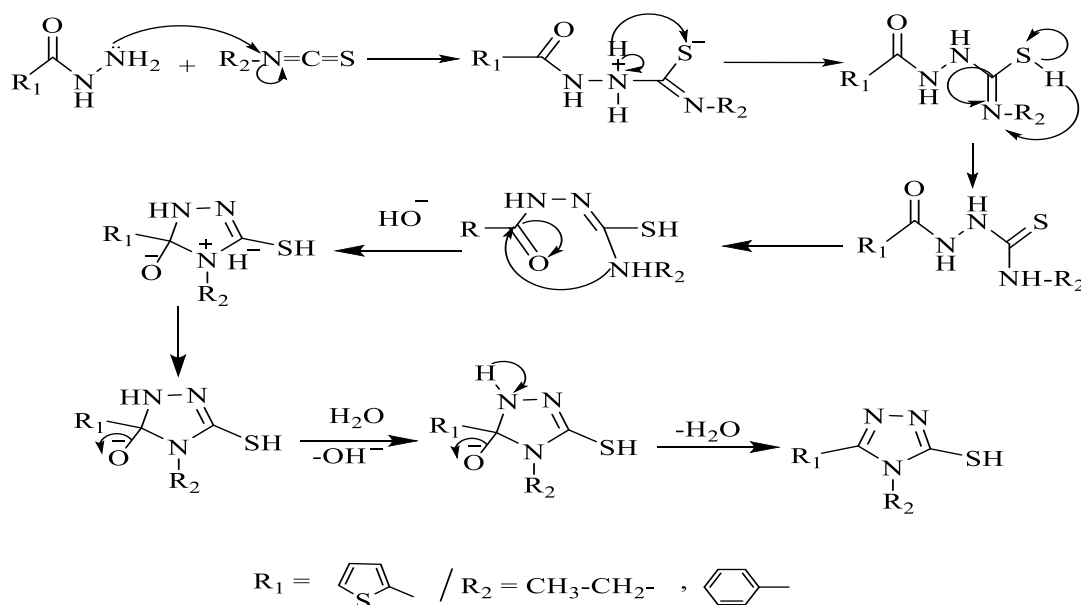
Figure 8.1. Reaction mechanism of synthesis 1,2,4-triazole derivatives.

This 1,2,4-triazole was formed to show the thiol-thione tautomer feature. The tautomer of 1,2,4-triazole formed as a result of the reaction is shown in Figure 8.2.
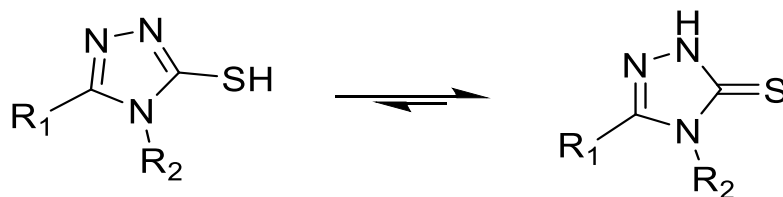
Figure 8.2. Tautomers of 1,2,4-triazole derivatives

8.2. Reaction Analysis of Sulfonyl Compounds Containing Triazole and Cyclobutane Ring

The 3,4,5-trisubstituted 1,2,4-triazoles obtained in the first step reacted with 2-chloro-1- (3-methyl-3-mesityl-cyclobutyl)-ethanone contain a cyclobutane ring by immersion in dry acetone containing K_2CO_3. 3,4,5-trisubstituted 1,2,4-triazole has been converted into sulfanyl compounds, see Figure 8.3.
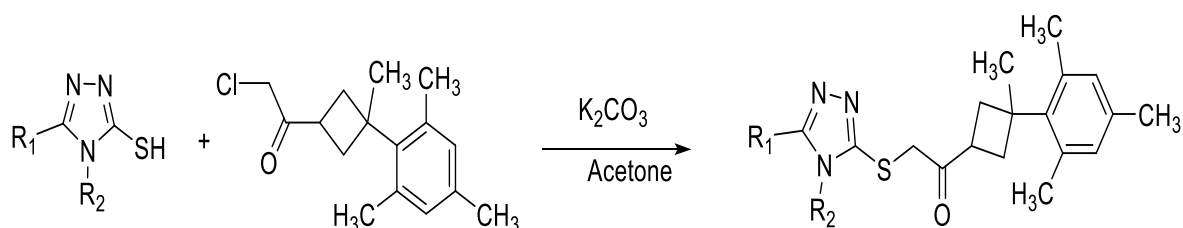
Figure 8.3. Reaction Analysis of Sulfonyl Compounds Containing Triazole and Cyclobutane Ring

3,4,5-trisubstituted 1,2,4-triazoles react with 2-chloro-1-(3-methyl-3-mesityl-cyclobutyl)-ethanone via the SN^2 reaction mechanism in the presence of K_2CO_3 to produced sulfanyl compounds containing triazole and cyclobutane ring, with a yield of 50-65%. The reaction mechanism is given in Figure 8.4.
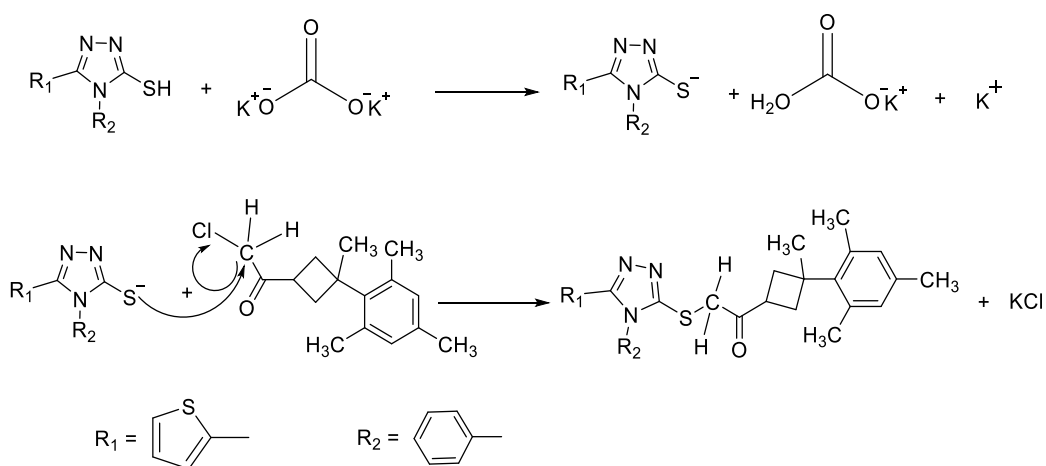
Figure 8.4. Reaction mechanism for the formation of sulfonyl compounds containing triazole and cyclobutane ring.

8.3. Reaction Analysis of Sulfonyl Compounds Containing Triazole and coumarin Ring

The 3,4,5-trisubstituted 1,2,4-triazoles obtained in the first step reacted with 4-(chloromethyl)-7-methyl coumarin contain a cyclobutane ring by immersion in dry acetone containing K_2CO_3. 3,4,5-trisubstituted 1,2,4-triazole has been converted into sulfanyl compounds, see Figure 8.5.
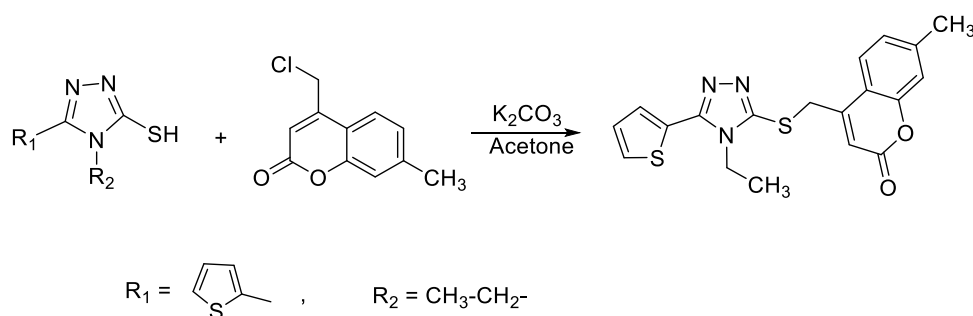
Figure 8.5. Reaction Analysis of Sulfonyl Compounds Containing Triazole and coumarin Ring

3,4,5-trisubstituted 1,2,4-triazoles react with 4-(chloromethyl)-7-methyl coumarin contain via the SN^2 reaction mechanism in the presence of K_2CO_3 to produced sulfanyl compounds containing triazole and coumarin compounds, with a yield of 65-75%. Figure 8.6 show the reaction mechanism.
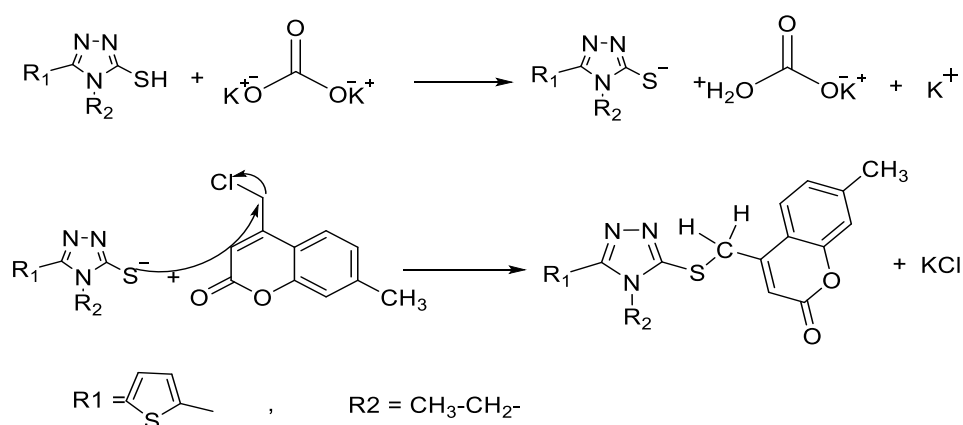
Figure 8.6. Reaction mechanism for the formation of sulfonyl compounds containing triazole and coumarin compounds.

8.4. FT-IR Analysis of Synthesized Compounds

When the FT-IR spectra of the synthesized 3,4,5-trisubstituted 1,2,4-triazoles were examined, it was observed that the C=O tension vibration between 1650-1690 cm^{-1} in carboxylic acid hydrazine derivatives disappeared. It was observed that instead of this peak, N-C=S peaks at 1584, 1265, 1085 and 980 cm^{-1} and C-N-C tension peak around 1180 cm^{-1}. Figure 8.7 shows the position of the C=O peak in the FT-IR spectrum of Benzoyl hydrazine [99]. N-C=S and C-N-C vibration frequencies of 4-Ethyl-5-(thiophene-2-yl)-4H-1,2,4-triazole-3-thiol are shown in Figure 8.8. In addition to these characteristic peaks, aromatic and allylic CH between 3025-3150 cm^{-1}, aliphatic CH between 2850-2965 cm^{-1}, C=N around 1550 cm^{-1}, C=S tension peaks around 1270 cm^{-1} and CH peaks was observed between 850-964 cm^{-1} are seen in 3,4,5-trisubstituted 1,2,4-triazole derivatives.
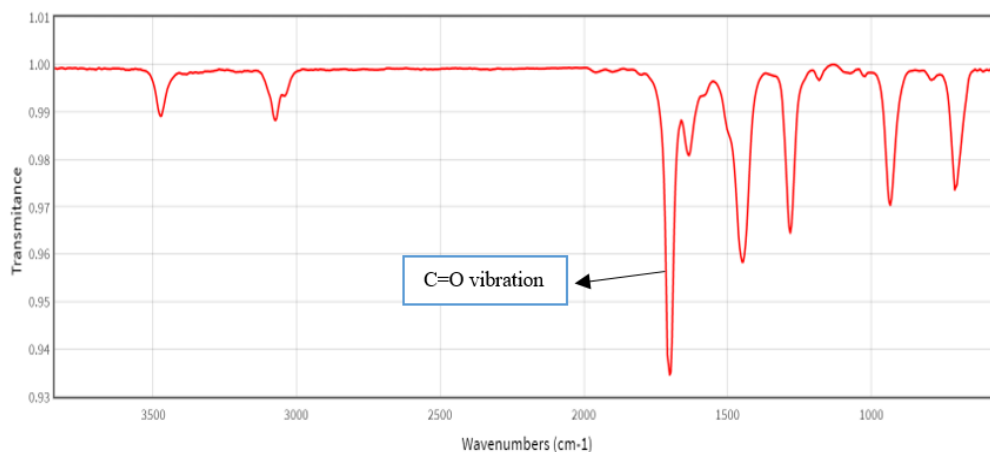
Figure 8.7. Representation of the peak of C = O stretch vibration in the FT-IR spectrum of Benzoyl hydrazine
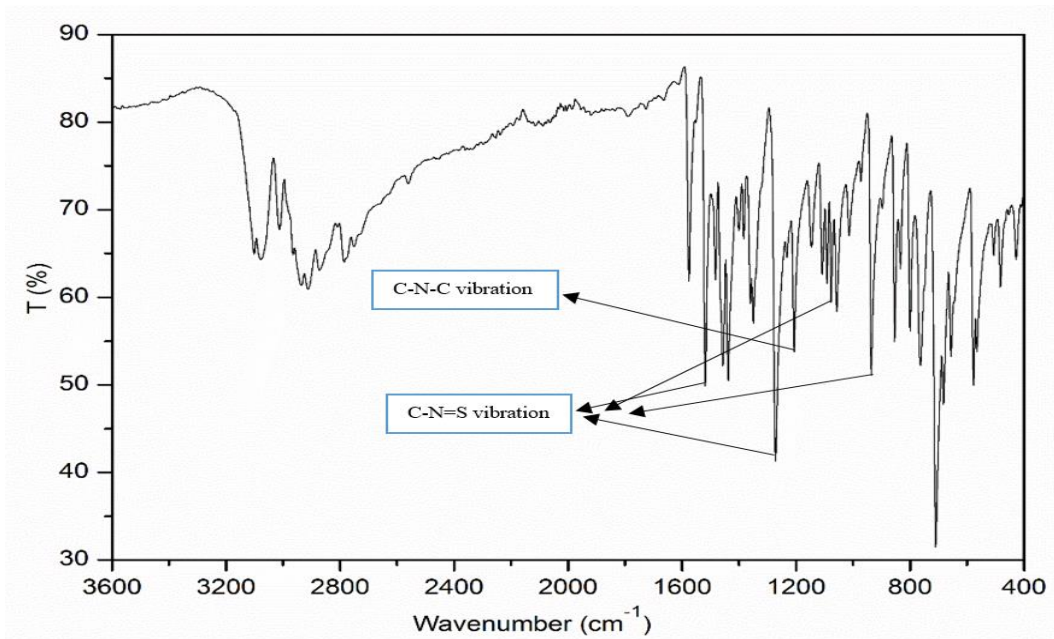
Figure 8.8. N-C = S and C-N-C vibration frequencies of 4-Ethyl-5-(thiophene-2-yl)-4H-1,2,4-triazole-3-thiol

The most characteristic peak in the 3,4,5-trisubstituted 1,2,4-triazole sulfonyl compound containing cyclobutane ring obtained in this study is the C=O peak. C=O stretch vibration occurs in 1697 cm^{-1} in the synthesized compounds. The C-S-C stretch peak, which is also peculiar to the structure, is approximately 774cm^{-1}. In addition to these peaks, Ar-H around 2955-3059 cm^{-1}, aliphatic C-H around 2866-2910 cm^{-1}, C-C stress peaks of the cyclobutane ring 1165 cm^{-1} and C=C stress peaks of mesityl ring around 1550 cm^{-1}. The characteristic peaks of the structure are shown in Figure 8.9.
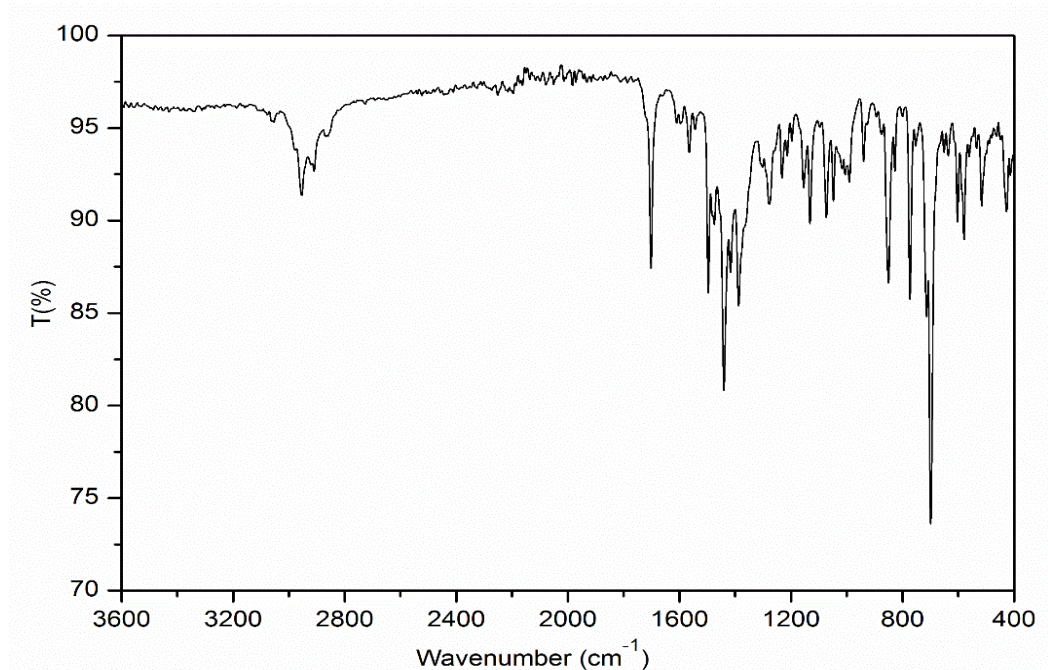
Figure 8.9. Representation of structure-specific characteristic peaks in the FTIR spectrum belonging to 1-(3-methyl-3-mesityl)-cyclobutyl-2–[[5-(thiophen-2-yl)-4-phenyl-4H-1,2,4 triazol-3- yl] sulfanyl]-ethanone

In the third step of this study prepared four different 1,2,4-triazole sulfonyl compounds containing coumarin (ETMC) compound which is different in the number of methyl groups and the position of the methyl groups. S–C, O–C, and C=O vibrations have the most distinct peaks in ETMC. The most S-C was vibrated at a range of 710-750 cm^{-1} and the computed results were show that at 750-780 cm^{-1}, this results was closed with the literature [100, 101]. At 1216-1262 and 1050-1150 cm^{-1}, O–C vibrations were detected. According to the literature previously the O-C vibration pack was observed at 1250-850 cm^{-1} [102, 103]. At 1720-1750 cm^{-1} was the frequency value for C=O, while at 1850 cm^{-1} appears as computed frequency value. Other notable peaks in ETMC include aromatic C–H, aliphatic C–H, and C=N. At 3000–3100 cm^{-1} is the range of aromatic C–H frequency values according to the reference [104, 105]. C–H aromatic frequency theoretical values are in the range of 3050–3150 cm^{-1}, while experimental values are in the range of 3050–3100 cm^{-1}. C–H aliphatic Experimental vibrated at 2920–2985 cm^{-1} and aliphatic C–H frequency values are computed at 3006–3026 cm^{-1}. The C=N vibrational frequency value was observed at 1605 cm^{-1}, while computed value was obtained at 1595 cm^{-1}, see Figure 8.10.
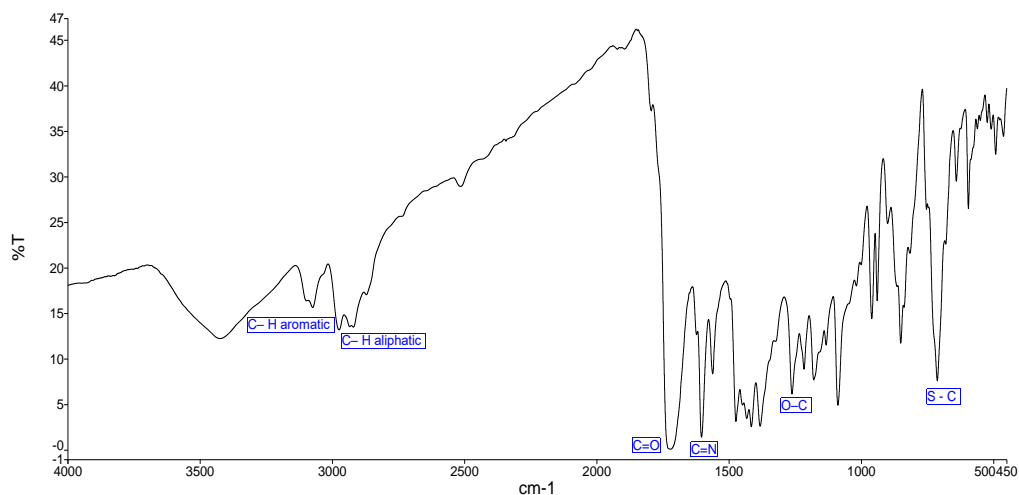
Figure 8.10. Representation of structure-specific characteristic peaks in the FTIR spectrum belonging to 4-(((4-ethyl-5-(thiophen-2-yl)-4H-1,2,4-triazol-3-yl)thio)methyl)-7,8-dimethyl-2H-chromen-2-one

8.5. NMR Analysis of Synthesized Compounds

The most characteristic peak of the synthesized 3,4,5-trisubstituted 1,2,4-triazoles is the SH/NH peak seen as a singlet in the range of 13.98-14.21ppm. This peak in the ^{1}H-NMR spectrum can be seen in Figure 8.11.
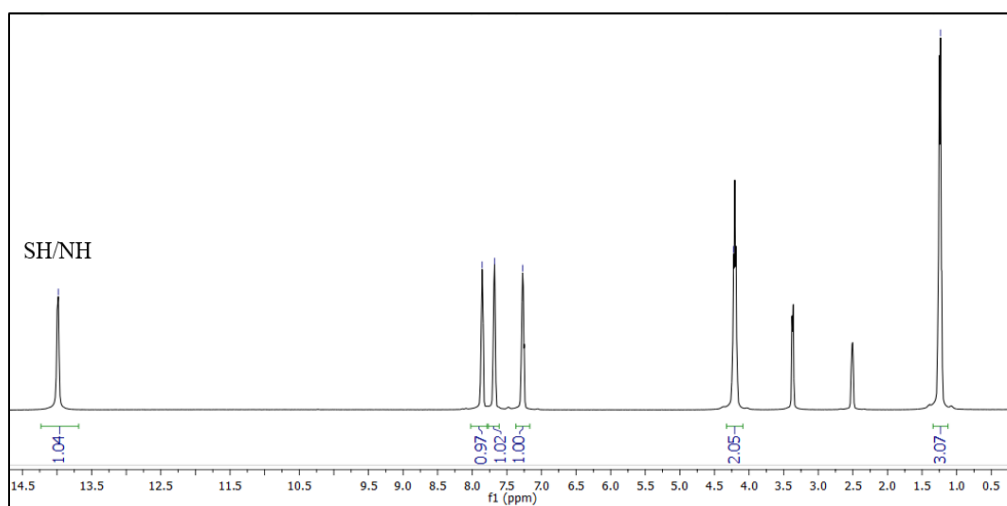
Figure 8.11. Representation of the SH/NH peak in the ^{1}H-NMR spectrum of the 4-ethyl-5-(thiophen-2-yl)-2,4-dihydro-3H-1,2,4-triazole-3-thione molecule

Besides this characteristic peak of SH/NH, there are some characteristic peaks in the substituents attached to the 1,2,4-triazole ring. The first example of these substituents is the ethyl fragment. It has been observed that the -CH$_2$- protons of N-CH$_2$-CH$_3$ in the 4- position give quartet

peaks between 4.05 and 4.45 ppm. The interaction constant of these quartet peaks is approximately 7.1 Hz. Likewise, –CH3- peaks were observed to give triplet peaks in the range of 1.09-1.24 ppm. The interaction constants of these triplet peaks are approximately 7.1 Hz. The places of the carbons belonging to the ethyl group in the ^{13}C-NMR spectrum are approximately 13.77 for CH_3 and 39.77 ppm for CH_2. The reason for the carbon and hydrogen being close to the nitrogen atom to come out in the low area is the high electronegativity of the nitrogen atom. Thus, the electron charge density shifted towards the nitrogen atom in these atoms and caused these atoms to resonate in a lower electric field. ^{13}C-NMR peaks of the ethyl group are shown in Figure 8.12.
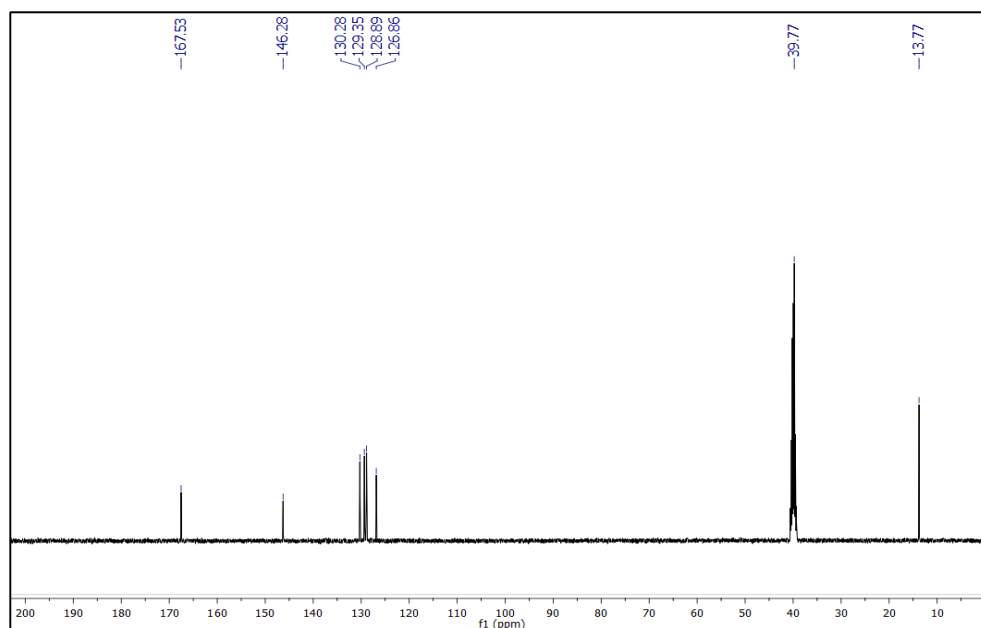
Figure 8.12. Representation of the ^{13}C-NMR spectrum of the 4-ethyl-5-(thiophen-2-yl)-2,4-dihydro-3H-1,2,4-triazole-3-thione molecule

In the protons of the phenyl group, those in the -orto and -meta positions have given two signals peck in the range of 7.0 and 6.6 ppm respectively. The representation of the signals belonging to the phenyl group of 4-phenyl-5-(thiophen-2-yl)-2,4-dihydro-3H-1,2,4-triazole-3-thione is given in Figure 8.13.
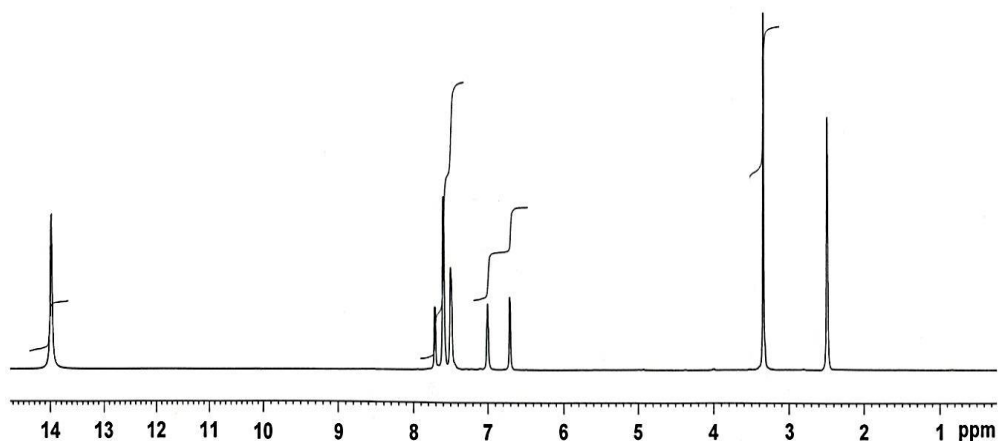
Figure 8.13. Representation of the phenyl peak in the ^{1}H-NMR spectrum of the 4-phenyl-5-(thiophen-2-yl)-2,4-dihydro-3H-1,2,4-triazole-3-thione molecule

The experimental and theoretical NMR calculation was founded for compound 5 (2-chloro-1-(3-methyl-3-mesityl-cyclobutyl)–ethanone), for experimental calculation used DMSO as a solvent and for the theoretical using B3LYP/ccpVDZ in a gas state.

For ^{1}H-NMR the clear peak was appear for two hydrogens on the benzene ring at 6.75ppm and the computed analysis was the show at 7.94ppm. The peaks for the two methyl groups in a benzene ring has appeared at 2.36ppm experimentally while computing show at 3.1ppm. Experimentally two hydrogen peaks for CH2 attached to chlorine atom were shifted to higher ppm lower filed (4.55ppm), the theoretical analysis show at 5.6ppm. Figure 8.14 was show the experiential ^{1}H-NMR peaks.
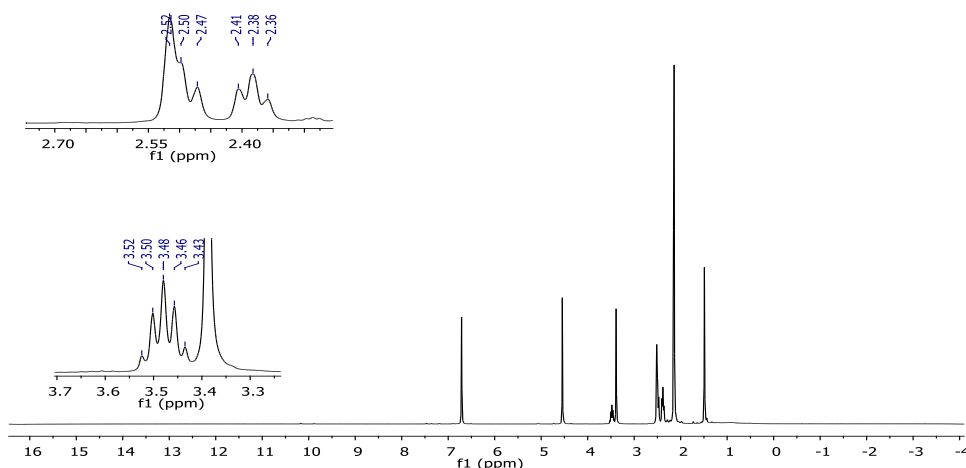
Figure 8.14. Experimental ^{1}H-NMR spectrum for 2-chloro-1-(3-methyl-3-mesityl-cyclobutyl)–ethanone in DMSO-d6

110

The ^{13}C-NMR spectrum for 2-chloro-1-(3-methyl-3-mesityl-cyclobutyl)–ethanone was analyzed in DMSO. The ^{13}C-NMR for three methyl groups on the benzene ring was found at 20.75, 20.75, 20.45ppm, the same carbon was determined theoretically at 30.47, 30.28, and 28.91ppm. The peak for C=O was found at 203.90 experimentally while computed founded at 211.06ppm. The experimental aromatic carbone for benzene ring appeared 143.94ppm and the theoretically show at 143.41ppm. The CH2 was attached to the chlorine atom and the carbonyl group shifted lower filed higher ppm (48.42) for experimental and for theoretical equal to 64.38ppm. The two-carbon of cyclobutane ring (C, CH2) was found in the solvent peaks (39.77 and 40.21ppm) experimentally and theoretically founded at 49.08 and 54.66ppm look in figure 8.15.
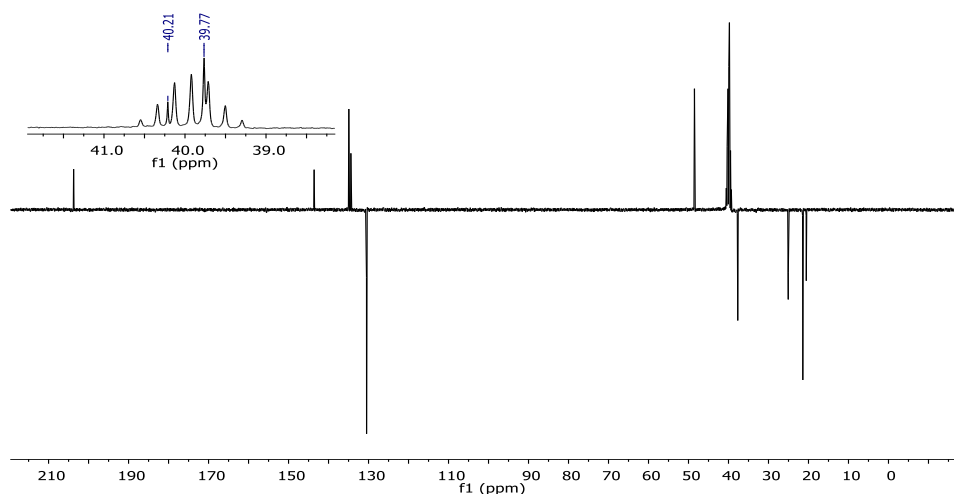
Figure 8.15. Experimental ^{13}C-NMR spectrum for 2-chloro-1-(3-methyl-3-mesityl-cyclobutyl)–ethanone in DMSO-d6

When the ^{1}H-NMR and ^{13}C-NMR were examined for coumarin compound 4-(((4-ethyl-5-(thiophen-2-yl)-4H-1,2,4-triazole-3-yl)thio) methyl)-6,7-dimethyl-2H-chromen-2-one we founded some peaks are representative for synthesis compounds. The proton peaks for CH2 which was attached to N-CH2-CH3 have observed quartet peaks at 4.09ppm experimentally, while theoretically was observed at range 4.84-4.28ppm. The CH3 peaks for the methyl group were observed at 1.18ppm this is the triplet peaks, also the computed result for the same peaks has appeared at range 2.22 - 1.73ppm.

For ^{13}C-NMR, the experimental peaks for each CH3 and CH2 (methyl group) were founded at 15.29 and 30.85ppm respectively, while theoretically found at 23.41 and 48.15ppm. According to electronegativity, the carbon and hydrogen atoms are closed to the atoms with the higher electronegativity was going to downfield and higher ppm. The ^{13}C-NMR for CH2-S peaks was mixt

in DMSO solvent. Look to the Figure 8.16 and 8.17 has H-NMR and C-NMR for coumarin compound (9).
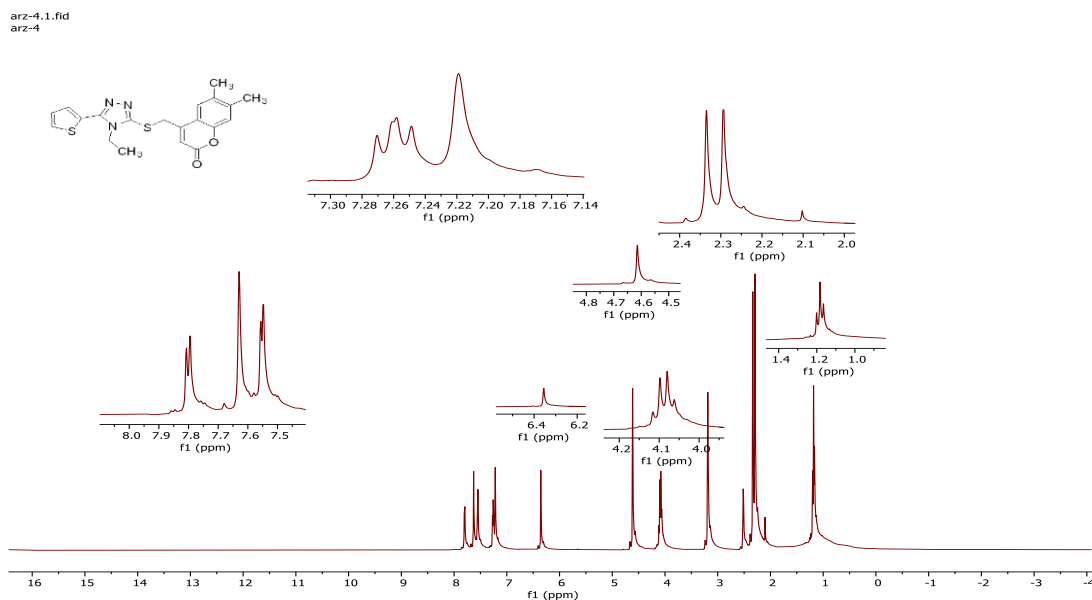
Figure 8.16. Experimental ^{1}H-NMR spectrum for 4-(((4-ethyl-5-(thiophen-2-yl)-4H-1,2,4-triazol-3-yl)thio) methyl)-6,7-dimethyl-2H-chromen-2-one in DMSO-d6
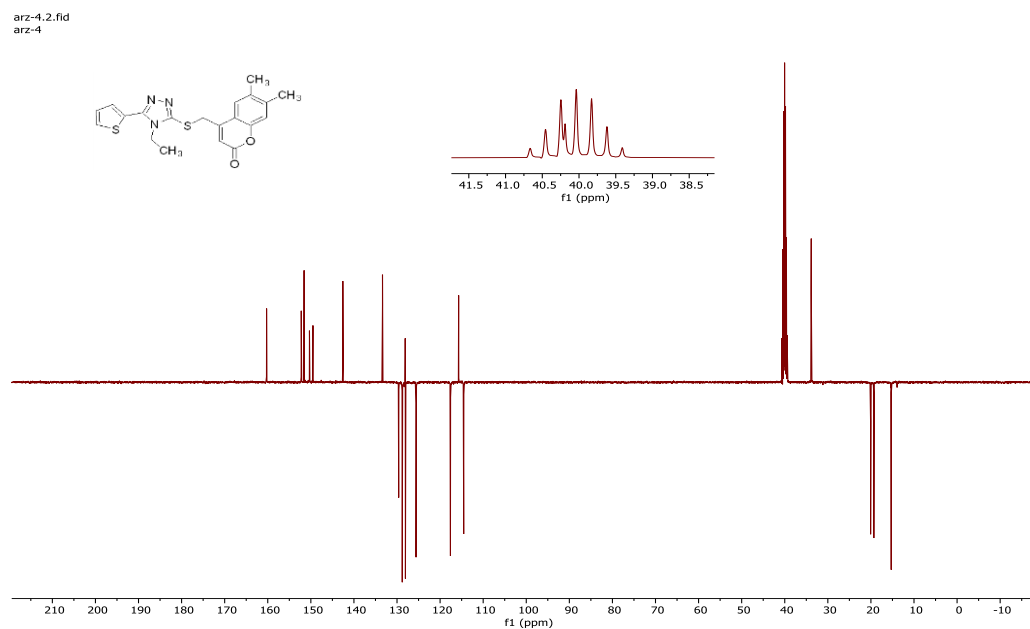
Figure 8.17. The experimental ^{13}C-NMR spectrum for 4-(((4-ethyl-5-(thiophen-2-yl)-4H-1,2,4-triazol-3-yl)thio) methyl)-6,7-dimethyl-2H-chromen-2-one in DMSO-d6

8.6. Investigation of Synthesized Molecules with Theoretical Calculations

Some theoretical calculations were made to elucidate the structures of some synthesized molecules in more detail. Within the scope of these studies, the three-dimensional geometry of the molecule, vibration frequencies, and ^{13}C-^1H NMR spectra graphs were calculated using the Gaussian package program and DFT method with B3LYP/cc-pVDZ base set. It has been seen that the experimental and theoretical findings obtained as a result of all these calculations are in harmony. In Figures 8.18, and 8.19 given below, correlation graphs are drawn to show the compatibility of NMR spectrums.

Equation	y = a + b*x
Plot	B
Weight	No Weighting
Intercept	10.07206 ± 1.5
Slope	0.97905 ± 0.01
Residual Sum of Sq	147.20233
Pearson's r	0.99842
R-Square (COD)	0.99683
Adj. R-Square	0.99666
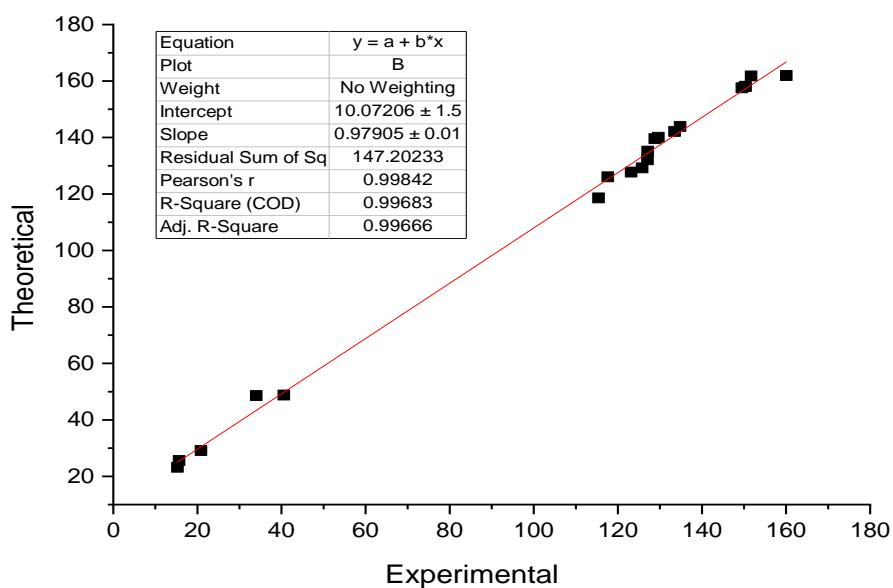
Figure 8.18. The ^{13}C-NMR correlation between experimental and theoretical calculation for 4-(((4-ethyl-5-(thiophen-2-yl)-4H-1,2,4-triazol-3-yl)thio)methyl)-6,8-dimethyl-2H-chromen-2-one

113
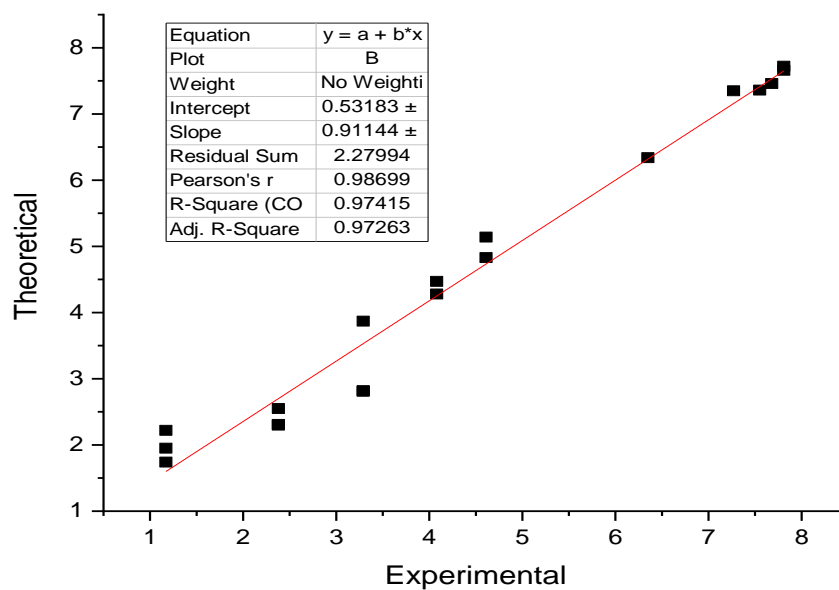
Figure 8.19. The ^{1}H-NMR correlation between experimental and theoretical calculation for 4-(((4-ethyl-5-(thiophen-2-yl)-4H-1,2,4-triazol-3-yl)thio)methyl)-7,8-dimethyl-2H-chromen-2-one

8.7. Study the molecular structure (geometrical structure)

The investigation of the molecular structure for our compounds to found the bond length, bond angle and dihedral angle, which are more important to determine the crystal structure. However, in the geometrical structure, we also found the globular all site reactivity of the molecule with dipole moment and energy of the molecule [106-108]. Also in the geometrical structure show the sit for capability and interaction for a large molecule like enzymes. Look Figure 8.20 was the geometrical structure for compound (10).
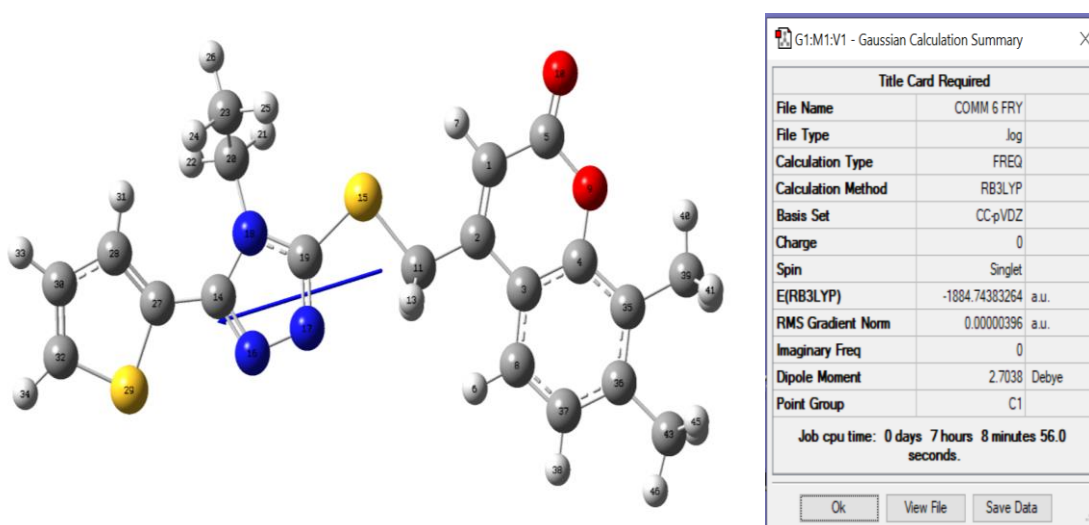
Figure 8.20. The geometrical structure for compound (10) and the summary of the calculation

114

8.8. Theoretical inhibitors parameters used to determine the activity of compounds

Determined the electronic structure for all molecules which are called electronic identified, including the following with the equations:

HOMO energy level is found from the output file of Gaussian   (1)

LUMO energy level is found from the output file of Gaussian   (2)

Dipolmoment (μ) is found from output file of Gaussian   (3)

Electronic affinity (I= -E_{HOMO}) [109, 110]   (4)

Ionization potential (A= -E_{LUMO}) [110]   (5)

Energy bandgap ($\Delta E = E_{HOMO} - E_{LUMO}$) [111]   (6)

Hardness (η) = (I – A)/2[112]   (7)

Softness (σ) = I/η[113]   (8)

Electronegativity (χ) = (I + A)/2 [114]   (9)

Chemical potential (Pi) = - χ [115]   (10)

Electrophilicity (ω) = Pi^2/2η [116]   (11)

Nucleophilicity (ϵ) = Pi. η [117]   (12)

$$\Delta N = \frac{(\chi \text{ metal} - \chi \text{ inhibitor})}{2 (\eta \text{ metal} - \eta \text{ inhibitor})} \text{ [115]}$$ (13)

The HOMO and LUMO energy level for the molecule has described the reactivity and stability of the molecule [118]. Electrophilicity ω is defined as the depletion of the energy because the electron is moved from transmitter to receiver [116]. The new molecular analysis is the nucleophilicity index looking at the equation (12). For determination ΔN equation (13) which is related to electrons relocated between inhibitor molecule and metal surface need calculations for each electronegativity and hardness [115]. The χ (electronegativity) and η (hardness) for our molecular inhibitor were calculated theoretically by DFT method with B3LYP/cc-pVDZ base set, while for metals (Fe bulk) equal to χ =7 and η = zero was founded from the literature [115, 117, 119].

HOMO is the capacity of the donating electronic in a molecule inhibitor. It's key in corrosion research in a theoretical study. It said that by increasing the value of the HOMO the inhibitor of the molecule was increasing. The is working on the absorption charge on the metal surface [120, 121]. From my study compound (C1) was a higher value for HOMO, while compound 5 was the lower

value see Figure 8.21. Looking at the order of the reactivity according to the HOMO value from Higher to lower degree.

$$HOMO = C1>C6>C2>C10>C9>C8>C7>C5$$

LUMO defines as a molecule that has ability to electron-accepting. The lower value of the LUMO means the inhibitor compound is adding a more negative charge on the metal surface. The higher value of the HOMO and LUMO the molecule reactivity for the inhibitor will be higher. For this reason, compound (C1) will be higher reactivity and compound (C7) was the lower reactivity using as an inhibitor. The order of the value of the LUMO from higher to lower is

$$LUMO = C5>C1>C2>C6>C9>C10>C8>C7$$

$E_{LUMO} = -1.205$

$\Delta E = 4.506$ eV

$E_{HOMO} = -5.712$

C1

$E_{LUMO} = -1.909$

$\Delta E = 3.976$ eV

$E_{HOMO} = -5.886$

C7
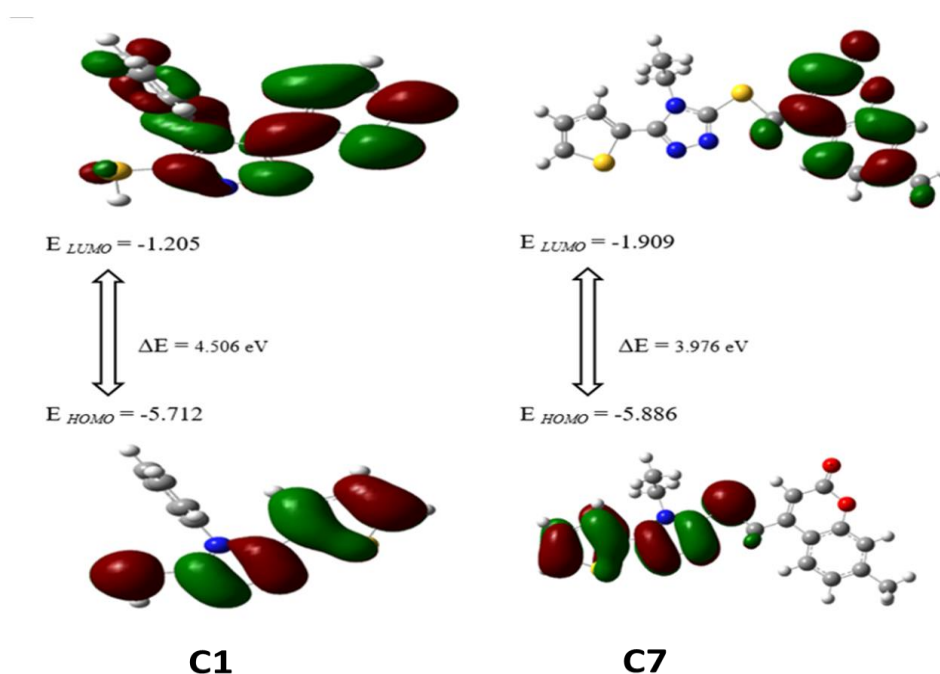
Figure 8.21. HOMO and LUMO energy level with ΔE for compounds 5 and 7.

The HOMO and LUMO energy bandgap were more important for the determination of inhibitor activity of the organic molecule, also the large significance in the molecular static reactivity. The order of the inhibitors for our molecule is as follows, based on the value of the energy band gaps from lower to a higher value.

$$\Delta E = C7>C8>C10>C9>C6>C1>C2>C5$$
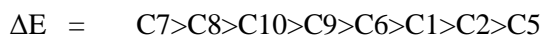
The energy band gaps were determined the reactivity of the molecule by compared the ΔE. The lower energy band gaps were inducted the molecule was more reactive. The value of the ΔE is

more related to the energy of the HOMO rather than LUMO, by increasing the energy of the HOMO the ΔE was decreased, it is good anti corrosion activity [120]. From the above sequence of the resulting compound 7 (C7) was lower energy band gap (ΔE), also it has more energy of HOMO, for this reason, it is good anti corrosion activity.

The used Mulliken charge distribution on the atoms in a molecule is one of the wide methods was using for determined the inhibitor activity [122]. With the presence of the negative charge on the heteroatoms, the inhibitor activity was increased due to the absorption on the metal surface this is maintained in the many kinds of literature [123]. Looking at the chart for charge distribution of the compound (7, 8, 9, 10) has a higher negative charge on the heteroatoms compared with another molecule (1, 2, 5, 6). The molecular electrostatic map potential (MEP) was clear shows the distribution of the charge on the atoms. The red color in MEP was representative of the negative charge and the red color going to the blue color illustrative the positive charge. Looking Figure 8.22 as an example for compound 9. The more negative charge was distributed on the heteroatoms like O, N, S, C.
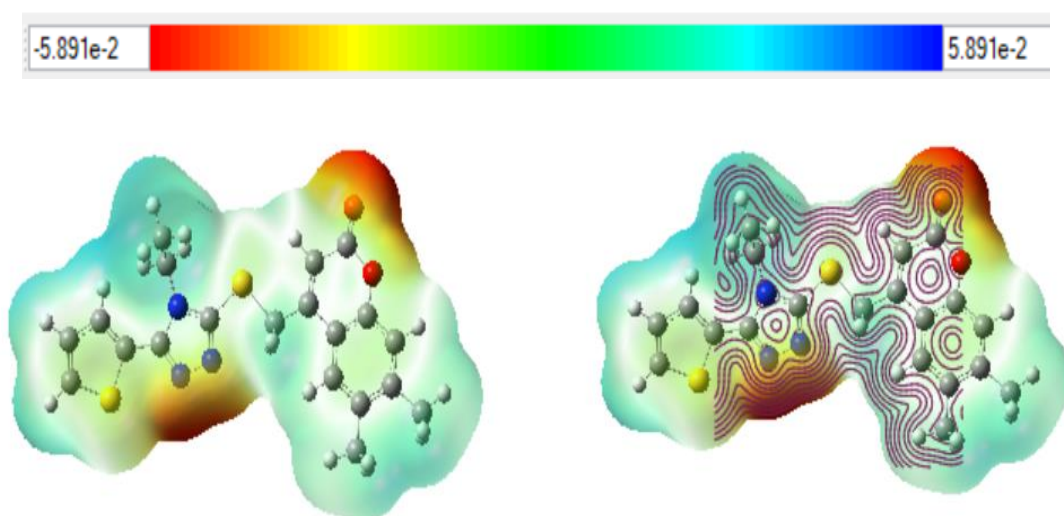
Figure 8.22. MEP for compound 10, show clear charge distribution on the atoms.

The other parameters chose for the inhibitor activity of an inhibitor and stable compound are η (eV) and σ (eV). The good corrosion inhibitors those compounds have soft and more lewis base [124, 125]. In this study the order of compounds from more soft to more hardness are the following:

$$\sigma > \eta \qquad C7 > C8 > C10 > C9 > C6 > C1 > C5 > C2$$

Compound 7 has higher energy of the HOMO and lower ΔE, it had more soft and lower hardness compared with other compounds. The compound 7 inhibitor has the most efficient inhibitory effect.

Two other parameters that have determined the inhibitor activities are electronegativity (χ) and chemical potential (Pi) which are inverse to each other. The following is the order of (χ) from higher value to lower value:

$$\chi \qquad C7>C8>C10>C9>C6>C5>C2>C1$$

The degree of the electronegativity inhibitor determined how the coordination covalent bonds are formed between the inhibitor compounds and metal surface. In this study, our compound was examined on the iron surface as a theoretical calculation. The theoretical χ value for inhibitor compounds was calculated, looking at Table 8.1. It has shown the χ inhibitor was less than iron metal, in this resonance the iron metal has formed a bond with the inhibitor by taking an electron. The chemical potential (Pi) for molecules was used as an inhibitor is more important, by increasing the (Pi) the anti-corrosion activity increase [126]. The calculation of chemical potential was sequenced as the following:

$$Pi \qquad C7>C8>C10>C9>C6>C5>C2>C1$$

Table 8.1 shows the result of ΔN which was obtained from the iron metal surface and inhibitor compounds. Generally, it is seen coumarin compounds (1>10>9=8>7) have more ΔN values than others (6>2>5). The higher value of ΔN means the compounds more electrons transfer to the metal surface [115].

Dipole moment (μ) is the other parameters that were found from the output file of the Gaussian calculation look Table 8.1. It has been not clear for many researchers to discuss the dipole moment change with inhibitor property. The same researcher said by increasing dipole moment the inhibitor property was increased the other researcher said with increasing dipole moment in a molecule the reactivity for inhibitor is decreasing. The coumarin compounds have a large value of the dipole moment compared with other compounds. This agrees with that researcher said by increasing the dipole moment the inhibitor activity is increasing.

The important parameters which are determined the corrosion inhibitors are the electrophilicity index (ω), nucleophilicity (ε) index. The ω for inhibitor molecule is represented for electron acceptance [116], while ε represents electron-donating [127]. The sequence of the molecule according to ω and ε from higher to lower value is a following:

$$\omega \qquad C6>C7>C8>C10>C9>C2>C1>C5$$

$$\varepsilon \qquad C10>C8>C7>C9>C1>C6>C2>C5$$

The inhibitor activity is increased with increasing ε value or decreasing value ω. Looking at the sequence study, compound 7 had higher inhibitor activity.

Table 8.1. Different parameters used for determination theoretical inhibitor activity

Parameters	Equations	Compound 1	Compound 2	Compound 5	Compound 6	Compound 7	Compound 8	Compound 9	Compound 10
Total Energy (a.u)		-1423.372	-1270.937	-1157.799	-2120.361	-1845.426	-1884.745	-1884.744	-1884.743
μ (D)		5.515	4.852	3.728	2.646	3.277	3.172	3.343	2.703
E_{LUMO} (eV)		-1.205	-1.221	-0.856	-1.344	-1.909	-1.883	-1.855	-1.87
E_{HOMO} (eV)		-5.712	-5.809	-6.235	-5.764	-5.886	-5.877	-5.87	-5.866
ΔE (eV)		4.507	4.588	5.379	4.42	3.977	3.994	4.015	3.996
I	$I = -E_{HOMO}$	5.712	5.809	6.235	5.764	5.886	5.877	5.87	5.866
A	$A = -E_{LUMO}$	1.205	1.221	0.856	1.344	1.909	1.883	1.855	1.87
χ (eV)	$\chi = (I + A) / 2$	3.4585	3.515	3.5455	3.554	3.8975	3.88	3.8625	3.868
η (eV)	$\eta = (I - A) / 2$	2.2535	2.294	2.6895	2.21	1.9885	1.997	2.0075	1.998
σ (eV)	$\sigma = 1/\eta$	0.4437	0.4359	0.3718	0.45248	0.5028	0.5007	0.4981	0.5005
Pi (eV)	$Pi = -\chi$	-3.4585	-3.515	-3.5455	-3.554	-3.8975	-3.88	-3.8625	-3.868
ω (eV)	$\omega = Pi^2/2\eta$	2.6539	2.6929	2.3369	2.8576	3.8195	3.7692	3.7157	3.7441
ε (eV)	$\varepsilon = Pi . \eta$	-7.7937	-8.0634	-9.5356	-7.8543	-7.7501	-7.7483	-7.7539	-7.7282
ΔN	$\Delta N = (\chi_{metal} - \chi_{inhibitor}) / 2. (\eta_{metal} - \eta_{inhibitor})$	0.7857	0.7595	0.6422	0.7796	0.7801	0.7811	0.7814	0.7837

9. CONCLUSION

In this thesis, eight organic compounds were synthesized. Experimentally the IR and NMR showed our compound was fully synthesized. Used B3LYP/cc-PVDZ for theoretical calculation, determined IR and NMR it is a good correlation with experimental characterization. Geometrical structure, molecular electrostatic map potential and thermodynamic was showing the properties of our compounds. Quantum chemical parameters show the inhibitor activity for the compounds. The HOMO and LUMO energy level was good coloration with inhibitor activity, by increasing the value of the HOMO and decreasing the value of the LUMO the inhibitor activity increased. This is because the increasing energy of HOMO is the tendency of the molecule to donating an electron on the metal surface (Fe bulk), while decreasing the energy value of LUMO indicates the molecule's ability to accept an electron. According to the energy of the HOMO and LUMO coumarin compounds has good anti-corrosion activity. The inhibition effectiveness of examined inhibitors is connected with the ΔE, which is a function of reactivity. As ΔE reduces, the inhibitor's reactivity on the iron surface was increased, this is clearly shown on the coumarins molecule. The softness and the hardness of the were linked to the ionization potential, the good softness compounds have good inhibitors, compound C7 has a higher softness value among all compounds. The parameters such as dipole moment (μ), electronegativity (χ), electrophilicity index (ω), nucleophilicity (ε) index and the fraction of transferred electrons (ΔN) which is related to transfer electron between inhibitor and metal surface supported that the coumarin compounds had more inhibitor activity. The lower value of electronegativity (χ) compared with the metal indicated the ΔN value was higher. The increasing value of ΔN the anti-corrosion was increased.

REFERENCES

[1]   Fang, B., Zhou, C.-H., and Rao, X.-C. (2010). Synthesis and biological activities of novel amine-derived bis-azoles as potential antibacterial and antifungal agents, *European journal of medicinal chemistry*, C Vol. 45 (9), pp: 4388-4398.

[2]   Zhou, C., Gan, L., Zhang, Y., Zhang, F., Wang, G., Jin, L., and Geng, R. (2009). Review on supermolecules as chemical drugs, *Science in China Series B: Chemistry*, C Vol. 52 (4), pp: 415-458.

[3]   Chang, J.-J., Wang, Y., Zhang, H.-Z., Zhou, C.-H., Geng, R.-X., and Ji, Q.-G. (2011). Recent advances in researches of triazole-based supramolecular chemistry and medicinal drugs, *Chemical Journal of Chinese Universities*, C Vol. 32 (9), pp: 1970-1985.

[4]   Omar, R., Koparir, P., and Koparir, M. (2021). Synthesis of 1, 3-Thiazole derivatives, *Indian Drugs*, C Vol. 1 58.

[5]   Mi, J., Wu, J., and Zhou, C. (2008). Progress in anti-tumor agents: triazoles, *West China Journal of Pharmacology Science*, C Vol. 23 84-86.

[6]   Jiali, M., Chenghe, Z., and Xue, B. (2010). Advances in triazole antimicrobial agents, Vol.

[7]   Wang, Y. and Zhou, C. (2011). Recent advances in the researches of triazole compounds as medicinal drugs, *Scientia Sinica Chimica*, C Vol. 41 (9), pp: 1429-1456.

[8]   Omer, R.A., Hughes, A., Hama, J.R., Wang, W., and Tai, H. (2015). Hydrogels from dextran and soybean oil by UV photo-polymerization, *Journal of Applied Polymer Science*, C Vol. 132 (6), pp.

[9]   Ouellette, W., Jones, S., and Zubieta, J. (2011). Solid state coordination chemistry of metal-1, 2, 4-triazolates and the related metal-4-pyridyltetrazolates, *CrystEngComm*, C Vol. 13 (14), pp: 4457-4485.

[10]   Liu, K., Shi, W., and Cheng, P. (2011). The coordination chemistry of Zn (II), Cd (II) and Hg (II) complexes with 1, 2, 4-triazole derivatives, *Dalton Transactions*, C Vol. 40 (34), pp: 8475-8490.

[11]   Zhou, C.-H., Zhang, Y.-Y., Yan, C.-Y., Wan, K., Gan, L.-L., and Shi, Y. (2010). Recent researches in metal supramolecular complexes as anticancer agents, *Anti-Cancer Agents in Medicinal Chemistry (Formerly Current Medicinal Chemistry-Anti-Cancer Agents)*, C Vol. 10 (5), pp: 371-395.

[12]   Rodriguez-Fernandez, E., Manzano, J.L., Benito, J.J., Hermosa, R., Monte, E., and Criado, J.J. (2005). Thiourea, triazole and thiadiazine compounds and their metal complexes as antifungal agents, *Journal of Inorganic Biochemistry*, C Vol. 99 (8), pp: 1558-1572.

[13]   Buzykin, B., Mironova, E., Nabiullin, V., Azancheev, N., Avvakumova, L., Rizvanov, I.K., Gubaidullin, A., Litvinov, I., and Syakaev, V. (2008). Tautomerism of aza cycles: II. Synthesis and structure of 5-substituted 3-(2-hydroxyethylsulfanyl)-1H-1, 2, 4-triazoles and their salts. Preference of the 1H, 4H-1, 2, 4-triazolium tautomers, *Russian Journal of General Chemistry*, C Vol. 78 (3), pp: 461.

[14]   Trzhtsinskaya, B., Aleksandrova, A., Apakina, E., Vinogradova, T., Shchegoleva, R., and Afonin, A. (1991). Synthesis and tuberculostatic activity of derivatives of 1, 2, 4-triazol-3-thione, *Pharmaceutical Chemistry Journal*, C Vol. 25 (3), pp: 171-173.

[15]   Mir, I., Siddiqui, M., and Comrie, A. (1970). Antituberculosis agents—I: α-[5-(2-Furyl)-1, 2, 4-triazol-3-ylthio] acethydrazide and related compounds, *Tetrahedron*, C Vol. 26 (22), pp: 5235-5238.

[16]   Ersan, S., Nacak, S., and Berkem, R. (1998). Synthesis and antimicrobial activity of N-[(α-methyl) benzylidene]-(3-substituted-1, 2, 4-triazol-5-yl-thio) acetohydrazides, *Il Farmaco*, C Vol. 53 (12), pp: 773-776.

[17]   Omar, R.A., Smail, A.K., and Omar, K.A. (2016). Study on the activity of Ag/Nylon 6, 10 nanocomposite against Escherichia coli, *Int. J. Curr. Microbiol. App. Sci*, C Vol. 5 (4), pp: 935-941.

[18]   Othman, R.S., Omar, R.A., Omar, K.A., Gheni, A.I., Ahmad, R.Q., Salih, S.M., and Hassan, A.N. (2019). Synthesis of Zinc Sulfide Nanoparticles by Chemical Coprecipitation Method and its Bactericidal Activity Application, *Polytechnic Journal*, C Vol. 9 (2), pp: 156-160.

[19]   Dembitsky, V.M. (2005). Astonishing diversity of natural surfactants: 5. Biologically active glycosides of aromatic metabolites, *Lipids*, C Vol. 40 (9), pp: 869-900.

[20]   Chakravarti, R., Gupta, K., Majors, A., Ruple, L., Aronica, M., and Stuehr, D.J. (2015). Novel insights in mammalian catalase heme maturation: effect of NO and thioredoxin-1, *Free Radical Biology and Medicine*, C Vol. 82 105-113.

[21]   El-Barbary, A., Abou-El-Ezz, A., Abdel-Kader, A., El-Daly, M., and Nielsen, C. (2004). Synthesis of some new 4-amino-1, 2, 4-triazole derivatives as potential anti-HIV and anti-HBV, *Phosphorus, Sulfur, and Silicon*, C Vol. 179 (8), pp: 1497-1508.

[22] Garratt, P., Katritzky, A., Rees, C., and Scriven, E. (1996). Comprehensive heterocyclic chemistry II, *AR Katritzky, CW Rees, EFV Scriven (Ed.)*, C Vol. 4 127-163.

[23] Barmin MI, M.V. (2002). Novyie amino-1, 2, 4-triazolil i tetrazolil alkany: monografia [New amino-1, 2, 4-triazolyl and tetrazolyl alkanes: monograph], *Sankt-Peterburg, SPHUTD*, C Vol.

[24] Omer, R.A., Hama, J.R., and Rashid, R.S.M. (2017). The effect of dextran molecular weight on the biodegradable hydrogel with oil, synthesized by the michael addition reaction, *Advances in Polymer Technology*, C Vol. 36 (1), pp: 120-127.

[25] Chenard, B., Lipinski, C., Dominy, B., Mena, E., Ronau, R., Butterfield, G., Marinovic, L., Pagnozzi, M., Butler, T., and Tsang, T. (1990). A unified approach to systematic isosteric substitution for acidic groups and application to NMDA antagonists related to 2-amino-7-phosphonoheptanoate, *Journal of medicinal chemistry*, C Vol. 33 (3), pp: 1077-1083.

[26] Wang, Z., Wu, B., Kuhen, K.L., Bursulaya, B., Nguyen, T.N., Nguyen, D.G., and He, Y. (2006). Synthesis and biological evaluations of sulfanyltriazoles as novel HIV-1 non-nucleoside reverse transcriptase inhibitors, *Bioorganic & medicinal chemistry letters*, C Vol. 16 (16), pp: 4174-4177.

[27] Shafiee, A., Sayadi, A., Roozbahani, M.H., Foroumadi, A., and Kamal, F. (2002). Synthesis and in vitro Antimicrobial Evaluation of 5-(1-Methyl-5-nitro-2-imidazolyl)-4H-1, 2, 4-triazoles, *Archiv der Pharmazie: An International Journal Pharmaceutical and Medicinal Chemistry*, C Vol. 335 (10), pp: 495-499.

[28] Nahrwold, M., Bogner, T., Eissler, S., Verma, S., and Sewald, N. (2010). "Clicktophycin-52": a bioactive cryptophycin-52 triazole analogue, *Organic Letters*, C Vol. 12 (5), pp: 1064-1067.

[29] Koca, M., Kirilmiş, C., and Arici, C. (2010). 1-(3-Mesityl-3-methylcyclobutyl)-2-phenoxyethanone, *Acta Crystallographica Section E: Structure Reports Online*, C Vol. 66 (3), pp: o523-o523.

[30] Dinçer, M., Özdemir, N., Yılmaz, İ., Çukurovalı, A., and Büyükgüngör, O. (2004). 1-Methyl-1-phenyl-3-[1-hydroxyimino-2-(succinimido) ethyl] cyclobutane, *Acta Crystallographica Section C: Crystal Structure Communications*, C Vol. 60 (9), pp: o674-o676.

[31] Özdemir, N., Dinçer, M., Yılmaz, İ., and Çukurovalı, A. (2004). 2-[2-Hydroxyimino-2-(3-methyl-3-phenylcyclobutyl) ethyl] isoindole-1, 3-dione, *Acta Crystallographica Section E: Structure Reports Online*, C Vol. 60 (1), pp: o145-o147.

[32] Zhu, Y., Olson, S.H., Graham, D., Patel, G., Hermanowski-Vosatka, A., Mundt, S., Shah, K., Springer, M., Thieringer, R., and Wright, S. (2008). Phenylcyclobutyl triazoles as selective inhibitors of 11β-hydroxysteroid dehydrogenase type I, *Bioorganic & medicinal chemistry letters*, C Vol. 18 (11), pp: 3412-3416.

[33] Ahmedzade, M., Cukurovali, A., and Koparir, M. (2003). Synthesis and Antimicrobial Activity of Some of New 1, 1, 3-Trisubstituted Cyclobutane Containing Thiazoles, Succinimide and Phthalimide Derivatives, *JOURNAL-CHEMICAL SOCIETY OF PAKISTAN*, C Vol. 25 (1), pp: 51-55.

[34] Greever, J.C., *Organic Chemistry, (Fessenden, Ralph J.; Fessenden, Joan S.)*, 1995, ACS Publications.

[35] Koparir, P., Parlak, A.E., Karatepe, A., and Omar, R.A. (2022). Elucidation of Potential Anticancer, Antioxidant and Antimicrobial Properties of Some New Triazole Compounds Bearing Pyridine-4-yl Moiety and Cyclobutane Ring, *Arabian Journal of Chemistry*, C Vol. 15 (27), pp: 103957.

[36] Bladin, J. (1885). Ueber von dicyanphenylhydrazin abgeleitete verbindungen, *Berichte der deutschen chemischen Gesellschaft*, C Vol. 18 (1), pp: 1544-1551.

[37] Vicentini, C.B., Manfrini, M., Veronese, A.C., and Guarneri, M. (1998). Synthesis of 4-(pyrazol-5-yl)-1, 2, 4-triazole-3-thiones, *Journal of heterocyclic chemistry*, C Vol. 35 (1), pp: 29-32.

[38] Klimešová, V., Zahajská, L., Waisser, K., Kaustová, J., and Möllmann, U. (2004). Synthesis and antimycobacterial activity of 1, 2, 4-triazole 3-benzylsulfanyl derivatives, *Il Farmaco*, C Vol. 59 (4), pp: 279-288.

[39] Potts, K. (1961). The Chemistry of 1, 2, 4-Triazoles, *Chemical reviews*, C Vol. 61 (2), pp: 87-127.

[40] Atkinson, M. and Polya, J. (1954). Triazoles. Part II. N-substitution of some 1: 2: 4-triazoles, *Journal of the Chemical Society (Resumed)*, C Vol. 141-145.

[41] Brunner, K. (1915). Eine neue Darstellungsweise von Triazolen, *Monatshefte für Chemie und verwandte Teile anderer Wissenschaften*, C Vol. 36 (7-8), pp: 509-534.

[42] Conde, S., Corral, C., and Madroñero, R. (1974). Synthesis and properties of 1H-1, 2, 4-benzotriazepines, *Tetrahedron*, C Vol. 30 (1), pp: 195-200.

[43] Castanedo, G.M., Seng, P.S., Blaquiere, N., Trapp, S., and Staben, S.T. (2011). Rapid synthesis of 1, 3, 5-substituted 1, 2, 4-triazoles from carboxylic acids, amidines, and hydrazines, *The Journal of Organic Chemistry*, C Vol. 76 (4), pp: 1177-1179.

[44] Palaska, E., Şahin, G., Kelicen, P., Durlu, N.T., and Altinok, G. (2002). Synthesis and anti-inflammatory activity of 1-acylthiosemicarbazides, 1, 3, 4-oxadiazoles, 1, 3, 4-thiadiazoles and 1, 2, 4-triazole-3-thiones, *Il Farmaco*, C Vol. 57 (2), pp: 101-107.

[45] Şahin, G., Palaska, E., Ekizoğlu, M., and Özalp, M. (2002). Synthesis and antimicrobial activity of some 1, 3, 4-oxadiazole derivatives, *Il Farmaco*, C Vol. 57 (7), pp: 539-542.

[46] Koparır, M., Cansız, A., and Demirdağ, A. (2004). Synthesis of some new 4, 5-substituted-4H-1, 2, 4-triazole-3-thiol derivatives, *Molecules*, C Vol. 9 (4), pp: 204-212.

[47] Cansız, A., Orek, C., Koparir, M., Koparir, P., and Cetin, A. (2012). 4-Allyl-5-pyridin-4-yl-2, 4-dihydro-3H-1, 2, 4-triazole-3-thione: Synthesis, experimental and theoretical characterization, *Spectrochimica Acta Part A: Molecular and Biomolecular Spectroscopy*, C Vol. 91 136-145.

[48] Koparir, M., Orek, C., Alayunt, N., Parlak, A.E., Koparir, P., Sarac, K., Dastan, S.D., and Cankaya, N. (2013). Synthesis, Structure Investigation, Spectral Characteristics and Biological Activitie of 4-Benzyl-3-(2-Hydroxyphenyl)-1H-1, 2, 4-Triazole-5 (4H)-Thione, *Communications in Computational Chemistry*, C Vol. 1 244-268.

[49] Koparır, M., Çetin, A., and Cansız, A. (2005). 5-Furan-2yl [1, 3, 4] oxadiazole-2-thiol, 5-furan-2yl-4H [1, 2, 4] triazole-3-thiol and their thiol-thione tautomerism, *Molecules*, C Vol. 10 (2), pp: 475-480.

[50] Omer, R.A., Koparir, P., and Ahmed, L.O. (2022). Characterization and Inhibitor Activity of Two Newly Synthesized Thiazole, *Journal of Bio-and Tribo-Corrosion*, C Vol. 8 (1), pp: 1-12.

[51] Öztürk, S., Akkurt, M., Cansız, A., Koparır, M., Şekerci, M., and Heinemann, F.W. (2004). 4-(4-Chlorophenyl)-3-(furan-2-yl)-1H-1, 2, 4-triazole-5 (4H)-thione, *Acta Crystallographica Section E: Structure Reports Online*, C Vol. 60 (3), pp: o425-o427.

[52] Heindel, N.D. and Reid, J.R. (1981). The Synthesis Of 3-R-7-Carbomethoxymethylene-7h-1, 2, 4-Triazolo [3, 4-B]-1, 3, 4-Thiadiazin-6-Ones, *Organic Preparations and Procedures International*, C Vol. 13 (2), pp: 123-126.

[53] Shivarama Holla, B., D'souza, A., and Kalluraya, B. (1991). Synthesis Of Some 2, 5-Diaryloxymethyl-1, 2, 4-Triazolo3, 4-B-1, 3, 4-Thiadiazoles, *Journal of the Indian Chemical Society*, C Vol. 68 (4), pp: 250-251.

[54] Eweiss, N. and Bahajaj, A. (1987). Synthesis of heterocycles. Part VII Synthesis and antimicrobial activity of some 7H-s-triazolo [3, 4-b][1, 3, 4] thiadiazine and s-triazolo [3, 4-b][1, 3, 4] thiadiazole derivatives, *Journal of heterocyclic chemistry*, C Vol. 24 (4), pp: 1173-1182.

[55] Heindel, N.D. and Reid, J.R. (1980). 4-Amino-3-mercapto-4H-1, 2, 4-triazoles and propargyl aldehydes: A new route to 3-R-8-aryl-1, 2, 4-triazolo [3, 4-b]-1, 3, 4-thiadiazepines, *Journal of heterocyclic chemistry*, C Vol. 17 (5), pp: 1087-1088.

[56] Meyer, V. (1883). Ueber den begleiter des benzols im steinkohlentheer, *Berichte der deutschen chemischen Gesellschaft*, C Vol. 16 (1), pp: 1465-1478.

[57] Patel, A.A. and Mehta, A.G. (2010). Synthesis of novel heterocyclic compounds and their biological evaluation, *Der Pharma Chemica*, C Vol. 2 (1), pp: 215-223.

[58] Joule, J. and Smith, G., *Heterocyclic Chemistry, van Norstrand Reinhold*, 1972, London.

[59] Jones, R.A. and Civcir, P.U. (1997). Extended heterocyclic systems 2. The synthesis and characterisation of (2-furyl) pyridines,(2-thienyl) pyridines, and furan-pyridine and thiophene-pyridine oligomers, *Tetrahedron*, C Vol. 53 (34), pp: 11529-11540.

[60] Freeman, F., Lee, M.Y., Lu, H., Wang, X., and Rodriguez, E. (1994). 1-Thia-cope rearrangements during the thionation of 2-endo-3-endo-bis (aroyl) bicyclo [2.2. 1] hept-5-enes, *The Journal of Organic Chemistry*, C Vol. 59 (13), pp: 3695-3698.

[61] Campaigne, E. and Foye, W.O. (1952). The synthesis of 2, 5-diarylthiophenes, *The Journal of Organic Chemistry*, C Vol. 17 (10), pp: 1405-1412.

[62] Gewald, K., Schinke, E., and Bottcher, H. (1966). 2-Amino-thiophene aus methylenaktiven Nitrilen, Carbonylverbindungen und Schwefel, *Chem. Ber*, C Vol. 99 94-100.

[63] Li, J.J. (2006). Fiesselmann thiophene synthesis, *Name Reactions: A Collection of Detailed Reaction Mechanisms*, C Vol. 230-232.

[64] Pinto, I.L., Jarvest, R.L., and Serafinowska, H.T. (2000). The synthesis of 5-alkoxy and 5-amino substituted thiophenes, *Tetrahedron Letters*, C Vol. 41 (10), pp: 1597-1600.

[65] Mishra, R., Jha, K., Kumar, S., and Tomer, I. (2011). Synthesis, properties and biological activity of thiophene: A review, *Der Pharma Chemica*, C Vol. 3 (4), pp: 38-54.

[66] Gronowitz, S., (2009). *Thiophene and Its Derivatives, Part 4*, John Wiley & Sons,

[67] Lew, H. (1963). CR N oller, *Org. Syn. Coll*, C Vol. 4 545.

[68] Barbarella, G., Melucci, M., and Sotgiu, G. (2005). The versatile thiophene: an overview of recent research on thiophene-based materials, *Advanced Materials*, C Vol. 17 (13), pp: 1581-1593.

[69] Hosmane, R.S. and Liebman, J.F. (1991). Aromaticity of heterocycles: experimental realization of dewar-breslow definition of aromaticity, *Tetrahedron Letters*, C Vol. 32 (32), pp: 3949-3952.

[70] Hartough, H.D. and Kosak, A.I. (1947). Acylation studies in the thiophene and furan series. IV. Strong inorganic oxyacids as catalysts, *Journal of the American Chemical Society*, C Vol. 69 (12), pp: 3093-3096.

[71] Maccarone, E. and Tomaselli, G. (1974). Leaving group effect in the reaction of 2-thiophenesulfonyl halides with anilines in methanol, *The Journal of Organic Chemistry*, C Vol. 39 (22), pp: 3286-3288.

[72] Marino, G., *Electrophilic substitutions of five-membered rings*, in *Advances in heterocyclic chemistry*1971, Elsevier. p. 235-314.

[73] Kuhn, S.J. and Olah, G.A. (1961). Aromatic Substitution. VII. 1 Friedel-Crafts Type Nitration of Aromatics2, *Journal of the American Chemical Society*, C Vol. 83 (22), pp: 4564-4571.

[74] Marino, G. (1965). A quantitative study of the uncatalysed halogenation of thiophene in acetic acid solution, *Tetrahedron*, C Vol. 21 (4), pp: 843-848.

[75] Hoffmann, R. and Davidson, R.B. (1971). Valence orbitals of cyclobutane, *Journal of the American Chemical Society*, C Vol. 93 (22), pp: 5699-5705.

[76] Heathcock, C.H. (1995). Molecular conformations--Stereochemistry of Organic Compounds by Ernest L. Eliel and Samuel H. Wilen with a chapter by Lewis N. Mander, *Science*, C Vol. 267 (5194), pp: 117.

[77] Crews, P., Rodriquez, J., Jaspars, M., and Crews, R.J. (1998). Organic structure analysis, Vol.

[78] Rosen, T. (1992). The Perkin Reaction, *Comprehensive Organic Synthesis*, C Vol. 2 395e408.

[79] Akhmedov, M., Sardarov, I., Akhmedov, I., Kostikov, R., Kisin, A., and Babaev, N. (1991). Formation of Substituted Cyclobutanes Under 2-(2-Methyl-2-Propenyl)-3-Chloromethyloxirane Interaction With Aromatic-Hydrocarbons, *Zhurnal Organicheskoi Khimii*, C Vol. 27 (7), pp: 1434-1440.

[80] Celikezen, F., Orek, C., Parlak, A., Sarac, K., Turkez, H., and Tozlu, Ö.Ö. (2020). Synthesis, structure, cytotoxic and antioxidant properties of 6-ethoxy-4-methylcoumarin, *Journal of Molecular Structure*, C Vol. 1205 127577.

[81] Davis, R.A., Vullo, D., Maresca, A., Supuran, C.T., and Poulsen, S.-A. (2013). Natural product coumarins that inhibit human carbonic anhydrases, *Bioorganic & medicinal chemistry*, C Vol. 21 (6), pp: 1539-1543.

[82] Zhang, L., Jiang, G., Yao, F., He, Y., Liang, G., Zhang, Y., Hu, B., Wu, Y., Li, Y., and Liu, H. (2012). Growth inhibition and apoptosis induced by osthole, a natural coumarin, in hepatocellular carcinoma, *PloS one*, C Vol. 7 (5), pp: e37865.

[83] Koparir, P., Sarac, K., Orek, C., and Koparir, M. (2016). Molecular structure, spectroscopic properties and quantum chemical calculations of 8-t-buthyl-4-methyl-2H-chromen-2-one, *Journal of Molecular Structure*, C Vol. 1123 407-415.

[84] Peng, X.-M., LV Damu, G., and Zhou, H. (2013). Current developments of coumarin compounds in medicinal chemistry, *Current pharmaceutical design*, C Vol. 19 (21), pp: 3884-3930.

[85] Thakur, A., Singla, R., and Jaitak, V. (2015). Coumarins as anticancer agents: A review on synthetic strategies, mechanism of action and SAR studies, *European Journal of Medicinal Chemistry*, C Vol. 101 476-495.

[86] Kumar, K.A., Renuka, N., Pavithra, G., and Kumar, G.V. (2015). Comprehensive review on coumarins: Molecules of potential chemical and pharmacological interest, *J Chem Pharm Res*, C Vol. 7 (9), pp: 67-81.

[87] Narayanaswamy, V.K., Gleiser, R.M., Kasumbwe, K., Aldhubiab, B.E., Attimarad, M.V., and Odhav, B. (2014). Evaluation of halogenated coumarins for antimosquito properties, *The Scientific World Journal*, C Vol. 2014.

[88] Potdar, M.K., Mohile, S.S., and Salunkhe, M.M. (2001). Coumarin syntheses via Pechmann condensation in Lewis acidic chloroaluminate ionic liquid, *Tetrahedron Letters*, C Vol. 42 (52), pp: 9285-9287.

[89] Perkin, W. (1868). XXIII.—On the hydride of aceto-salicyl, *Journal of the Chemical Society*, C Vol. 21 181-186.

[90] Knoevenagel, E. (1898). Condensation of malonic acid with aromatic aldehydes with ammonia and amines, *J. Am. Chem. Soc*, C Vol. 31 2596-2619.

[91] Akman, F. and Sarac, K. (2016). Molecular structure, vibration properties and quantum chemical calculations of 4-(chloromethyl)-7-methoxycoumarin and 4-(chloromethyl)-7-methyl-coumarin, *Natural Science and Discovery*, C Vol. 2 (2), pp: 26-35.

[92] Saraç, K. (2021). Spectroscopic characterization and structural insights of 4-Coumarinyl-4-nitrobenzoate using vibrational and quantum chemical calculations, *Bitlis Eren University Journal of Science and Technology*, C Vol. 11 (1), pp: 17-21.

[93] Gündüz, C., (2001). *Bazı Polihidroksikumarin Türevi Makrohalkalı Eterlerin Sentezi, Yüksek Lisans Tezi, MÜ Fen Bilimleri Enstitüsü, İstanbul*. Ph.D. thesis,

[94] Koparir, P., Sarac, K., and Omar, R.A. (2022). Synthesis, molecular characterization, biological and computational studies of new molecule contain 1, 2, 4-triazole, and Coumarin bearing 6, 8-dimethyl, *Biointerface Research in Applied Chemistry*, C Vol. 12 (1), pp: 809-823.

[95] Rebaz, O., Koparir, P., Qader, I., and Ahmed, L. Theoretical Determination of Corrosion Inhibitor Activities of Naphthalene and Tetralin, *Gazi University Journal of Science*, C Vol. 1-1.

[96] Koparir, P., Rebaz, O., Karatepe, M., and Ahmed, L. (2020). Synthesis, Characterization, and theoretical inhibitor study for (1E, 1'E)-2, 2'-thiobis (1-(3-mesityl-3-methylcyclobutyl) ethan-1-one) dioxime, *El-Cezeri*, C Vol. 8 (3), pp: 1495-1510.

[97] Ahmed, L. and Rebaz, O. (2021). 1H-Pyrrole, Furan, and Thiophene Molecule Corrosion Inhibitor Behaviors, *Journal of Physical Chemistry and Functional Materials*, C Vol. 4 (2), pp: 1-4.

[98] Koparir, P., Omer, R.A., Karatepe, A., and Ahmed, L.O. (2022). Theoretical determination of corrosion inhibitor activities of 4-allyl-5-(pyridin-4-yl)-4H-1, 2, 4-triazole-3-thiol-thione tautomerism, *Indian Journal of Chemical Technology*, C Vol. 29 75-81.

[99] Linstrom, P.J. and Mallard, W.G. (2001). The NIST Chemistry WebBook: A chemical data resource on the internet, *Journal of Chemical & Engineering Data*, C Vol. 46 (5), pp: 1059-1063.

[100] Rao, C., Venkataraghavan, R., and Kasturi, T. (1964). Contribution to the infrared spectra of organosulphur compounds, *Canadian journal of chemistry*, C Vol. 42 (1), pp: 36-42.

[101] Rebaz, O., Koparir, P., Ahmed, L., and Koparir, M. (2020). Computational determination the reactivity of salbutamol and propranolol drugs, *Turkish Computational and Theoretical Chemistry*, C Vol. 4 (2), pp: 67-75.

[102] Sajan, D., Erdogdu, Y., Reshmy, R., Dereli, Ö., Thomas, K.K., and Joe, I.H. (2011). DFT-based molecular modeling, NBO analysis and vibrational spectroscopic study of 3-(bromoacetyl) coumarin, *Spectrochimica Acta Part A: Molecular and Biomolecular Spectroscopy*, C Vol. 82 (1), pp: 118-125.

[103] Ahmed, L. and Rebaz, O. (2020). Spectroscopic properties of Vitamin C: A theoretical work, *Cumhuriyet Science Journal*, C Vol. 41 (4), pp: 916-928.

[104] Silverstein, R.M. and Bassler, G.C. (1962). Spectrometric identification of organic compounds, *Journal of Chemical Education*, C Vol. 39 (11), pp: 546.

[105] Omer, L.A. and Rebaz, O. (2020). Computational Study on Paracetamol Drug, *Journal of Physical Chemistry and Functional Materials*, C Vol. 3 (1), pp: 9-13.

[106] Omer, R.A., Koparir, P., Ahmed, L., and Koparir, M. (2021). Computational and spectroscopy study of melatonin, *Indian Journal of Chemistry-Section B (IJC-B)*, C Vol. 60 (5), pp: 732-741.

[107] Omer, R.A., Ahmed, L.O., Koparir, M., and Koparir, P. (2020). Theoretical analysis of the reactivity of chloroquine and hydroxychloroquine, *Indian Journal of Chemistry-Section A (IJCA)*, C Vol. 59 (12), pp: 1828-1834.

[108] Omer, L.A. and Anwer, R.O. (2020). Population Analysis and UV-Vis spectra of Dopamine Molecule Using Gaussian 09, *Journal of Physical Chemistry and Functional Materials*, C Vol. 3 (2), pp: 48-58.

[109] Koopmans, T. (1934). Über die Zuordnung von Wellenfunktionen und Eigenwerten zu den einzelnen Elektronen eines Atoms, *Physica*, C Vol. 1 (1-6), pp: 104-113.

[110] Plakhutin, B.N. and Davidson, E.R. (2009). Koopmans' Theorem in the Restricted Open-Shell Hartree− Fock Method. 1. A Variational Approach, *The Journal of Physical Chemistry A*, C Vol. 113 (45), pp: 12386-12395.

[111] Jesudason, E.P., Sridhar, S., Malar, E.P., Shanmugapandiyan, P., Inayathullah, M., Arul, V., Selvaraj, D., and Jayakumar, R. (2009). Synthesis, pharmacological screening, quantum chemical and in vitro permeability studies of N-Mannich bases of benzimidazoles through bovine cornea, *European journal of medicinal chemistry*, C Vol. 44 (5), pp: 2307-2312.

[112] Gökce, H. and Bahceli, S. (2011). A study on quantum chemical calculations of 3-, 4-nitrobenzaldehyde oximes, *Spectrochimica Acta Part A: Molecular and Biomolecular Spectroscopy*, C Vol. 79 (5), pp: 1783-1793.

[113] Arivazhagan, M. and Subhasini, V. (2012). Quantum chemical studies on structure of 2-amino-5-nitropyrimidine, *Spectrochimica Acta Part A: Molecular and Biomolecular Spectroscopy*, C Vol. 91 402-410.

[114] Masoud, M.S., Ali, A.E., Shaker, M.A., and Elasala, G.S. (2012). Synthesis, computational, spectroscopic, thermal and antimicrobial activity studies on some metal–urate complexes, *Spectrochimica Acta Part A: Molecular and Biomolecular Spectroscopy*, C Vol. 90 93-108.

[115] Musa, A.Y., Jalgham, R.T., and Mohamad, A.B. (2012). Molecular dynamic and quantum chemical calculations for phthalazine derivatives as corrosion inhibitors of mild steel in 1 M HCl, *Corrosion Science*, C Vol. 56 176-183.

[116] Kiyooka, S.-i., Kaneno, D., and Fujiyama, R. (2013). Parr's index to describe both electrophilicity and nucleophilicity, *Tetrahedron Letters*, C Vol. 54 (4), pp: 339-342.

[117] Pearson, R.G. (1988). Absolute electronegativity and hardness: application to inorganic chemistry, *Inorganic chemistry*, C Vol. 27 (4), pp: 734-740.

[118] Ahmed, L. and Rebaz, O. (2019). A theoretical study on Dopamine molecule, *Journal of Physical Chemistry and Functional Materials*, C Vol. 2 (2), pp: 66-72.

[119] Arslan, T., Kandemirli, F., Ebenso, E.E., Love, I., and Alemu, H. (2009). Quantum chemical studies on the corrosion inhibition of some sulphonamides on mild steel in acidic medium, *Corrosion Science*, C Vol. 51 (1), pp: 35-47.

[120] Chen, S., He, B., Liu, Y., Wang, Y., and Zhu, J. (2014). Quantum chemical study of some benzimidazole and its derivatives as corrosion ınhibitors of steel in HCl solution, *Int. J. Electrochem. Sci*, C Vol. 9 5400-5408.

[121] Ahmed, L. and Rebaz, O. The Role of the Various Solvent Polarities on Piperine Reactivity and Stability, *Journal of Physical Chemistry and Functional Materials*, C Vol. 4 (2), pp: 10-16.

[122] Rebaz, O., Koparir, P., Qader, I.N., and Ahmed, L. (2021). Structure reactivity analysis for Phenylalanine and Tyrosine, *Cumhuriyet Science Journal*, C Vol. 42 (3), pp: 576-585.

[123] El Adnani, Z., Mcharfi, M., Sfaira, M., Benzakour, M., Benjelloun, A., and Touhami, M.E. (2013). DFT theoretical study of 7-R-3methylquinoxalin-2 (1H)-thiones (RH; CH3; Cl) as corrosion inhibitors in hydrochloric acid, *Corrosion Science*, C Vol. 68 223-230.

[124] Fujioka, E., Nishihara, H., and Aramaki, K. (1996). The inhibition of pit nucleation and growth on the passive surface of iron in a borate buffer solution containing Cl− by oxidizing inhibitors, *Corrosion Science*, C Vol. 38 (11), pp: 1915-1933.

[125] Koch, E.C. (2005). Acid-Base Interactions in Energetic Materials: I. The Hard and Soft Acids and Bases (HSAB) Principle–Insights to Reactivity and Sensitivity of Energetic Materials, *Propellants, Explosives, Pyrotechnics: An International Journal Dealing with Scientific and Technological Aspects of Energetic Materials*, C Vol. 30 (1), pp: 5-16.

[126] Kaya, S., Kariper, S.E., Üngördü, A., and Kaya, C. (2014). Effect of some electron donor and electron acceptor groups on stability of complexes according to the principle of HSAB, *Journal of New Results in Science*, C Vol. 3 (4), pp: 1-1.

[127] Erkan, S., Sayın, K., and Karakaş, D. (2014). Theoretical studies on eight oxovanadium (IV) complexes with salicylaldehyde and aniline ligands, *Hacettepe J Biol Chem*, C Vol. 42 337-342.

APPENDICES

APPENDIX- 1:

Figure A. 1. Synthesis 4-phenyl-5-(thiophen-2-yl)-4H-1,2,4-triazole-3-thiol

Figure A. 2. Synthesis 4-ethyl-5-(thiophen-2-yl)-4H-1,2,4-triazole-3-thiol

Figure A. 3. The powder of 4-phenyl-5-(thiophen-2-yl)-4H-1,2,4-triazole-3-thiol
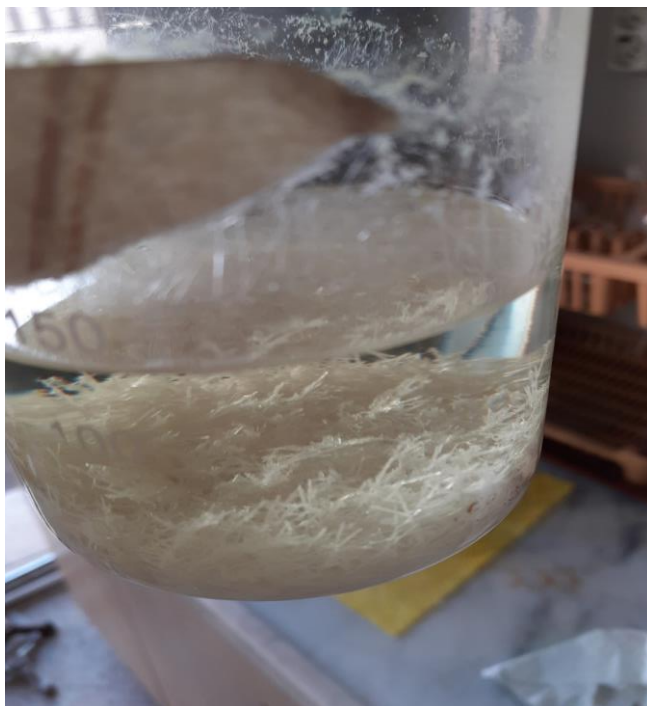
Figure A. 4. Recrytallzation of 4-phenyl-5-(thiophen-2-yl)-4H-1,2,4-triazole-3-thiol

Figure A. 5. Perkin Elmer 1600 FT-IR spectrophotometer

Figure A. 6. Bruker advance III 400 MHz NMR spectrophotometer

CURRICULUM VITAE

Rebaz OMER

PERSONAL INFORMATION

Birth of Place	: **Iraq- Erbil- Koya**
Birth of Date	: 23/9/1983
Nationality	: Iraqi
Address	: Iraq-Erbil-koya-Koya university
E-mail	: rebaz.anwar@koyauniversity.org
Languages	: Turkish (B1), English (B2), Arabic (B2)

RESEARCHER INFORMATION

Student Orcid ID	: **0000-0002-3774-6071**
Advisor Orcid ID	: **0000-0003-1031-783X**

EDUCATION

Master Degree	:"Synthesis Hydrogels from dextran and soybean oil by UV photo-polymerization" Bangor University, Environmental Graduate School, Department of Chemistry, 2012 Supervisor: Dr. Hongyun Tai
Bachelor	: Koya University, Faculty of health and Science, Department of Chemistry, 2008
High School	: High School for Boy, Koya, 2004

RESEARCH EXPERIENCES

- ✓ FT-IR, NMR, TGA, and XRF
- ✓ Computer programs (Microsoft Office Word, Excel, PowerPoint, EndNote, Origin Lab, Gaussian, ChemBioDraw Ultra, and ChemBio3D Ultra)
- ✓

WORK EXPERIENCE

2008 – 2009 : Worked in Laboratory as assistant chemistry/ koya University/ chemistry department.

2013 – 2016 : Assistant Lecturer at Koya University \ Faculty of Science and Health \ Chemistry Dept. Teaching polymer Chemistry for 4th year students (Theoretical and practical). Teaching analytical and organic chemistry for Biology and petroleum (Theoretical and practical) engineering department.

2016 - 2017 : Lecture at koya university/ Faculty of Science and Health/ Teaching organic for 3rd year student (Theoretical).

ACADEMIC ACTIVITIES

Paper:

1. Koparir, P., Parlak, A.E., Karatepe, A., and Omar, R.A. (2022). Elucidation of Potential Anticancer, Antioxidant and Antimicrobial Properties of Some New Triazole Compounds Bearing Pyridine-4-yl Moiety and Cyclobutane Ring, *Arabian Journal of Chemistry*, C Vol. 15 (27), pp: 103957.

2. Ahmed, L.O., Omer, R.A., Qader, I.N., Koparir, P, (2022). Theoretical Analysis of the Reactivity of Carmustine and Lomustine Drugs. *Journal of Physical Chemistry and Functional Materials*, Volume 5, Issue 1 (2022) 84-96.

3. Omar, R.A., Ahmed, L.O., Hama ,J.R., Koparir, P., (2022). Structural Analysis of Epinephrine by Combination of Density Functional Theory and Hartree-Fock Methods. *El-Cezerî Journal of Science and Engineering*, Vol: 9, No: 2.

4. Omer, R.A., Ahmed, L.O., Koparir, P., Hama, J.R., (2022). Impact of Solvent Polarity on the Molecular Properties of Dimetridazole. *El-Cezerî Journal of Science and Engineering*, (9), No: 2.

5. Koparir, P, Omer, R.A., Karatepe, A., Ahmed, L.O., (2022). Theoretical determination of corrosion inhibitor activities of 4-allyl-5-(pyridin-4-yl)-4H-1, 2, 4-triazole-3-thiol-thione tautomerism. *Indian Journal of Chemical Technology*, Vol. 29, January, pp. 75-81.

6. Omer, R.A., Koparir, P., Qader, I.N., Ahmed, L.O, (2022). Theoretical Determination of Corrosion Inhibitor Activities of Naphthalene and Tetralin. *Gazi University Journal of Science*, 35 (2), 434-444

7. Omer, R.A., Koparir, P., Ahmed, L.O., (2022). Characterization and Inhibitor Activity of Two Newly Synthesized Thiazole. *Journal of Bio-and Tribo-Corrosion*, 8 (1), 1-12.

8. Koparir, P., Sarac, K., Omar, R.A., (2022). Synthesis, Molecular Characterization, Biological and Computational Studies of New Molecule Contain 1, 2, 4-Triazole, and Coumarin Bearing 6, 8-Dimethyl. *Biointerface Research in Applied Chemistry*, Volume 12, Issue 1, 2022, 809 – 823.

9. Omer, R.A. Koparir, M., (2021). Synthesis, Quantum Chemical Calculation and Biological Activity of 4-Phenyl-5-(Thiophen-2-yl)-4H-1,2,4-Triazole-3-Thiol. *2nd International Hazar Scientific Researches Conference*, Baku, Azerbaijan.

10. Koparir, P., Omer, R.A., Karatepe, M., Ahmed, L.O., (2021). Synthesis, Characterization, and theoretical inhibitor study for (1E, 1'E)-2, 2'-thiobis (1-(3-mesityl-3-methylcyclobutyl) ethan-1-one) dioxime. *El-Cezeri*, 8 (3), 1495-1510.

11. Ahmed, L.O., Omer, R.A., (2021). 1H-Pyrrole, Furan, and Thiophene Molecule Corrosion Inhibitor Behaviors. *Journal of Physical Chemistry and Functional Materials,* 4 (2), 1-4.

12. Ahmed, L.O., Omer, R.A., (2021). The Role of the Various Solvent Polarities on Piperine Reactivity and Stability. *Journal of Physical Chemistry and Functional Materials,* 4 (2), 10-16.

13. Omer, R.A., Koparir, P., Qader, I.N., Ahmed, L.O., (2021). Structure reactivity analysis for Phenylalanine and Tyrosine. *Cumhuriyet Science Journal,* 42 (3), 576-585.

14. Ahmed, L.O, Al-Arif, M., Chaqmaqchee, F., Omer, R.O., (2021). Risk Elements in Drinking Water of Koya City. *Letters in Applied NanoBioScience,* 11 (2), 3488-3497.

15. Omer, R.A., Koparir, P., Ahmed, L.O, Koparir, M., (2021). Computational and spectroscopy study of melatonin. *Indian Journal of Chemistry-Section B (IJC-B)*, 60 (5), 732-741.

16. Omar, R.A, Koparir, P., Koparir, M., (2021). Synthesis of 1, 3-Thiazole Derivatives, *Indian Drugs*, 58 (1), 7-19

17. Ahmed, L.O., Omer, R.A., (2020). Spectroscopic properties of Vitamin C: A theoretical work. *Cumhuriyet Science Journal,* 41 (4), 916-928.

18. Ahmed, L.O., Omer, R.A., (2020). Population Analysis and UV-Vis spectra of Dopamine Molecule Using Gaussian 09. *Journal of Physical Chemistry and Functional Materials*, 3 (2), 48-58.

19. Ahmed, L.O., Omer, R.A., (2020). Computational Study on Paracetamol Drug. *Journal of Physical Chemistry and Functional Materials*, 3 (1), 9-13.

20. Omer, R.A., Ahmed, L.O., Koparir, M., Koparir, P., (2020). Theoretical analysis of the reactivity of chloroquine and hydroxychloroquine. *Indian Journal of Chemistry-Section A (IJCA),* 59 (12), 1828-1834.

21. Omer, R.A., Koparir, P., Ahmed, L.O., Koparir, M., (2020). Computational determination the reactivity of salbutamol and propranolol drugs. *Turkish Computational and Theoretical Chemistry,* 4 (2), 67-75.

22. Omer, R.A., Gheni, A.I., Omar, K.A., Ahmed, L.O., (2019). Antimicrobial Activity of Nylon Nanocomposites Against Staphylococcus Aureus and Escherichia Coli Bacteria. *Science Journal of University of Zakho* 7 (4), 138-143.

23. Roshna, S.O, Omar, R.A., Omar, K.A., Gheni, A.I., Ahmad, R.Q., Salih, S.M., (2019). Synthesis of Zinc Sulfide Nanoparticles by Chemical Coprecipitation Method and its Bactericidal Activity Application. *Polytechnic Journal*, 9 (2), 156-160.

24. Ahmed, L.O., Omer, R.A., Kebiroglu, H., (2019). A theoretical study on Dopamine molecule. *Journal of Physical Chemistry and Functional Materials*, 2 (2), 66-72.